Department of Material Science and Engineering
Faculty of Mechanical, Maritime and Materials Engineering
Delft University of Technology

Kinetics of Austenite to Ferrite Transformation and Microstructure Modelling in Steels

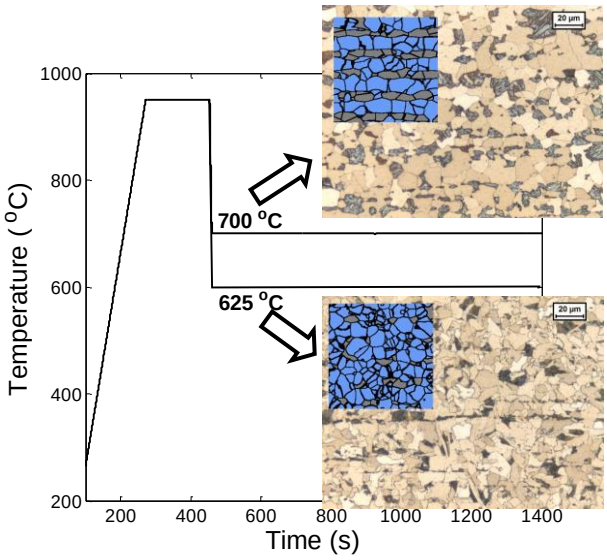

Harini Pattabhiraman
MSc Material Science and Engineering

MSc Thesis
20th June 2013

Supervisors:
Prof. dr. ir. J. Sietsma (TU Delft)
Dr. ir. C. Bos (Tata Steel)
Dr. M. G. Mecozzi (TU Delft)

Committee Members:
Prof. dr. ir. J. Sietsma
Dr. ir. C. Bos
Dr. M. G. Mecozzi
Dr. ir. M. H. F. Sluiter

Abstract

The mechanical properties of steel are influenced by its microstructure, which is obtained as a result of processing conditions. It is, thus, important to study the effect of these conditions on the microstructure. A three dimensional microstructure model, based on a cellular automata (CA) model, was previously developed. The model is capable of reproducing a number of trends caused by the difference in processing conditions, like temperature and cooling rate, with respect to the microstructure and growth kinetics. However, a single set of nucleation and growth parameters to define the behaviour through a range of conditions have not been found yet. Thus, the goal of this project is to optimise the cellular automata model with a single set of nucleation and growth parameters which makes it capable of predicting the microstructure and growth kinetics at different processing conditions.

The CA model uses a simplified calculation of the carbon concentration profile in the austenite. Validation of this simplified calculation, termed as the 'semi analytical model', was performed. This was necessary to ascertain that the error obtained in the calculation of the CA model is not a result of this simplification. It was found that the accuracy of the semi analytical model depends on the nature of the transformation. The error increases when the transformation becomes more diffusion controlled in nature.

The improvement in the CA model was carried out in terms of its ability to deal with the interaction of the solutes with the austenite-ferrite interface. This, in turn, affects the thermodynamic conditions applicable at the interface. The two extreme equilibrium conditions which are generally defined are the para-equilibrium (PE) and the local equilibrium with negligible partitioning (LENP). The former represents a constrained equilibrium resulting in faster kinetics, while the latter is associated with short range diffusion leading to slower kinetics. In order to account for the slowing down of the kinetics at the end of the transformation, a transition from PE to LENP was proposed. This 'gradual transition approach' is based on the interface velocity and accounts for equilibrium states intermediate to that of the PE and LENP conditions.

Isothermal austenite-to-ferrite transformation in a dual phase steel, DP600, at temperatures of 625, 650 and 700 °C was studied. The general trends with respect to the ferrite transformation rate, final ferrite fraction and ferrite microstructure were predicted

by the model using a single set of parameters. However, in order to explain the trend with respect to the ferrite grain size, the parameter describing the amount of edge cells used for nucleation had to be manually adjusted at different temperatures. A greater contribution of edge nucleation was required with decrease in temperature. The fraction of edge cells used for nucleation was 0.3, 0.1 and 0 at temperatures of 625, 650 and 700 °C respectively.

Acknowledgements

Firstly, I would like to thank my supervisors, Jilt Sietsma, Kees Bos and Pina Mecozzi, for introducing me to the world of computational sciences and giving me an opportunity to work on this project. I would also like to thank Pieter van der Wolk (Tata Steel) for letting me to carry out the project in his group.

The monthly meetings with Pina, Jilt and Kees was a major driving force behind this work. The long insightful discussions during those meetings played a crucial role in understanding and exploring many concepts. Writing those meeting summaries prepared me better to write this thesis. Thank you for motivating me to think and work independently.

A special thanks to Kees for being available for those numerous small discussions throughout the day and working on the programs during the weekends. I can hardly envisage the disturbance I would have caused to your work.

A special mention goes to a number of people for explaining me the basic concepts involved: Pina and Kees for cellular automata model, Kees for finite difference model and Dennis den Ouden for MATLAB®. It would have been more difficult if not for you. I would also like to thank Nico Geerlofs, Stefan van Boheman and Theo Kop for helping me with the dilatometric experiments and its analysis and Floor Twisk and Maxim Aarnts for the metallographic experiments.

Next, I would like to thank Theo Kop for the Dutch talks. It was a welcome distraction in the middle of technically challenging days. The list will be incomplete, without the mention of the location of Tata Steel and the Dutch weather for making me physically stronger by forcing me to bike in the wind, rain and snow.

Finally, I would like to thank my brother, Sriram, and my parents, Usha and Pattabhiraman, for their support during the course of my study, and my fiancé, Santosh, for putting up with my daily cribbing.

Contents

Chapter 1

Introduction

The mechanical properties of a metal or an alloy is a result of its constituent microstructure. The microstructure is a result of its chemical composition, processing and heat treatment. It is important to study and understand the formation of microstructures in order to develop new products for specific applications.

1.1 Steel and its Applications

Iron is one of the most abundantly present metals on the surface of the earth and constitutes up to 35 % of its mass. Its application is numerous owing to its relatively easy accessibility and extractability. In addition, its combination of low cost and good mechanical properties makes it a suitable candidate for various important applications like automobiles and mechanical structures. (Savran [2009])

Steel is an alloy of iron and carbon. Though iron and carbon are the major constituents of all kinds of steel, various grades of steels are formed by the addition of several alloying elements. These alloying elements aim at improving certain properties of steel in accordance to its application. In addition to changing its composition, the mechanical properties of steel can also be influenced by various heat treatment processes.

The wide range of alloy compositions, mechanical properties and product forms makes steel one of the most versatile materials currently available. It, thus, finds application in almost every sphere of life ranging from small applications like home appliances and packaging cans to structural applications like the construction and transport sectors. It is also widely used in electrical and magnetic devices. (SteelUniversity [2013])

1.2 Steel in the Automobile Industry

The automobile industry today aims at reducing the fuel consumption and resource utilisation and maximise the recyclability of the product. This is catered by reducing

the weight of the automobiles by using thinner gauges of sheet material. In order to adhere to the safety norms, this also means that the material used needs to be much stronger. This need of strong and light materials has given rise to a new class of steel termed as 'Advanced High Strength Steels'. The distribution of steel grades used in the automobile body structure is given in Figure 1.1. It can be noted that dual phase (DP) steel is the most widely used grade of advanced high strength steel. (Tsipouridis [2006])

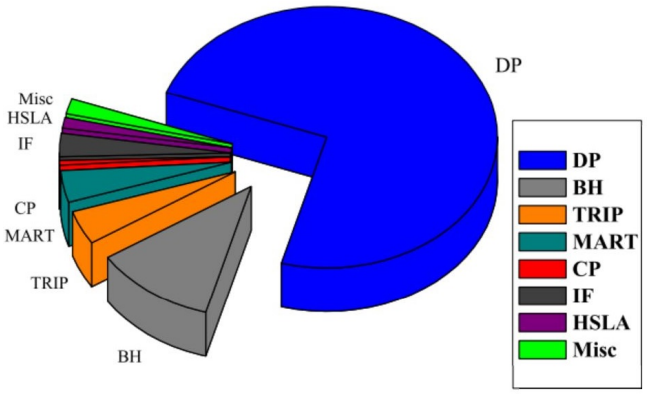

Figure 1.1: Distribution of steel grades in automobile body structure (Tsipouridis [2006])

1.3 Dual Phase Steel

Industrially, dual phase steels contain less than 0.2 wt.% of carbon. In addition, Manganese, Chromium, Molybdenum, Silicon and Aluminium are added individually or in combination. These additions help in attaining unique set of mechanical properties, in addition to increased hardenability and better resistance spot welding capability. (WorldAutoSteel [2013]) A commonly used form of the dual phase steel has a microstructure consisting of a softer ferrite matrix (about 75-95 %) and much stronger martensite. This microstructure results in a combination of high strength, good energy absorption characteristics, good ductility and formability. (TATASteel [2013])

The parts wherein dual phase steel is used in the automobile chassis is shown in Figure 1.2. These include, the A-, B- C- pillars, crash boxes and support components. The excellent fatigue properties and good energy absorption characteristics of the dual phase steel makes it an ideal material for structural and reinforcement structures, especially in the crash structure.

For use in automobiles, dual phase steel is initially processed into strips by hot rolling. These strips are then further processed to obtain the necessary shapes. The heat treatment cycle during processing affects the final microstructure of the steel. One of the possible heat treatment cycles for the creation of a dual phase microstructure is explained by Bos et al. [2010]. At the start of the annealing cycle, the alloy consists

Figure 1.2: Application of Dual Phase steel in the automobile chassis (SalzgitterFlachstahl [2013])

of a microstructure of deformed ferrite and pearlite. The material is heated up to the intercritical annealing temperature, wherein the ferrite is recrystallised to an extent determined by the heating rate and the strain energy. This is followed by an isothermal hold at that temperature. The transformation of pearlite- and ferrite-to-austenite takes place during heating and isothermal hold. A two-phase microstructure consisting of ferrite and austenite is, thus, obtained. The holding period is followed by a short slow cooling period and a quench. During slow cooling, a part of austenite is transformed to ferrite and the remaining austenite is transformed to martensite during quenching.

It can be summarised that the set of mechanical properties of the dual phase steel is a result of its microstructure, which in turn depends on the heat treatment. Thus, it becomes important to study the microstructure formation and transformation behaviour of the steel during its processing. This project aims at fine tuning a model for simulating the microstructure and transformation behaviour of the dual phase steel in the run-out table of a hot strip mill.

A cellular automata (CA) model was developed by Bos et al. [2010] to describe the kinetics of the austenite-to-ferrite transformation along with a description of the final ferrite microstructure. However, it has been observed that the final ferrite fraction as simulated by the model is much larger than the experimentally observed fractions. (Pattabhiraman [2012]) This could be due to the absence of a description of interaction of the alloying elements with the moving interface in the CA model. This is addressed by focussing on the thermodynamic conditions present at the moving austenite-ferrite interface. It deals with the transition from one thermodynamic equilibrium condition to another. This is based on the ability of the moving interface to exist in conditions intermediate to those defined by various equilibrium conditions. After obtaining a correct description of the transformation kinetics, the cellular automata model is optimised with a universal set of nucleation and growth parameters in order to describe the transformation behaviour of various alloys. This would act as a useful tool in product development.

1.4 Thesis Outline

Chapter 2 deals with the basic physical principles used in the modelling of phase transformations. The various models used in this work are explained. In Chapter 3, the basic thermodynamic principles involved in phase transformations are discussed. An overview of various transition models is also given. The techniques involved in various experimental studies and the results obtained from them are given in Chapter 4. Chapter 5 concerns with the implementation of different models in MATLAB® and their validation. The formulation of a new transition approach and its subsequent implementation is given in Chapter 6. Results of simulations of isothermal austenite-to-ferrite transformation of a dual phase steel, DP600, obtained using the CA model are discussed in Chapter 7. The conclusions and recommendations for future work are given in Chapter 8.

Chapter 2

Background Theory

In this chapter, the fundamental principles of physical metallurgy related to steel are discussed. This includes the phases present in steel and the transformation reactions between them. Further, the computational principles required for modelling phase transformations are explained. This is followed by an explanation of the cellular automata model used in this study.

2.1 Solid State Transformations in Steel

The major solid state transformations in steel are a result of the allotropic nature of its main constituent, iron. Iron exists in a body centered cubic (BCC) structure at low (<910 °C) and very high temperatures (1394-1538 °C) and in a face centered cubic structure (FCC) at intermediate temperatures (910-1394 °C). A similar behaviour is observed in case of steels. The FCC phase is termed as 'austenite' (γ) and the low temperature BCC phase is termed as 'ferrite' (α). The temperature ranges in which a certain phase can be expected to be present in equilibrium is explained with the help of a 'phase diagram'. The iron-carbon phase diagram is shown in Figure 2.1. It is a plot between the carbon content and temperature. The austenite and ferrite phases can be noted. The phase formed at higher carbon concentrations is termed as 'cementite'. At lower temperatures, alternate lamellae of ferrite and cementite is formed, which is termed as 'pearlite'. It can be noted that the transition between any two phases is not sharp and occurs over a range of temperatures and compositions. This is in sharp contrast with the allotropic transitions in iron, which occur at a constant temperature.

Industrially, the formation of ferrite from austenite is encountered during hot processing of steel when the steel is cooled from a higher temperature, consisting of full or partial austenitic microstructure, to the room temperature. This transformation, generally, forms the final step of processing and thus, dictates the microstructure at room temperature. This makes it highly important and relevant and thus, has been widely

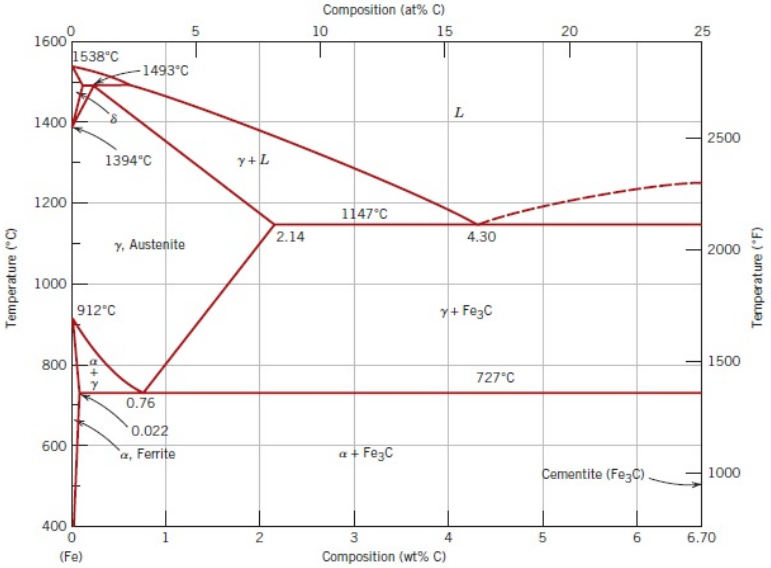

Figure 2.1: The iron-iron carbide phase diagram (Callister [2007])

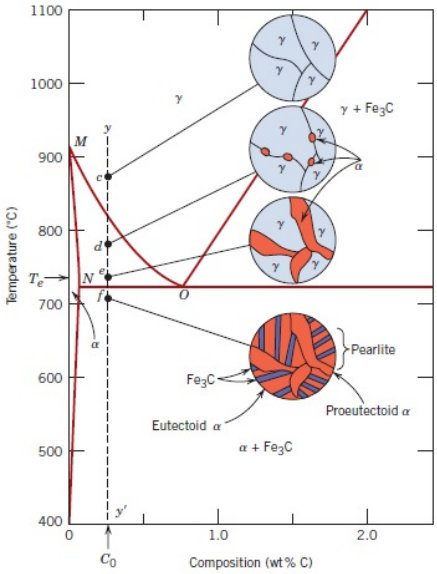

Figure 2.2: Schematic representation of the microstructural changes in a iron-carbon alloy during cooling (Callister [2007])

studied and documented. (van Leeuwen [2000], Mecozzi [2007], Kop [2000]) The kinetics of this transformation depends on the chemical composition, microstructure before transformation and the temperature of transformation. The microstructural variation during cooling for an alloy containing $C_\circ$ wt% carbon is shown in Figure 2.2. Initially, the microstructure is completely austenitic in nature. No transformation occurs in it till the transition temperature is reached. At the transition temperature, ferrite starts to form at the austenite grain boundaries as a result of the nucleation process. The

amount of ferrite increases with time as a result of the growth process. Finally, at lower temperatures, the remaining austenite is converted to pearlite.

Various alloying elements are added to steel in order to obtain a desired set of properties. However, this greatly affects the thermodynamics and kinetics of the austenite-to-ferrite transformation. In general, two classes of alloying elements can be distinguished, namely interstitial and substitutional elements. As the name suggests, interstitial elements, like C and N, occupy the interstitial sites in the lattice and the substitutional elements, like Mn and Cr, substitute an iron atom from the lattice. (Kop [2000])

2.2 Modelling of Transformations

The increase in industrial demand for more stronger and ductile materials has led to the production of steels with complex chemistry. The use of a simple plain carbon steel with only iron and carbon is becoming quite limited. This requires understanding of such complex systems in terms of its thermodynamics and kinetics. Carrying out large number of experimental studies on such complex systems is quite challenging. An ideal alternative is offered by the use of various computational tools. These tools help in understanding the underlying physical principles which, in turn, can lead to the development of new grades of steel. The numerous computer simulations aim at describing the various transformations by predicting the following:

1. The changes in the microstructure
2. The effect of alloying element on the kinetics of phase transformation
3. The effect of heat treatments

One of the major parameters required for describing the system in a computational domain is the thermodynamics of the multi-component systems as a function of the chemical composition. This involves the prediction of the necessary phase diagram for a given composition. This acts as the basis for calculation of the driving force. Such thermodynamic data can be obtained from a database such as Thermo-calc®. The second major requirement is that of the kinetic parameters. This involves the description of the diffusivities and interface mobilities. These input parameters along with a numerical description of the transformation are implemented in a computational domain to define the transformation. (Inden and Hutchinson [2003])

2.2.1 Austenite to Ferrite Transformation

The austenite (γ) to ferrite (α) transformation in steels can be considered to involve two components, namely a structural rearrangement from a FCC to a BCC system and a long-range distribution of carbon from ferrite to austenite. The solubility of carbon,

being interstitially dissolved in steels, is highly dependent on the crystal structure of the parent phase, iron. The solubility in ferrite is almost two orders of magnitude lower than in austenite and this requires long range diffusion of carbon atoms during the transformation. (van Leeuwen [2000])

Depending on whether the majority of the free energy is dissipated by the interfacial process or the carbon diffusion, the transformation can be described either as interface controlled or diffusion controlled in nature. (Hutchinson et al. [2004]) In the interface controlled transformation, diffusion is assumed to be infinitely fast. Whereas in the diffusion controlled transformation, the interface movement is assumed to be infinitely fast. However, it has been shown that neither of these approaches can accurately describe the growth kinetics of the entire transformation. Consequently, a mixed-mode model, which takes both these effects into account, was proposed by Sietsma and van der Zwaag [2004] and was later reformulated by Bos and Sietsma [2007].

In order to numerically describe the transformation in a computational domain, a description of the moving austenite-ferrite interface along with the equilibrium condition acting on it is required. Three kinds of models are used for describing the migrating interface, namely the sharp interface, finite interface and diffuse interface models. The sharp interface model is the simplest among the three and is widely used for describing diffusion controlled transformations. Here, the interface velocity is calculated either by considering the individual jumps of the atoms across the interface or the fluxes across the interface and in the two phases. Interfaces with finite width account for a composition profile within the interface. The solute phase inside the interface and its subsequent migration along with the interface accounts for the solute drag description. (Purdy et al. [2011]) One of the widely used diffuse interface models is the phase field model wherein the moving interface is described in terms of so-called phase field parameters. These parameters have a constant value in the bulk of the phase and change continuously across the width of the interface. The position of the interface is then derived from the contour of the phase field parameter. However, a fine grid size is required to reduce the anomalous effects arising from the description of the diffuse interface and thus, results in a large amount of computational time. (Mecozzi et al. [2012])

The equilibrium condition at the interface depends on the elements present in steel. In this chapter, modelling of austenite-to-ferrite transformation occurring in steels containing only iron and carbon is explained. The addition of a substitutional alloying element, like Mn or Cr, leads to complexities in the equilibrium conditions. This is due to the fact that the diffusion of the substitutional alloying element is a few orders of magnitude slower than the interstitial alloying elements. These are explained in Chapter 3.

Here, the formulation of a mixed mode model to describe the austenite-to-ferrite transformation is given. This is followed by an explanation of a three-dimensional mi-

crostructural model where the mixed mode model is used. This model is based on a cellular automata description and uses sharp interfaces between the phases.

2.3 Mixed Mode Model

In the mixed mode model formulated by Sietsma and van der Zwaag [2004], the velocity of the interface between ferrite (α) and austenite (γ) is calculated as

$$v = M\Delta G(T, x_{\mathrm{C}}^{\gamma}), \tag{2.1}$$

where M is the interface mobility, ΔG is the driving force, which is a function of temperature (T) and the interface carbon concentration in austenite (x_{C}^{γ}). The interface mobility is given by an Arrhenius type equation,

$$M = M_{\circ} \cdot e^{\frac{-Q_G}{RT}}, \tag{2.2}$$

where $M_{\circ}$ is the pre-exponential constant and Q_G is the activation energy for interface movement and has a value of 140 KJ/mol. (Bos and Sietsma [2007])

Consider an alloy of average carbon concentration x_{C}°, such that $x_{\mathrm{C}}^{\alpha\gamma} < x_{\mathrm{C}}^{\circ} < x_{\mathrm{C}}^{\gamma\alpha}$, where $x_{\mathrm{C}}^{\alpha\gamma}$ is the carbon concentration of ferrite in equilibrium with austenite and $x_{\mathrm{C}}^{\gamma\alpha}$ is the carbon concentration of austenite in equilibrium with ferrite. Partitioning of carbon at the moving interface takes place from ferrite to austenite as shown in Figure 2.3. Partitioning refers to the redistribution of substitutional solute over distances much larger than the interfacial region. The rate of partitioning is determined by the interface velocity. Diffusion of carbon takes place in austenite with a flux given by Fick's law.

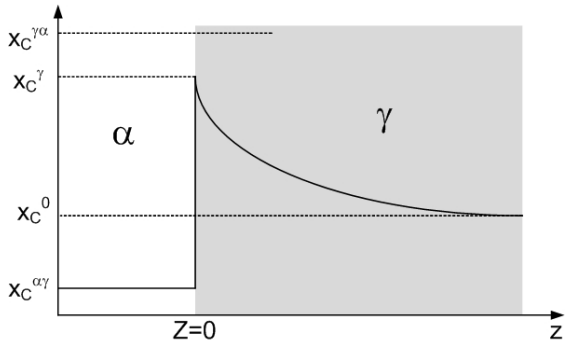

Figure 2.3: Carbon concentration profile near the moving interface (Bos and Sietsma [2007])

Numerically, this moving boundary problem can be solved using the Murray-Landis finite difference method (Murray and Landis [1959]), but it is computationally expensive. This method of solving the problem is termed as the fully numerical model. An altern-

ative, computationally faster, semi analytical model was proposed by Bos and Sietsma [2007].

2.3.1 Semi Analytical Mixed Mode Model

In the semi analytical model, the interface carbon concentration in the austenite, x_{C}^{γ}, is calculated on the basis of a few assumptions. The driving force is assumed to be a function of the difference between the austenite equilibrium carbon concentration and the interface carbon concentration and is calculated as

$$\Delta G = \chi(x_{\mathrm{C}}^{\gamma\alpha} - x_{\mathrm{C}}^{\gamma}), \tag{2.3}$$

where χ is a proportionality factor calculated from Thermo-calc®.

The carbon concentration profile in the austenite is described as a function of the distance from the interface, z. The concentration profile is assumed to be exponential in nature and can be expressed as

$$x_{\mathrm{C}} = x_{\mathrm{C}}^{\circ} - (x_{\mathrm{C}}^{\gamma} - x_{\mathrm{C}}^{\circ})\exp\left(-\frac{z}{z_{\circ}}\right), \tag{2.4}$$

where $z_{\circ}$ defines the width of the profile. The value of z at the interface is zero as shown in Figure 2.3.

The value of $z_{\circ}$ is calculated from the mass balance of a single ferrite grain growing in an infinitely large austenite grain. The mass balance can be represented as

$$V_{\alpha}(x_{\mathrm{C}}^{\circ} - x_{\mathrm{C}}^{\alpha\gamma}) = \int_0^{\infty} A(z)(x_{\mathrm{C}}^{\gamma} - x_{\mathrm{C}}^{\circ})\mathrm{d}z, \tag{2.5}$$

where V_{α} is the volume of the ferrite grain, $A(z)$ is the surface area of the grain at position z.

$z_{\circ}$ is then given by

$$z_{\circ} = \frac{V_{\alpha}}{\Omega A_{\alpha}}\left(\frac{x_{\mathrm{C}}^{\circ} - x_{\mathrm{C}}^{\alpha\gamma}}{x_{\mathrm{C}}^{\gamma} - x_{\mathrm{C}}^{\circ}}\right), \tag{2.6}$$

where A_{α} is the area of the ferrite grain and Ω is a factor dependent on the radius of the ferrite particle (r_{α}). Ω can be calculated as

$$\Omega_{1D} = 1,$$

$$\Omega_{2D} = 1 + \frac{z_{\circ}}{r_{\alpha}},$$

and

$$\Omega_{3D} = 1 + 2\frac{z_{\circ}}{r_{\alpha}} + 2\left(\frac{z_{\circ}}{r_{\alpha}}\right)^2$$

for one-, two- and three-dimensional systems respectively. Two-dimensional systems

include rod like geometries and three-dimensional systems include spherical geometries.

A quadratic equation for the interface concentration is obtained by equating the rate of partitioning at the interface (determined by the interface velocity as given in Equation 2.1) and the diffusion flux (determined by Fick's law written as $J = -\delta x_{\mathrm{C}}/\delta z$) and combining it with equation 2.6.

$$x_{\mathrm{C}}^{\gamma} = \frac{Z x_{\mathrm{C}}^{\circ} + \Delta x_{\mathrm{C}}^{\circ} x_{\mathrm{C}}^{\alpha+\gamma} + \left[(Z x_{\mathrm{C}}^{\circ} + \Delta x_{\mathrm{C}}^{\circ} x_{\mathrm{C}}^{\alpha+\gamma})^2 - (Z + 2\Delta x_{\mathrm{C}}^{\circ})(Z (x_{\mathrm{C}}^{\circ})^2 + 2\Delta x_{\mathrm{C}}^{\circ} x_{\mathrm{C}}^{\alpha\gamma} x_{\mathrm{C}}^{\gamma\alpha}) \right]^{\frac{1}{2}}}{Z + 2\Delta x_{\mathrm{C}}^{\circ}}, \tag{2.7}$$

where $\Delta x_{\mathrm{C}}^{\circ} = x_{\mathrm{C}}^{\circ} - x_{\mathrm{C}}^{\alpha\gamma}$, $x_{\mathrm{C}}^{\alpha+\gamma} = x_{\mathrm{C}}^{\alpha\gamma} + x_{\mathrm{C}}^{\gamma\alpha}$ and

$$Z = 2\Omega \frac{D}{M\chi} \frac{A_{\alpha}}{V_{\alpha}}.$$

x_{C}^{γ} is solved in an iterative manner over equations 2.6 and 2.7 because of the dependency of Ω on z_o. Generally, the solution converges in less than ten iterations.

In order to describe the nature of the transformation, mode parameter, S, is defined as

$$S = \frac{x_{\mathrm{C}}^{\gamma\alpha} - x_{\mathrm{C}}^{\gamma}}{x_{\mathrm{C}}^{\gamma\alpha} - x_{\mathrm{C}}^{\circ}}. \tag{2.8}$$

The mode parameter varies from zero for completely diffusion controlled transformations to unity for completely interface controlled transformations.

As the ferrite grains grow, they start to approach each other and their surrounding concentration profiles start to overlap. This effect, termed as soft-impingement, is accounted for by a mean-field approximation. If the carbon would redistribute completely in the austenite, then the homogeneous carbon concentration, $x_{\mathrm{C}}^{\gamma,h}$, will be given by

$$x_{\mathrm{C}}^{\gamma,h} = \frac{x_{\mathrm{C}}^{\circ} - f_{\alpha} x_{\mathrm{C}}^{\alpha\gamma}}{1 - f_{\alpha}}, \tag{2.9}$$

where f_{α} is the transformed ferrite fraction.

Then, the corrected interface carbon concentration, x_{C}^{*}, is calculated as

$$x_{\mathrm{C}}^{*} = x_{\mathrm{C}}^{\gamma\alpha} - S\left(x_{\mathrm{C}}^{\gamma\alpha} - x_{\mathrm{C}}^{\gamma,h} \right). \tag{2.10}$$

This concentration is then used to calculate the driving force and subsequently the interface velocity. This soft-impingement correction is termed as 'mode factor soft-impingement'.

An alternative soft-impingement correction was proposed by Van Bohemen et al. [2011]. In this 'fraction soft-impingement' approach, the corrected interface carbon con-

centration is calculated as

$$x_{\mathrm{C}}^{*} = x_{\mathrm{C}}^{\gamma} + \frac{f_{\alpha}}{f_{\alpha}^{eq}}(x_{\mathrm{C}}^{\gamma\alpha} - x_{\mathrm{C}}^{\gamma}), \tag{2.11}$$

where f_{α} is the volume fraction of ferrite formed at a given time and f_{α}^{eq} is the equilibrium volume fraction of ferrite calculated using the lever rule in the Fe-C phase diagram.

2.4 Cellular Automata Model

A three dimensional cellular automata (CA) model was developed by Bos et al. [2010] in order to study the microstructural evolution during the annealing of dual phase steels. The model addresses ferrite recrystallisation, pearlite- or ferrite-to-austenite and austenite-to-ferrite transformations.

The CA model considers a discretized volume consisting of a grid of cubic cells of dimension, δ, with periodic boundary conditions. At a given time, t, each cell is associated with its growth length (l_{cell}^{i}) and the grain to which it belongs. The grain to which a cell belongs helps in identifying the 'grain boundary cells' and the transformation equations are applied to these cells alone. The growth length of the cell is calculated at each time step (Δt) by Euler time integration of the grain-boundary velocity given (v_{cell}^{i}) by

$$l_{\mathrm{cell}}^{i}(t + \Delta t) = l_{\mathrm{cell}}^{i}(t) + v_{\mathrm{cell}}^{i}\Delta t. \tag{2.12}$$

When the growth length of a particular cell (l_{cell}^{i}) reaches a value equal to the grid spacing (δ), the nearest neighbour cells are transformed into cells of the concerned grain i. Subsequently, when the growth length (l_{cell}^{i}) exceeds the value of the length of the face diagonal ($\delta\sqrt{2}$) and the body diagonal of a cubic cell ($\delta\sqrt{3}$), the next-nearest neighbour and the last neighbour cells are respectively transformed. A cell ceases to be a grain boundary cell when all its neighbour cells have been transformed. During the cases when more than one cell grows into a shared neighbour cell, the cell which reaches the critical length early determines which grain the shared neighbour cell transforms to. Also, a hierarchy in the transformation, based on the required driving force, decides the preference of a transformation over another. For example, an austenite-to-ferrite transformation is ranked higher than a recrystallisation process. The maximum allowed time step (Δt) depends on the criterion

$$\Delta t < \left(\sqrt{3} - \sqrt{2}\right)\frac{\delta}{v}. \tag{2.13}$$

Grains are formed by a collection of cells and have their own set of properties, namely: the collection of cells that belong to them, phase of the grain (ferrite, austenite or pearlite), strain energy, average carbon concentration and carbon concentration at

the interface. For each grain, the grain-boundary velocity is calculated as

$$v = M\Delta G, \tag{2.14}$$

where M is the interface mobility and ΔG is the driving force for transformation.

The driving force for transformation is calculated using the Thermo-calc® database. In a multi-component system, the driving force for the formation of a new phase from the parent phase is given by

$$\Delta G = \sum_{i=1}^{N} x_i^n \left(\mu_i^p - \mu_i^n\right), \tag{2.15}$$

where N is the number of components in the system, x_i^n is the concentration of the element i in the new phase, μ_i^p and μ_i^n are the chemical potentials of the parent and new phase respectively.

Different submodels are employed for defining the various metallurgical transformations, each with its own nucleation and growth modules. The austenite-to-ferrite transformation submodel is explained here.

The nucleation of ferrite from austenite is explained in terms of a continuous nucleation description. The nucleation rate, based on the classical nucleation theory was formulated by Bos et al. [2011] as

$$\frac{dN}{dt} = K\frac{k_B T}{h}\exp\left(-\frac{Q_d}{k_B T}\right)\exp\left(-\frac{L}{k_B T(T_{\mathrm{Ae3}} - T)^2}\right), \tag{2.16}$$

where K is a nucleation pre-exponential constant, k_B is the Boltzmann constant, h is the Planck constant, Q_d is the activation energy for Fe self-diffusion(in case of steel) and T_{Ae3} is the temperature at which austenite starts to decompose to ferrite.

The factor L in Equation 2.16 can be considered as an 'effective activation energy for nucleation' and is given as

$$L = \frac{\Psi}{\chi^2}, \tag{2.17}$$

where Ψ is a factor that takes into account the shape of the nucleus and the interfacial energies and χ is a proportionality constant between the driving force for nucleation (Δg_v) and undercooling (ΔT) such that $\Delta g_v = \chi \Delta T$.

Once the nucleation rate is calculated using Equation 2.16, the nucleation behaviour is interpreted by the model by considering the probability of nucleation taking place at a specific site during a time interval (Δt). The probability (P_N) is given by

$$P_N = \Delta t \frac{\mathrm{d}N}{\mathrm{d}t}. \tag{2.18}$$

At each time step, for every available potential nucleation site, the probability P_N

is evaluated. This is then compared with a random number R, which is obtained from a uniform distribution. If $R < P_N$, then the potential ferrite nucleation site becomes an active ferrite nucleus.

Once nucleated, the growth of the nucleus (and later, the ferrite grain) is described in terms of the semi analytical mixed mode model described in Section 2.3.1.

In this chapter, the basic thermodynamic and computational principles used for describing the austenite-to-ferrite transformation for a Fe-C alloy was explained. Addition of a substitutional alloying element, like Mn or Cr, influences the thermodynamic conditions at the interface. This will be explained in Chapter 3.

Chapter 3

Equilibrium at the Interface

This chapter focusses on the importance of defining the conditions at the moving austenite-ferrite interface in order to effectively and efficiently describe the transformation behaviour. In this chapter, the fundamental tools for determining the equilibrium conditions in a ternary system are explained. This is followed by a description of two widely used equilibrium conditions, namely the Local Equilibrium with Negligible Partitioning (LENP) and Para Equilibrium (PE). Then, an overview of various approaches which describe the kinetic transition between the two above mentioned equilibrium conditions is given. Finally, a summary of the proposed 'Gradual Transition Approach' is given.

3.1 Equilibrium Conditions at the Interface

In binary Fe-C alloys, the equilibrium between ferrite and austenite is well-defined for a given alloy composition, temperature and pressure. For a diffusion controlled transformation occurring under atmospheric pressure, the interfacial conditions at the moving γ/α interface at a given temperature can be obtained from the equilibrium phase diagram as shown in Figure 3.1. The figure shows the equilibrium carbon concentration in austenite and ferrite for a steel with bulk carbon concentration B at a certain temperature. Under such conditions, the chemical potential of Fe and C is the same in austenite and ferrite at the interface and there exists no driving force for interface migration.

However, in the mixed-mode approach, the finite interface mobility will affect the interfacial composition of the austenite and ferrite phases and a lower velocity of the interface is observed. In contrast to the diffusion controlled transformation, the interfacial condition is a variable. The interfacial carbon concentration of austenite increases continuously from the bulk (x_{C}°) to the equilibrium value ($x_{\mathrm{C}}^{\gamma\alpha}$) as the transformation proceeds. (Mecozzi [2007])

Most industrially relevant steels generally contain a few substitutional alloying elements, such as Mn, Ni, Cr, Si, Al, in addition to the interstitial element carbon. The

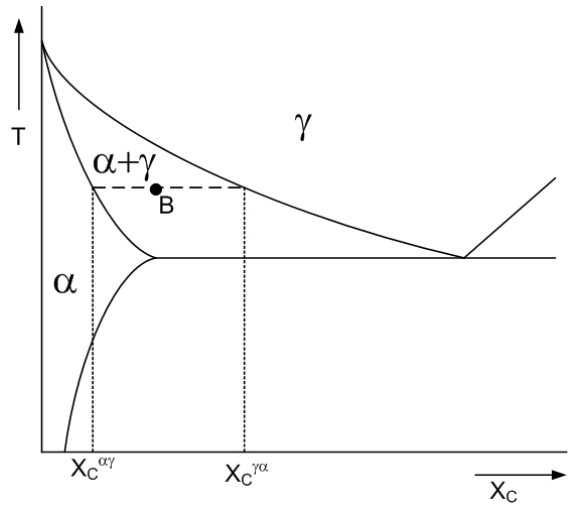

Figure 3.1: Schematic representation of the equilibrium carbon concentration of ferrite and austenite at a given temperature in a binary system

addition of an alloying element increases the number of variables in the system. In general, three concepts are widely used to describe the equilibrium condition at the interface in such systems. They are termed as, 'Local Equilibrium', 'Local Equilibrium with Negligible Partitioning' and 'Para Equilibrium'. These equilibrium conditions differ from each other in the way in which the substitutional alloying elements are considered. This gives rise to the construction of different tie-lines according to the equilibrium.

In a ternary system, the equilibrium between two phases can be identified by the help of a plane which is tangential to the free energy surfaces of both the phases. A line which describes the equilibrium concentration in this common tangential plane is called a tie-line. It is represented in an isothermal section of the equilibrium phase diagram, as shown in Figure 3.2. The figure is plotted between the carbon concentration and the substitutional element concentration at a given temperature. The dashed lines in the figure represent possible tie-lines.

The influence of substitutional alloying element is mainly attributed to the difference in diffusivities between the substitutional and interstitial alloying elements at the temperature of interest. Thus, a tie-line passing through the bulk alloy composition does not simultaneously satisfy the mass balances for both alloying elements at the interface. In addition to the difference in diffusivity, the solubilities of the alloying elements in the parent and product phases also plays an important role. This gives rise to the possibilities of partitioned and un-partitioned product formation. Partitioning refers to the redistribution of substitutional solute over distances much larger than the interfacial region and thus, involves long-range diffusion. (Inden and Hutchinson [2003], Inden [2003], Hillert and Agren [2004], Hutchinson et al. [2004])

Two of the equilibrium conditions, namely 'Local Equilibrium with Negligible Parti-

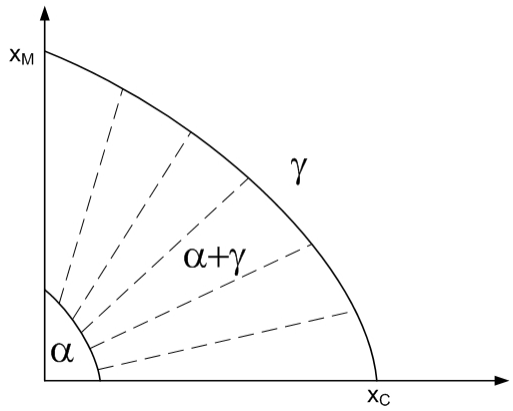

Figure 3.2: Schematic representation of tie-lines in an isothermal section of a ternary phase diagram

tioning' and 'Para Equilibrium' are explained here.

3.1.1 Local Equilibrium with Negligible Partitioning

Local equilibrium with negligible partitioning (LENP) constitutes the equilibrium at higher undercoolings where it is thermodynamically possible for ferrite to grow without bulk redistribution of the substitutional element. Local equilibrium, referred to as the equality of chemical potentials of the species across the interface, of carbon and substitutional element is maintained at all times. Mathematically, it can be expressed as

$$\mu_C^\gamma = \mu_C^\alpha \tag{3.1}$$

$$\mu_X^\gamma = \mu_X^\alpha, \tag{3.2}$$

where μ_C^γ and μ_C^α refers to the chemical potential of carbon in austenite and ferrite respectively and μ_X^γ and μ_X^α refers to the chemical potential of substitutional element in austenite and ferrite respectively.

In the compositional domain where LENP is valid, the carbon chemical potential in austenite at the interface is higher than in the bulk. This accounts for the driving force required to transport carbon released from ferrite away from the interface, thereby leading to ferrite growth. Even though no long range diffusion of the substitutional element takes place, a short range diffusion is required to maintain equilibrium and is seen as a 'spike' in the front of the moving interface. The 'spike' can be visualised as a pointed concentration profile in a one-dimensional system. In a three-dimensional system, this refers to a curved plane of negligible thickness located at the austenite side of the interface. (Chen and van der Zwaag [2012])

A schematic of a LENP operating tie-line in a Fe-C-Mn alloy is shown in Figure 3.3. For an alloy of bulk composition B, the concentration of austenite and ferrite

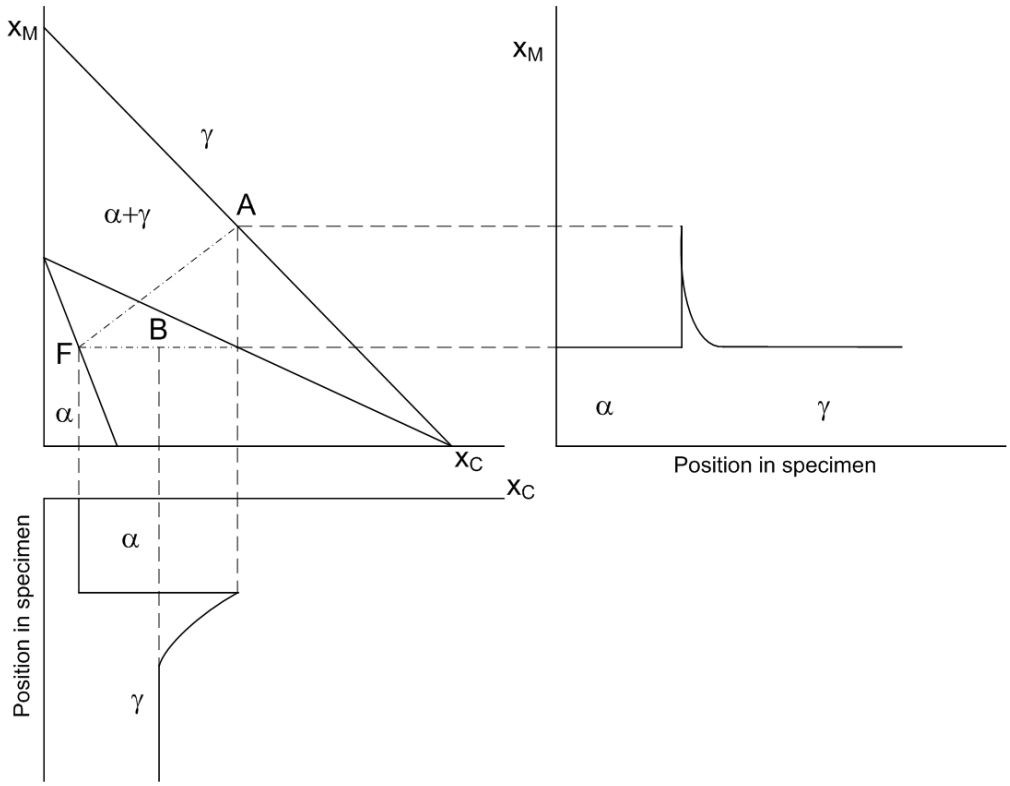

Figure 3.3: C and Mn concentration profiles in α and γ in a Fe-C-Mn system under LENP condition (van der Ven and Delaey [1996])

in equilibrium with each other, under LENP conditions, will be given by A and F respectively. This is represented by the tie-line AF. The growing ferrite phase has the same Mn concentration as the bulk austenite phase. The 'spike' in the Mn concentration profile in austenite can be noted. (van der Ven and Delaey [1996])

3.1.2 Para Equilibrium

Para equilibrium (PE) represents a constrained equilibrium wherein local equilibrium of carbon is established across the interface and the substitutional elements are assumed to be undisturbed by the passage of the interface. This suggests that the substitutional atoms are immobile compared to the interface velocity and therefore, the equilibrium with respect to these elements cannot be attained across the interface. It is defined by three conditions at the interface, namely

1. Equal ratio of alloying elements to iron on both sides

2. Equal chemical potential of carbon on both sides

3. Equal chemical potential of weighted average of iron and alloying elements

Mathematically, it can be expressed as

$$\mu_{\mathrm{C}}^{\gamma} = \mu_{\mathrm{C}}^{\alpha} \tag{3.3}$$

$$U_{\mathrm{X}} \cdot (\mu_{\mathrm{X}}^{\gamma} - \mu_{\mathrm{X}}^{\alpha}) = -U_{\mathrm{Fe}} \cdot (\mu_{\mathrm{Fe}}^{\gamma} - \mu_{\mathrm{Fe}}^{\alpha}), \tag{3.4}$$

where U_i refers to the site fraction of element i defined as $\dfrac{x_i^{\circ}}{x_X^{\circ} + x_{Fe}^{\circ}}$.

The driving force for the transformation is assumed to be governed entirely by the carbon diffusion. The PE interface conditions and transformation kinetics can be obtained by solving the diffusion equations for carbon in both ferrite and austenite, together with the mass balance for carbon at the interface and the above PE conditions. The tie-lines, thus obtained, are parallel to the carbon axis and no alloying element 'spike' exists. (Zurob et al. [2012], Hutchinson et al. [2004])

Physically, this can be observed as the formation of ferrite with the same concentration of the substitutional alloying element as the bulk austenite. This is shown in Figure 3.4. The line AF is the tie-line under PE conditions for an alloy of given bulk composition B. It can be noted that there exists no concentration profile with respect to the substitutional element. However, a carbon concentration profile in austenite does exist.

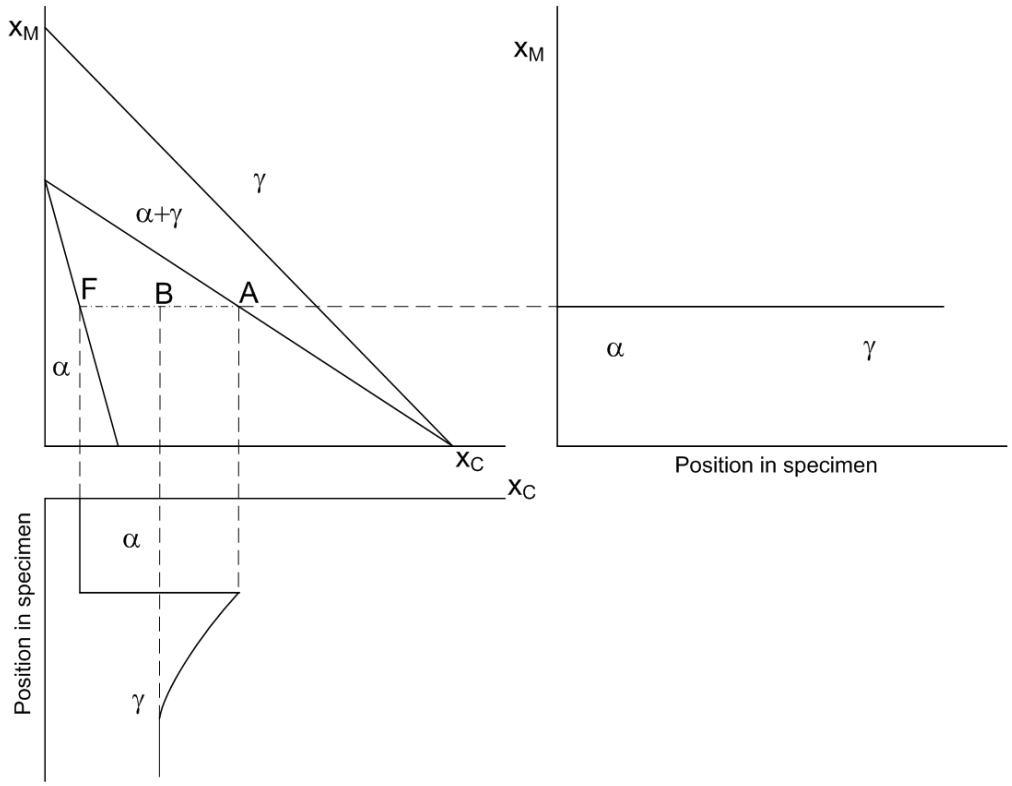

Figure 3.4: C and Mn concentration profiles in α and γ in a Fe-C-Mn system under PE condition (Capdevila et al. [2011])

3.2 PE-LENP Transition Models

The interaction of the alloying elements with the moving austenite-ferrite interface could be dealt using two approaches, namely the solute drag and the kinetic transition. Solute drag refers to the dragging of the solute atoms along with the moving interface. The amount of free energy dissipation due to the drag is consumed from the driving force for transformation. This leads to slowing down of the interface velocity. In the second approach, the slowing down of the transformation is explained by the transition from PE to LENP equilibrium condition. This is termed as 'kinetic transition'. Considering an initial period of growth by PE, a number of instances have been reported wherein the experimental ferrite fraction at the end of the transformation is found to be much lower than that predicted by the PE limit. The transition from PE to LENP helps in accounting for this slower growth at the end of the transformation. (Zurob et al. [2008], Hutchinson et al. [2004])

In general, the LENP and PE equilibrium conditions are the limiting cases and intermediate states are, in principle, possible. Thus, the transition can be explained either with or without the presence of intermediate states, i.e. the transition being sharp or gradual in nature. A number of approaches have been used to model this transition by considering a diffusion controlled transformation. An overview of various approaches is given.

3.2.1 Maximum Penetration Distance Approach

A few approaches to define the transition are based on the maximum penetration distance of the substitutional alloying element ahead of the interface, as introduced by Bradley and Aaronson [1981].

It is stated that, some amount of volume diffusion of the substitutional element in austenite ahead of the moving interface is necessary to maintain the interface boundary in full equilibrium or in LENP condition. The penetration distance should be greater than the austenite lattice parameter. This, in turn, acts as a necessary condition for local equilibrium to exist. The maximum penetration distance (l_{max}) is given by

$$l_{\max} = \frac{2D_X^{\gamma} t^{1/2}}{\alpha}, \tag{3.5}$$

where D_X^{γ} is the diffusivity of the substitutional alloying element (X) in austenite, t is the growth time and α is the growth rate constant (in $\mathrm{ms}^{-1/2}$). The half-thickness, r, of a growing ferrite particle is explained in terms of the rate constant as $r = \alpha\sqrt{t}$.

In the following approaches, a criterion for the kinetic transition is obtained as a function of the maximum penetration distance.

Enomoto [2006] defined a P-factor equal to the maximum penetration distance of

the substitutional alloying element as

$$P = \frac{D_X^\gamma}{v} = \frac{2D_X^\gamma t^{1/2}}{\alpha}, \tag{3.6}$$

where v is the interface velocity. PE condition was assumed to be maintained for spike width in the order of a few atomic distance and LENP condition for spike width greater than ten times the atomic spacing.

A similar criteria had been proposed much earlier by Coates [1972], wherein PE condition is considered to be valid when the P-factor is comparable to the interface thickness, i.e. $\Delta S < 10$ Å and local equilibrium when $\Delta S > 50$ Å.

Capdevila et al. [2011] considered grain boundary diffusion of the substitutional alloying element in the definition of the P-factor.

$$P = \frac{{}^{GB}D_{\mathrm{Mn}}^\gamma}{v} = 2n\frac{D_{\mathrm{Mn}}^\gamma t^{1/2}}{\alpha}, \tag{3.7}$$

where ${}^{GB}D_{\mathrm{Mn}}^\gamma$ is the austenite grain boundary diffusivity for Mn, which is determined as n times the bulk diffusivity (D_{Mn}^γ).

PE condition is initially assumed at the interface. The difference in chemical potentials of Mn and Fe is assumed to cause an unbalanced flux of Mn to flow across the interface, which, in turn, builds up a spike. It was also considered that the width of the Mn spike increases faster when the velocity of the interface becomes lower compared to Mn diffusivity i.e. cross-interfacial jumps become more efficient. The transition is assumed to occur when the interface velocity is low enough to allow some Mn diffusion ahead of the interface. In other words, the P-factor achieves a certain threshold value. However, it is also suggested that in reality the Mn spike develops progressively and thus, an abrupt transition cannot be considered. The critical value of P-factor was chosen such that the resulting ferrite transformation curve forms a good fit with the experimental data set.

Capdevila et al. [2011] carried out isothermal studies on a Fe-0.37C-1.8Mn (wt.%) steel at 973 K (700 °C). A coarse prior austenite grain size of 76 μm at 1523 K (1250 °C) is used in order to avoid a large influence of the nucleation process on the transformation behaviour. The transformation model described nucleation according to the classical nucleation theory and growth was assumed to be diffusion controlled. The soft impingement correction is based on the volume fraction of ferrite formed. The simulated and experimental fraction curves are given in Figure 3.5. A critical P-factor of 1.62×10^{-10} m was used.

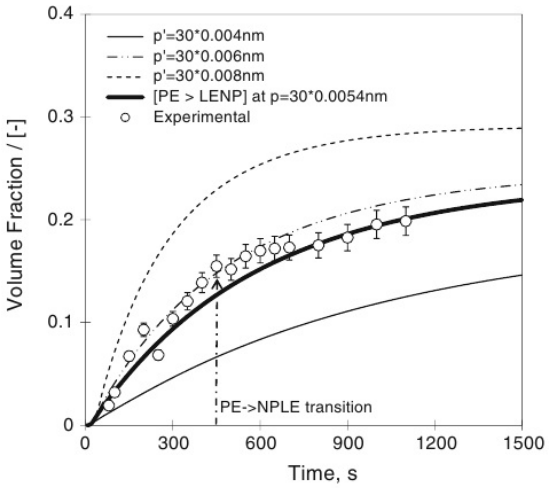

Figure 3.5: Postulated PE-LENP transition on the basis of good fitting to experimental dataset (Capdevila et al. [2011])

3.2.2 Alloying Element Concentration Approach

In the following approaches, the nature of the transformation is expressed on the basis of the chemical condition of the substitutional element in the interface or the spike. This includes the substitutional alloying element content or its concentration profile.

Mn Concentration in the Spike

The presence of kinetic states intermediate to those defined by the LENP and PE conditions was experimentally observed by Zurob et al. [2008]. Isothermal decarburisation studies were carried out on a Fe-0.57C-0.94Mn (wt.%) steel and the ferrite layer thickness as a function of time and temperature was studied. Stable intermediate states were observed in the temperature range of 775 to 825 °C. However, LENP conditions were found to be operational in the lower temperature range of 725 to 775 °C and PE conditions in the higher temperatures between 825 °C and $T_\circ$ as shown in Figure 3.6.

The proposed model considered the segregation of solute towards the interface to be different in nature from the building up of the spike in austenite. The spike represents the thermodynamic properties of the bulk phases and the segregation is the result of the binding energy between the interface and solute atoms. The transformation is described as a result of a 'two-jump' process to transfer the solute across the interface. The building up of the spike is affected by the relative values $^\circ\Delta G^{\text{trans}}$ and $^\circ\Delta G^{\text{seg}}$. The difference in chemical potential between the two phases is represented as $^\circ\Delta G^{\text{trans}}$. The contribution of the segregation energy to the definition of chemical potential at the interface is represented as $^\circ\Delta G^{\text{seg}}$. A relatively large $^\circ\Delta G^{\text{trans}}$ promotes the building up of spike while a larger $^\circ\Delta G^{\text{seg}}$ prevents the spike build up. Large values of $^\circ\Delta G^{\text{seg}}$

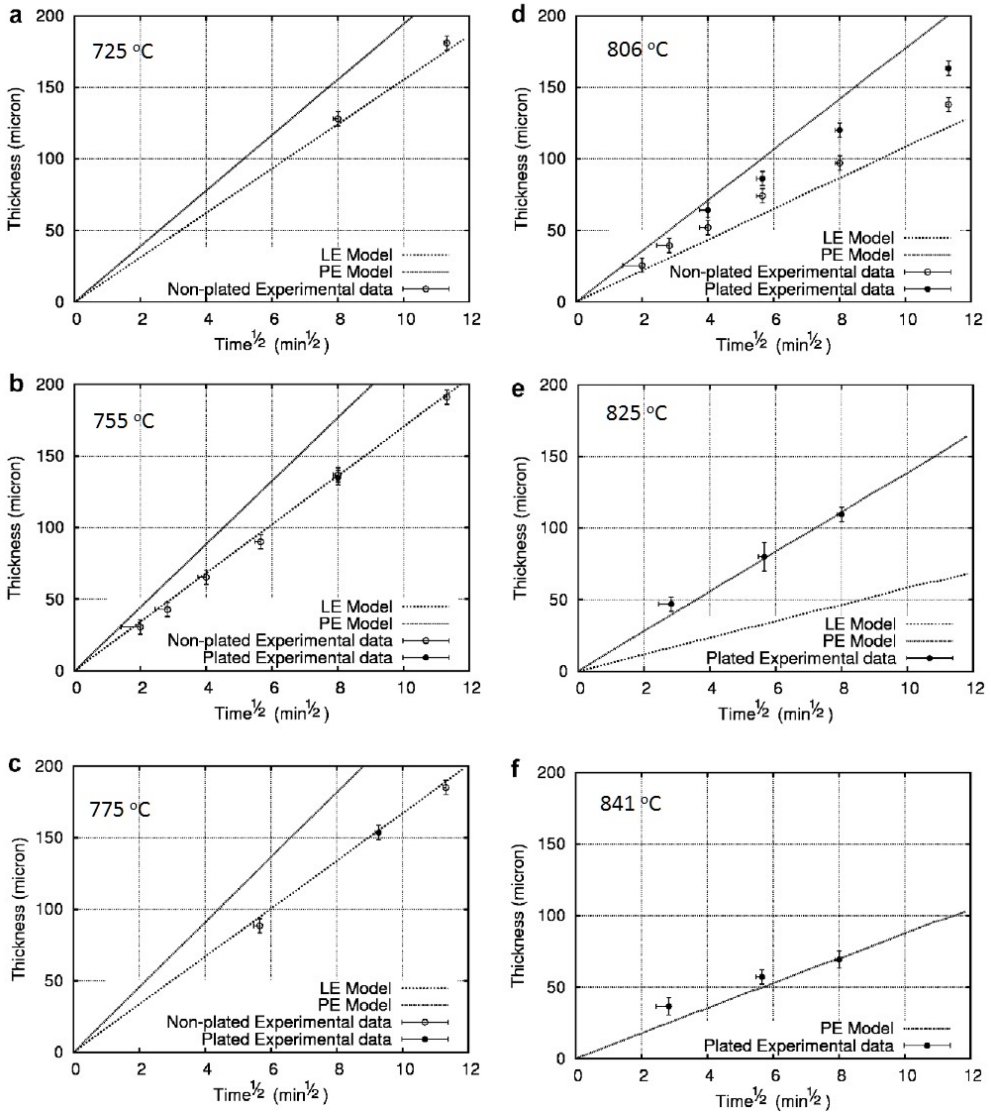

Figure 3.6: Isothermal growth kinetics of ferrite at various temperatures (a)725 °C (b)755 °C (c)775 °C (d)806 °C (e)825 °C (f)841 °C (Zurob et al. [2008])

and $^{\circ}\Delta G^{\text{trans}}$ are expected occur at higher and lower temperatures respectively. The transformation is studied by obtaining the concentration profile across the interface with time.

The transition is specified in terms of the normalised Mn concentration in the spike, which is defined as

$$x_{\text{Mn}}^{norm} = \frac{x_{\text{Mn}}^{i/\gamma}}{x_{\text{Mn}}^{\circ}}, \tag{3.8}$$

where $x_{\text{Mn}}^{i/\gamma}$ is the Mn concentration in the austenite side of the interface and x_{Mn}° is the bulk Mn concentration.

Assuming that ferrite grows under PE in the initial stages and that the interface

velocity reduces continuously, a certain value of P-factor is reached when the normalised Mn concentration in the spike reaches 1.05. This point is considered to indicate the deviation from PE condition and thus, the beginning of building up of the spike. This, however, does not specify a criterion when the spike is fully formed. For the same driving force for Mn diffusion across the interface, segregation at the interface will increase the range of velocities where PE can exist.

The value of P-factor is found to be dependent on temperature and varies between 0.041 nm at 725 °C and 0.071 nm at 825 °C. The diffusivity of Mn across the interface is considered for the calculations.

Alloying Element Capacity of the Interface

Zurob et al. [2009] further developed the above mentioned model by considering the interface as a separate phase. In order to describe the flux of Mn from ferrite to interface, the equation by Hutchinson et al. [2004] was used. An additional term describing the maximum Mn capacity of the interface was introduced. The flux equation can be written as

$$J_{\mathrm{Mn}}^{\alpha\to I} = \underbrace{\left(\frac{x_{\mathrm{Mn}}^{b}\cdot M_{\mathrm{Mn}}^{\mathrm{trans-int}}}{V_m}\cdot\frac{\mu_{\mathrm{Mn}}^{I}-\mu_{\mathrm{Mn}}^{\alpha}}{\delta}\right)}_{\mathrm{I}}\underbrace{\left(1-\exp\left(\frac{-D_{\mathrm{Mn}}^{\mathrm{trans-int}}}{v\delta}\right)\right)}_{\mathrm{II}}\underbrace{\left(1-\frac{x_{\mathrm{Mn}}^{I}}{x_{\mathrm{Mn}}^{*}}\right)}_{\mathrm{III}}, \tag{3.9}$$

where x_{Mn}^{b} is the bulk Mn concentration, x_{Mn}^{I} is the Mn concentration within the interface, $(\mu_{\mathrm{Mn}}^{I}-\mu_{\mathrm{Mn}}^{\alpha})$ is the chemical potential difference between interface and ferrite, δ is the thickness of the interface (taken as 1 nm), V_m is the molar volume, and $M_{\mathrm{Mn}}^{\mathrm{trans-int}}$ and $D_{\mathrm{Mn}}^{\mathrm{trans-int}}$ are trans-interface mobility and diffusivity of Mn respectively. x_{Mn}^{*} is the interface capacity for Mn and is chosen so as to obtain a good agreement with the experimental results. It is defined as

$$x_{\mathrm{Mn}}^{*} = 205\cdot x_{\mathrm{Mn}}^{b}\cdot x_{\mathrm{Mn}}^{\gamma\alpha}, \tag{3.10}$$

where $x_{\mathrm{Mn}}^{\gamma\alpha}$ is the Mn concentration in the austenite side of the interface.

The first term in the equation is a measure of the driving force for the transfer of Mn atoms from ferrite to the interface. The second term describes the 'efficiency of Mn jump', which depends on the ratio of the residence time of the moving interface (δ/v) to the diffusion time across the interface $(\delta^2/D_{\mathrm{Mn}})$.

The third term in the equation defines the maximum Mn capacity of the moving interface. It acts in a way such that the flux of Mn from ferrite to the interface goes to zero when the interface Mn concentration reaches the maximum Mn capacity. It, therefore, makes it possible to cap the accumulation of Mn inside the interface even in the presence of a thermodynamic driving force for accumulation. The interface capacity

capacity for Mn, x^*_{Mn}, decreases with increase in temperature, leading to partial or no spike development at higher temperatures.

3.2.3 Mixed Equilibrium Approach

Thibaux [2006] proposed a mixed equilibrium approach which accommodates both the LENP and PE equilibrium conditions. The equilibrium conditions are differentiated by the dissipation of energy in the spike, such that the dissipation can vary from zero to the LENP value. The maximum dissipation in the spike is calculated as

$$\zeta^{\mathrm{Max}} = G^{\gamma\alpha}_{\mathrm{LENP}} - G^{\alpha\gamma}_{\mathrm{LENP}} + (x^{\gamma\alpha}_{\mathrm{C,LENP}} - x^{\alpha\gamma}_{\mathrm{C,LENP}}) \cdot (\mu^{\gamma\alpha}_{\mathrm{Fe,LENP}} - \mu^{\alpha\gamma}_{\mathrm{C,LENP}}), \tag{3.11}$$

where ζ is the dissipation in the spike, G is the free energy and μ is the chemical potential. The dissipation in the spike is schematically shown in Figure 3.7.

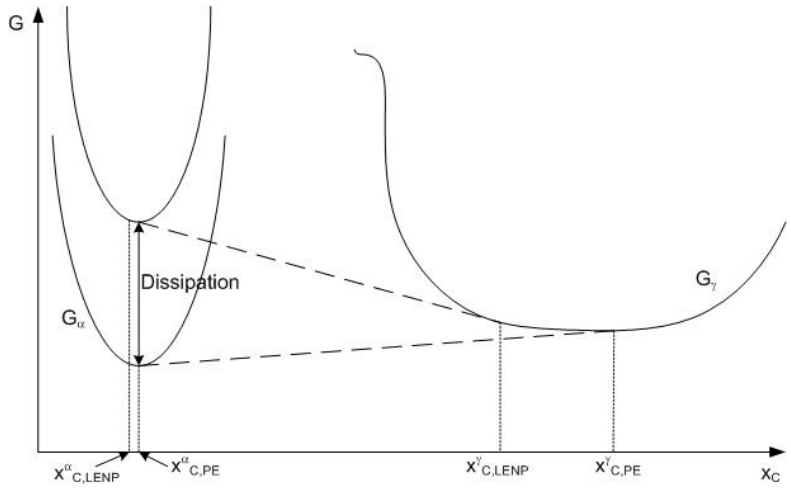

Figure 3.7: Calculation of maximum dissipation of energy in the spike (Thibaux [2006])

The dissipation in the mixed condition is calculated as

$$\zeta = \frac{L \cdot \zeta^{\mathrm{LENP}}}{L + \frac{v}{V_m} \cdot \frac{\zeta^{\mathrm{LENP}}}{(\Delta\mu)^2}}, \tag{3.12}$$

where the transition from PE to LENP is a function of L_{int} and the interface velocity (v). The condition tends towards PE at higher velocities and LENP at lower velocities. Considering grain boundary diffusion, L is expressed as

$$L = \lambda_t \frac{D^{\mathrm{GB,fcc}}_{\mathrm{Ni}}}{a} \cdot \frac{dx_{\mathrm{C}}}{d\mu}. \tag{3.13}$$

L varies from zero in LENP to infinity in PE.

The value of λ_t is chosen in order to obtain a good fit with the experimental data.

The transformation kinetics described using the mixed condition for a Fe-0.0715C-2.76Ni (wt.%) steel with a λ_t of 100 is given in Figure 3.8. The dashed and dotted lines represent the transformation under complete PE and LENP conditions. The mixed equilibrium is represented by the solid line. It can be noted that the mixed condition provides a better description of the transformation kinetics than either PE or LENP.

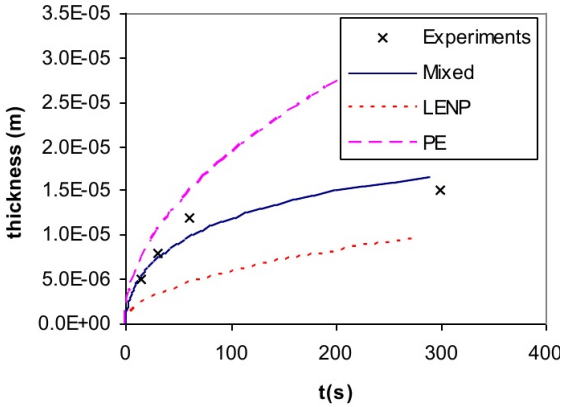

Figure 3.8: Transformation behaviour using mixed equilibrium conditions (Thibaux [2006])

3.3 Proposed Transition Approach

All the transition approaches described in the previous section are applied for explaining the transition during a diffusion controlled transformation. The present work is an attempt to incorporate the same in a mixed mode model.

In the present work, the PE-LENP transition is modelled on the basis of the concept of P-factor described by Capdevila et al. [2011] and the mixed equilibrium approach by Thibaux [2006]. The transition between the two equilibrium conditions is gradual in nature. It is assumed that in the austenite to ferrite transformation, the nucleation and initial growth takes place under PE condition. The growth of ferrite is associated with a decrease in interface velocity. It is proposed that the alloying element spike starts to build-up when a certain interface velocity is reached and is completely built-up at a much lower interface velocity. The system is in a mixed equilibrium between these values. The limits for transition are explained in terms of the P-factor. This approach is, hereby, named as 'Gradual Transition Approach'.

3.4 Specific Objectives

The principles of the semi analytical mixed mode model was discussed in Chapter 2. It is a computationally inexpensive method to study phase transformations in comparison

to the fully numerical model. However, a critical assessment of its validity in comparison to the fully numerical model has not been carried out previously.

The interaction of the solute with the interface can be described by means of a transition from PE to LENP equilibrium condition. Various approaches to describe this transition have been documented for diffusion controlled transformations. However, no attempt has been made to incorporate the same in a mixed mode transformation definition.

Based on the previous works carried out, the following specific objectives are defined for this work:

- Implement the fully numerical and semi analytical mixed mode models in MATLAB® and study the validity of the semi analytical model
- Mathematically formulate the gradual transition approach
- Implement the transition in the MATLAB® models and study the transition characteristics
- Implement the transition in the CA model and test its validity by studying the transformation kinetics of a dual phase steel under different thermal conditions

Chapter 4

Experimental Study

In this chapter, the details of various alloys and experimental techniques used in this work are given. Various experimental studies were carried out to obtain the necessary data in order to validate the model in terms of microstructure and transformation kinetics. The experimental techniques are explained on the basis of their underlying principles and the results obtained from them.

4.1 Alloy Compositions

This work focusses on the microstructure and kinetics of phase transformation of a dual phase steel. The concerned experimental studies were carried out on a ferritic-martensitic dual phase steel, DP600, with a chemical composition as given in Table 4.1. The material was obtained from Tata Steel, IJmuiden.

C	Mn	Si	Cr	Fe
0.090	1.630	0.250	0.550	remaining

Table 4.1: Chemical composition of DP600 in wt.%

The other alloy used in the work was a hypo-eutectoid plain carbon steel, A36. The composition of the alloy is given in Table 4.2. This alloy was chosen owing to the availability of reliable data in literature. This grade was extensively researched by Militzer et al. [1996].

C	Mn	Si	Cr	P	S	Cu	Ni	Al	Fe
0.17	0.74	0.012	0.019	0.009	0.008	0.016	0.01	0.04	remaining

Table 4.2: Chemical composition of A36 in wt.% (Militzer et al. [1996])

4.2 Dilatometry

A dilatometer is used to measure the length changes in a sample occurring as a result of phase transformation during a certain heat treatment cycle. The length change is associated with the change in specific volume of the material due to the change in lattice structure. For example, in steel, when austenite transforms to ferrite during cooling, the volume expansion is in the order of 1.6 %. This is because of the transformation from a more closely packed FCC to a less closely packed BCC structure. The expansion or contraction of the sample, during heating or cooling respectively in case of steel, is assumed to be isotropic for all practical purposes. (Kop [2000])

The austenite-to-ferrite transformation in DP600 was studied during isothermal annealing after austenization treatment. The sample was cooled at a rate of 40 °C/s to the required temperature after austenizing at 950 °C for 3 minutes. The isothermal transformation at 625, 650 and 700 °C for 1000 seconds was recorded. In order to study the prior austenite grain size in DP600, a completely martensitic microstructure was created by quenching the sample to room temperature after austenization. It was, then, tempered at 500 °C for 5 minutes.

The temperature programs are shown in Figure 4.1. The samples used were 10 mm in length and 2 mm thick. A thermocouple was spot welded on to the sample, which was then clamped between two push rods. The schematic of the dilatometry experimental setup is given in Figure 4.2. The change in length of the sample is measured by a linear variable differential transformer (LVDT).

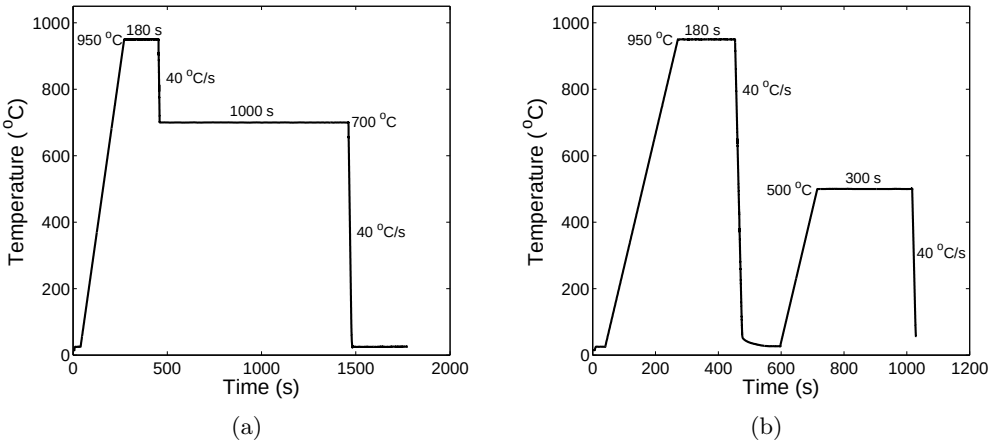

(a) (b)

Figure 4.1: Temperature programs used in the dilatometry experiments for studying (a) isothermal transformation and (b) prior austenite microstructure determination

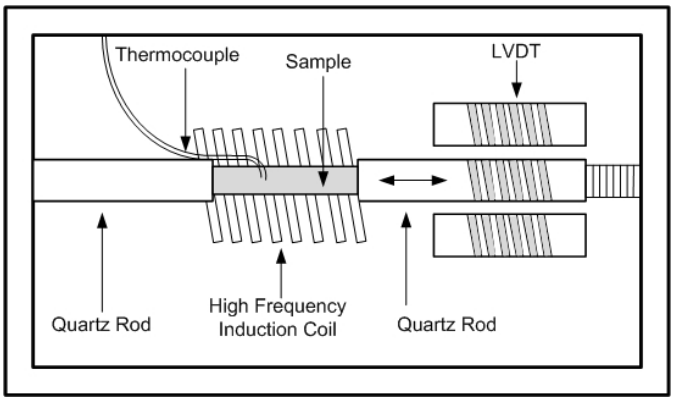

Figure 4.2: Schematic of the dilatometry experimental setup (Kop [2000])

4.3 Ferrite Fraction Curves

The ferrite fraction curves were obtained from the dilatation data using the lever-rule method. (Van Bohemen) In this method, the remaining austenite fraction is interpolated as a function of temperature considering the linear expansion between a temperature where no transformation occurs and the required temperature. Proportionality is assumed between the decomposed ferrite fraction and the observed length change. The fraction transformed is then determined as

$$\phi = \frac{\Delta L - \Delta L_e^{\gamma}}{\Delta L_e^{\alpha} - \Delta L_e^{\gamma}}, \tag{4.1}$$

where ΔL is the measured dilatation and ΔL_e^{γ} and ΔL_e^{α} are the extrapolated dilatation in the high-temperature and low-temperature range respectively as shown in Figure 4.3.

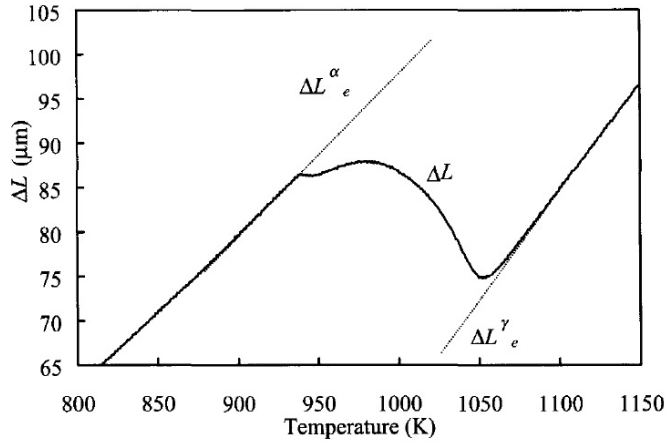

Figure 4.3: Lever-rule method for calculating the ferrite fraction (Kop [2000])

This, however, gives the total transformed fraction, which is sum of the ferrite and pearlite formed.

Generally, the lever-rule method is used for single, non-partitioning phase transformations. In case of the austenite-to-ferrite transformations, this method is not advisable due to two reasons, namely

1. Enrichment of carbon in austenite due to the limited solubility in ferrite, thereby leading to increase in specific volume of austenite
2. Difference in the nature of volume change during the formation of ferrite and pearlite from austenite

However, it was reported by Kop [2000], that the relative error and absolute error in the determination of the ferrite fraction between the lever-rule method and a method considering the above to factors is in the order of 0.2 and 0.06 respectively for a steel containing about 0.4 at.% carbon. It is, thus, assumed that owing to the low carbon content of the alloy, the error between them is not significant and the lever-rule method can be used.

The dilatation data obtained from the dilatometric experiments are given in Figure 4.4. The dilatation plot at higher temperature of 700 °C shown in the figure, shows the presence of a transformation taking place during cooling after the isothermal holding period, as indicated by the change in the slope of the line. This is marked by an arrow in the figure. This, however, is absent in the lower temperatures of 625 and 650 °C. Thus, at these temperatures, the austenite completely transforms to ferrite and pearlite during the isothermal holding. The pearlitic transformation is assumed to start when the obtained transformed fraction from the dilatation curve equals the ferrite fraction obtained from optical micrographs.

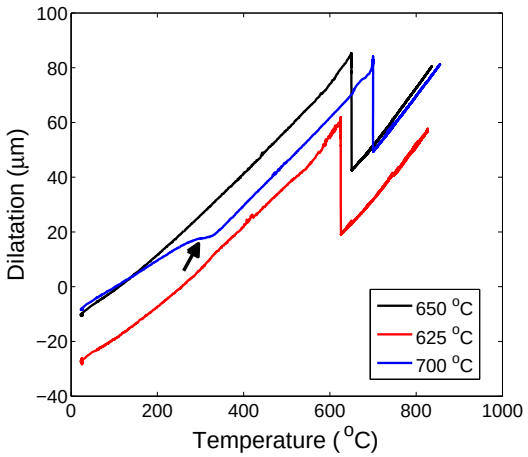

Figure 4.4: Variation of dilatation length with temperature in DP600

The ferrite fraction obtained from optical micrographs is shown in Table 4.3. The ferrite fraction was calculated from five different micrographs for each isothermal holding temperature.

Sample	700 °C	650 °C	625 °C
1	0.750	0.872	0.882
2	0.749	0.884	0.883
3	0.728	0.866	0.888
4	0.758	0.881	0.887
5	0.732	0.858	0.870
Average	0.743	0.872	0.882

Table 4.3: Ferrite fraction obtained from optical microscopy for various isothermal transformation temperatures in DP600

The transformed fraction curves obtained from dilatometry using the lever-rule method are given in Figure 4.5. Figure 4.5a shows the complete transformation curves and Figure 4.5b shows only the region of ferrite transformation. The curves are plotted from a temperature of 1100 K (826.85 °C). The oscillation observed in the plots of 625 °C can be attributed to experimental errors.

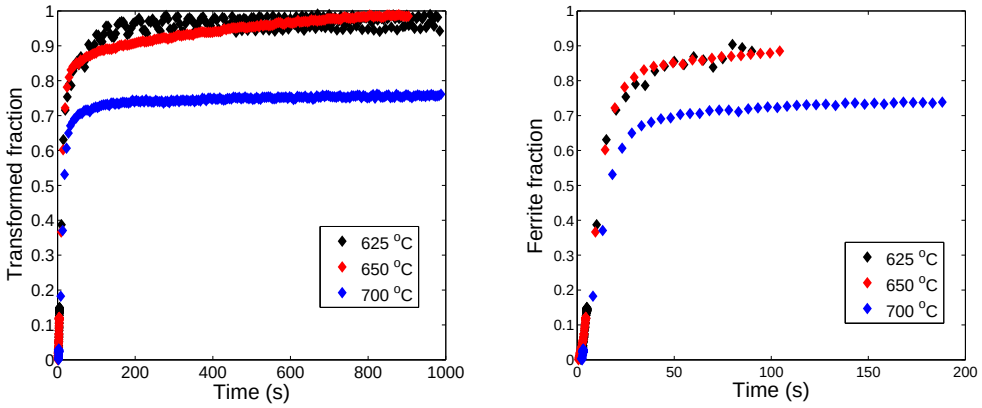

(a) (b)

Figure 4.5: (a) Transformation curves and (b) Ferrite fraction curves obtained from dilatometry for DP600 at various temperatures

4.4 Optical Microscopy

Metallographic studies were performed on DP600 in order to obtain the microstructure after ferrite transformation. A microstructure consisting of ferrite and pearlite is expected at the end of the heat treatment cycle.

The austenite microstructure obtained after the heat treating cycle in Figure 4.1b is shown in Figure 4.6. The completely martensitic sample obtained was etched with saturated picral solution. The initial austenite size was measured manually by intersecting-lines method. The number averaged austenite grain size was found to be 11.5 μm. The

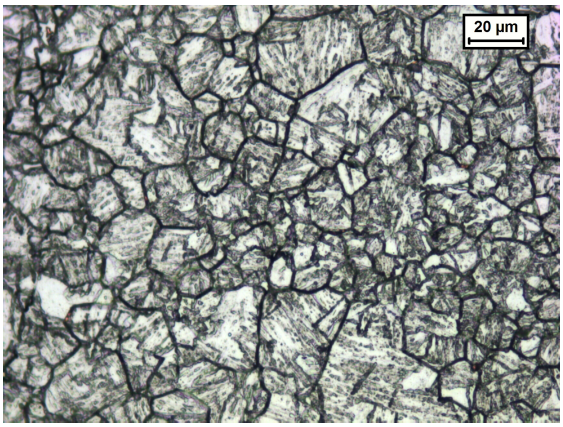

Figure 4.6: Austenite microstructure obtained after etching with saturation picral solution at a magnification of 500x

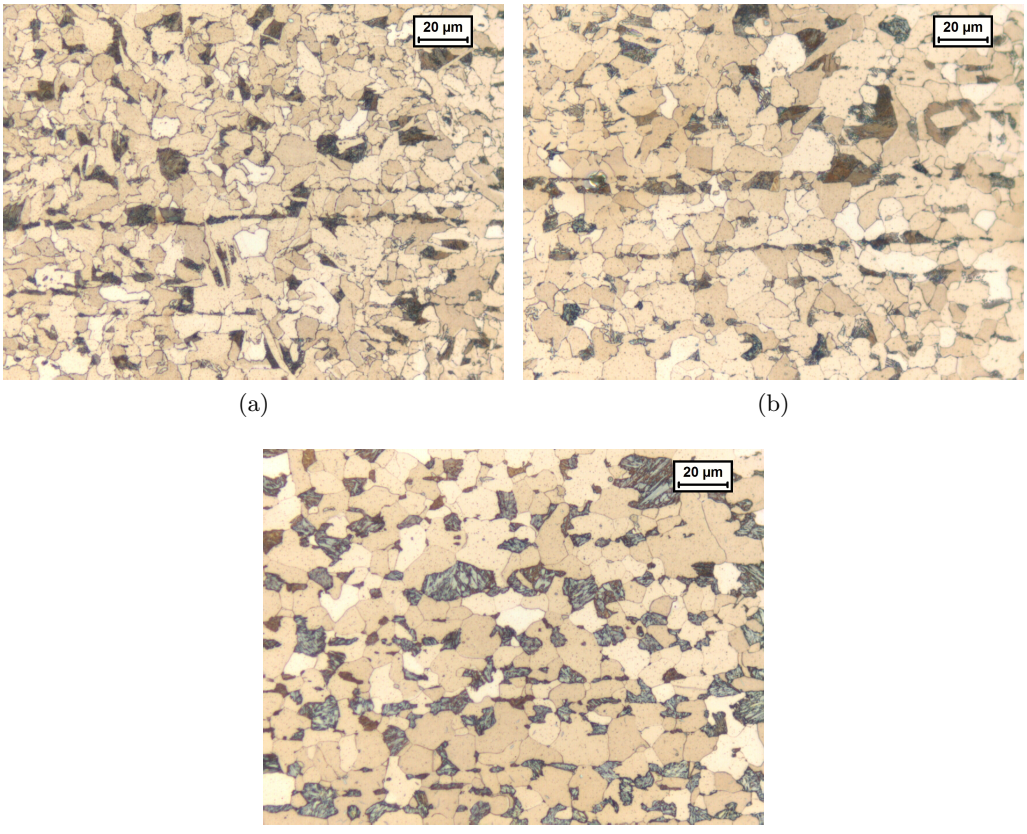

(a) (b)

(c)

Figure 4.7: Final microstructures obtained after isothermal transformation at (a) 625 °C (b) 650 °C (c) 700 °C obtained after etching with SMB solution at a magnification of 500x

final microstructures obtained after isothermal transformation are given in Figure 4.7. The ferrite (brown) and pearlite (grey) phases can be noted. These samples were etched

using sodium metabisulfite (SMB) solution. The number averaged ferrite grain size was measured to be 8.7, 6.5 and 5.2 μm for holding temperatures of 700, 650 and 625 °C respectively. An increase in the grain size and amount of banding in the microstructure with increase in temperature can be noted.

Chapter 5

Implementation and Validation

This chapter explains the principles involved in the implementation of the fully numerical and semi analytical models, described in Chapter 2, to describe the formation of ferrite from austenite. Both models were implemented in MATLAB®. The fully numerical model implemented in MATLAB® was first compared with the original fully numerical model used by Bos and Sietsma [2007]. It was, then, used to benchmark the semi analytical model. The semi analytical model was thoroughly analysed for its validity in a range of conditions in order to determine its range of application. It was previously observed that the fraction curves obtained using the cellular automata model does not match with the experimental curves. (Pattabhiraman [2012]) Thus, the validation of the semi analytical model was carried out to ascertain that this difference is not due to the simplification of the carbon profile in this model.

5.1 Model Implementation

The fully numerical model is a computationally expensive method to describe the austenite-to-ferrite transformation. The semi analytical model is a computationally faster alternative proposed by Bos and Sietsma [2007]. Both models were implemented in MATLAB® in order to verify the suitability of the semi analytical model on a common computational platform.

5.1.1 Fully Numerical Model

In the fully numerical model, the transformation behaviour is explained by taking into account both the carbon diffusion and the interface movement. The diffusion of carbon in the austenite is uniquely described for each grid point by solving the concerned diffusion equation. The fully numerical model MATLAB® is based on the mixed mode model by Bos and Sietsma [2007].

The interface velocity is calculated as described in Equation 2.1. The diffusion of carbon in austenite is given by Fick's law and can be written as

$$\frac{\partial x_{\mathrm{C}}}{\partial t} = D_C^{\gamma} \frac{\partial^2 x_{\mathrm{C}}}{\partial y^2}, \tag{5.1}$$

where D_C^{γ} is the diffusion coefficient of carbon in austenite and x_{C} is the carbon concentration calculated in the y direction.

In terms of one-dimensional finite difference method based on equidistant grids, the above equation for a given grid point i at time j can be written as

$$\frac{\partial x^i_{\mathrm{C},j}}{\partial t} = D_C^{\gamma} \frac{x^{i-1}_{\mathrm{C},j} - 2C^i_j + x^{i+1}_{\mathrm{C},j}}{\Delta y^2}, \tag{5.2}$$

where Δy is the grid spacing.

It is assumed that the ferrite is formed with the equilibrium carbon concentration at each time step and that the carbon is distributed homogeneously through the ferrite. It is a reasonable assumption owing to the fact that the diffusivity of carbon in ferrite is about three orders of magnitude larger than that in austenite.

Equation 5.2 gives the change in concentration profile due to diffusion of carbon in austenite for a stationary interface. In order to describe a moving interface, the position and concentration of each grid point must be corrected. This is performed by the Murray-Landis method. (Murray and Landis [1959]) The equation is then written as

$$\frac{\partial x^i_{\mathrm{C},j}}{\partial t} = D_C^{\gamma} \left(\frac{x^{i-1}_{\mathrm{C},j} - 2x^i_{\mathrm{C},j} + x^{i+1}_{\mathrm{C},j}}{\Delta y^2} \right) + v \frac{N-i}{E-\epsilon^i_j} \left(\frac{x^{i+1}_{\mathrm{C},j} - x^{i-1}_{\mathrm{C},j}}{2} \right), \tag{5.3}$$

where N is the total number of grid points, E is the system size, ϵ^i_j is the position of grid point i at time j.

For a three-dimensional description, a finite spherical system representing the growth of a ferrite grain from the centre to the periphery is considered. A schematic of such a system is shown in Figure 5.1. The equation for this system can be written as

$$\frac{\partial x^i_{\mathrm{C},j}}{\partial t} = D_C^{\gamma} \left[\left(\frac{x^{i-1}_{\mathrm{C},j} - 2x^i_{\mathrm{C},j} + x^{i+1}_{\mathrm{C},j}}{\Delta y^2} \right) + \left(\frac{2}{r^i_j} . \frac{x^{i+1}_{\mathrm{C},j} - x^{i-1}_{\mathrm{C},j}}{2\Delta y} \right) \right] + v \frac{N-i}{E-\epsilon^i_j} \left(\frac{x^{i+1}_{\mathrm{C},j} - x^{i-1}_{\mathrm{C},j}}{2} \right), \tag{5.4}$$

where r^i_j is the radius of the i^{th} grid point at time j.

The concentration of each grid point is then obtained by Euler implicit time integration as

$$x^i_{\mathrm{C},j+1} = x^i_{\mathrm{C},j} + \Delta t \frac{\partial x^i_{\mathrm{C},j+1}}{\partial t}. \tag{5.5}$$

Considering

$$\frac{\partial x_{\mathrm{C},j+1}}{\partial t} = \mathbf{A} \ . \ \mathbf{X}_{\mathrm{C},j+1}, \tag{5.6}$$

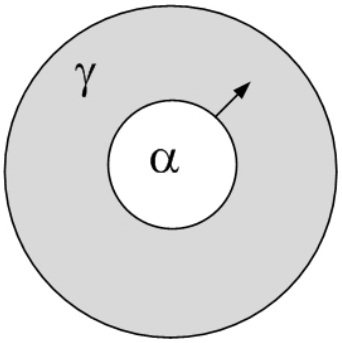

Figure 5.1: Schematic of spherical geometry used in the simulations

where $\mathbf{A}$ is a matrix containing the non-concentration terms in the equation and $\mathbf{X}_{\mathrm{C}}$ is a column matrix containing the concentration terms.

The Euler integration can then be re-written as

$$\mathbf{X}_{\mathrm{C},j+1} = \left(\mathbf{I} - \Delta t.\mathbf{A}\right)^{-1} \mathbf{X}_{\mathrm{C},j}, \tag{5.7}$$

where I is an identity matrix.

This approach is different from that of the original fully numerical method by Bos and Sietsma [2007]. In the later, the diffusion and the grid shift were accommodated in two separate steps. The diffusion step according to Fick's law was performed first and subsequently, the carbon concentration at each grid point was modified due to grid shift. The change in carbon concentration was calculated as

$$x_{\mathrm{C},j}^{i,\mathrm{new}} = x_{\mathrm{C},j}^{i,\mathrm{old}} + \left(\frac{\epsilon_j^i - \epsilon_{j-1}^i}{\epsilon_{j-1}^{i+1} - \epsilon_{j-1}^i}\right)\left(x_{\mathrm{C},j}^{i+1,\mathrm{old}} - x_{\mathrm{C},j}^{i,\mathrm{old}}\right), \tag{5.8}$$

where the superscripts old and new refer to the carbon concentration before and after the grid shift correction. Also, the original method used the Euler explicit method for time integration.

The interface carbon concentration is calculated by carbon mass balance calculations, i.e. the total carbon in the system remains constant. The amount of carbon in the austenite is calculated as the difference between the total carbon content and the amount of carbon in ferrite as

$$\mathrm{C}_j^{\gamma} = \mathrm{C}^{\mathrm{total}} - \mathrm{C}_j^{\alpha}, \tag{5.9}$$

where $\mathrm{C}^{\mathrm{total}}$ is the total carbon content of the system and C_j^{α} and C_j^{γ} are the amount of carbon in ferrite and austenite respectively.

The interface carbon concentration is then calculated as the difference between the amount of carbon in austenite and the carbon present in austenite except the interface

grid point. For a three-dimensional system, it can be written as

$$x^{\gamma}_{C,j} = \frac{\mathrm{C}^{\gamma}_{j} - \mathrm{C}^{\gamma,\mathrm{rest}}_{j}}{0.5 \cdot V_{int}} - x^{a+1}_{C,j}, \tag{5.10}$$

where $\mathrm{C}^{\gamma,\mathrm{rest}}_{j}$ is the amount of carbon in the austenite except the interface, V_{int} is the volume of the interface and a is the position of the interface (in terms of grid points).

The mobility (in molm/Js) is calculated using the following equation (Bos and Sietsma [2007])

$$M = M_{\circ} \times \exp\left(\frac{-140 \times 10^{3}\,\mathrm{KJ/mol}}{\mathrm{RT}}\right), \tag{5.11}$$

where M_o is the mobility pre exponential factor and R is the gas constant.

The diffusion coefficients for carbon in ferrite and austenite (in m^2/s) are calculated as (Murch [2001])

$$D^{\alpha}_{\mathrm{C}} = \left(2 \times 10^{-6}\,\mathrm{m}^2/\mathrm{s}\right) \times \exp\left(\frac{-8.414 \times 10^{4}\,\mathrm{KJ/mol}}{\mathrm{RT}}\right) \tag{5.12}$$

and

$$D^{\gamma}_{\mathrm{C}} = \left(1.5 \times 10^{-5}\,\mathrm{m}^2/\mathrm{s}\right) \times \exp\left(\frac{-1.42 \times 10^{5}\,\mathrm{KJ/mol}}{\mathrm{RT}}\right). \tag{5.13}$$

Grid and Time Independency Study

A number of simulations were carried out in order to identify a reasonable grid size and time step size for the given system. The simulation details are given in Table 5.1. The sets of various grid size and time step size was compared in terms of their final ferrite fraction. Though an implicit method was used, care was taken to select a stable grid and time step size given by

$$\frac{D^{\gamma}_{\mathrm{C}} \times \Delta t}{\Delta y^2} \leq 0.5. \tag{5.14}$$

Parameter	Value
Material	DP600 (Table 4.1)
Equilibrium condition	LENP
Temperature	950 K (676.85 °C)
Time	5 s
$\mathrm{M}_{\circ}$	0.2 molm/Js
System size	10 μm
Geometry	3-D spherical

Table 5.1: Simulation details for grid and time independency studies

The various time steps and grid sizes used are given in Table 5.2. The corresponding final ferrite fraction is plotted in Figure 5.2. In Figure 5.2a, each line represents a

Time step size (s)	Number of grid points		
	Austenite	Ferrite	Total
0.1	90	10	100
0.01	180	20	200
0.001	270	30	300
0.0001	360	40	400
	450	50	500

Table 5.2: Details of time step sizes and grids used

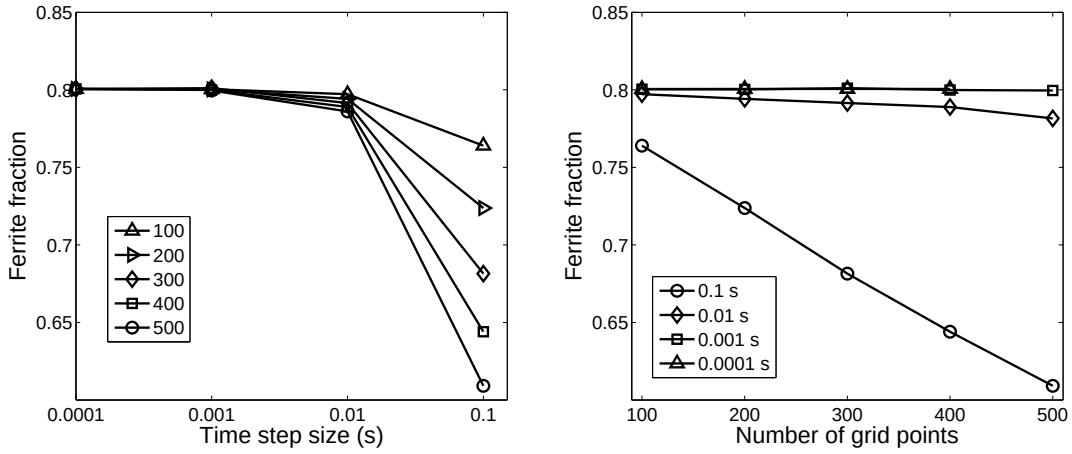

(a) (b)

Figure 5.2: Effect of time step size and grid size on final ferrite fraction

different grid size and in Figure 5.2b, a different time step size. For larger time step sizes, a large scatter in the results can be observed. Also, it is observed that the final ferrite fraction decreases with increase in the number of grid points. This behaviour is in contrast with the universal observation of higher accuracy with larger number of grid points.

According to Equation 5.14, a smaller time step size has to be used for a smaller grid size (i.e. larger number of grid points) in order to obtain a stable system. The maximum time step size that can be used with various grid sizes is given in Table 5.3. It is, thus, noted that certain time step sizes used in the simulations (0.01 and 0.1 s) are larger than the calculated stable sizes. This could be the reason behind the larger deviation of the final ferrite fraction at these time step sizes. Also, the deviation of the time step size used in the simulations from the stable size is larger for smaller grid sizes. This explains the decrease in final ferrite fraction with decreasing grid sizes. Thus, for obtaining a stable system, a time step size less than 0.01 s needs to be used.

The time taken for simulation at different time step and grid sizes is given in Figure 5.3. It can be noted that the time taken for simulation increases with decrease in grid

Grid points	Δy (m)	Δt (s)
100	1.0×10^{-7}	0.033
200	5.0×10^{-8}	0.008
300	3.3×10^{-8}	0.003
400	2.5×10^{-8}	0.002
500	2.0×10^{-8}	0.001

Table 5.3: Stable time step size for different grid sizes

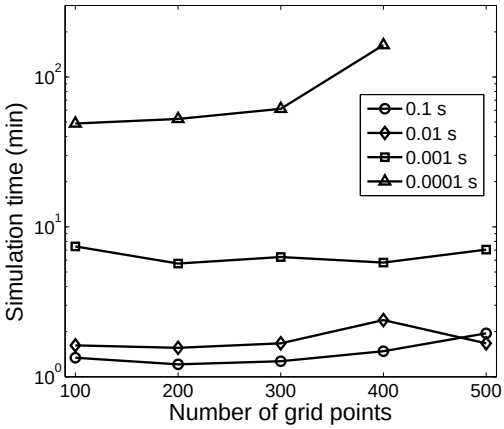

Figure 5.3: Time taken for simulation as a function of grid size and time step size

size and time step size. From Figure 5.2, it can be noted that the final ferrite fraction is not affected by the number of grid points for a time step size lower than 0.01 s. Thus, considering the computational time required, a system of 200 grid points with a time step size of 0.001 s was chosen for further simulations.

5.1.2 Semi Analytical Model

The semi analytical model, including both soft-impingement corrections, as explained in Section 2.3.1 is implemented in MATLAB®. The model is implemented with adaptive time stepping which uses the 'ode45' differential equation solver to calculate the ferrite radius as a function of time. The initial ferrite radius at the start of the transformation is known. This solver uses a variable step size 'Runge-Kutta' method to numerically solve differential equations.

Variable step size or adaptive time stepping works through a feedback loop. At each time step, the error in the result of the previous time step is calculated. It is then decided if this calculated error is acceptable and the time step size is modified accordingly. This enables the model to take larger time steps whenever possible, i.e. improves the accuracy of the solution while maintaining the efficiency as much as possible. In this case, however, the maximum time step size was fixed at 0.001 s in order to maintain consistency between

the semi analytical and fully numerical models.

5.2 Model Validation

The model implemented in MATLAB® was first benchmarked with the original fully numerical model by Bos and Sietsma [2007] in order to assess its accuracy. It was then used as the basis to validate the semi analytical model.

5.2.1 Fully Numerical Model

The two fully numerical models were compared on the basis of rate of ferrite formation. The simulations were carried out for DP600 under PE conditions at a temperature of 800 K (526.85 °C) with a system size of 10 μm. A system of 200 austenite grid points and 10 ferrite grid points was used for the simulation in one-dimensional system. For the three-dimensional simulations, a system of 256 austenite grid points with no ferrite grid point was used. The ferrite fraction curves obtained from both models were compared and are shown in Figure 5.4

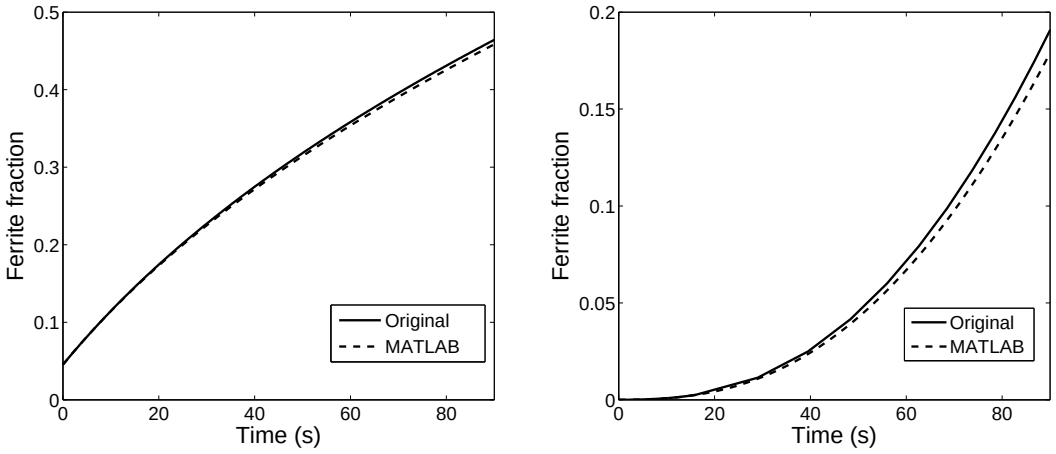

(a) (b)

Figure 5.4: Comparison between the two fully numerical models for (a) one dimensional and (b) three dimensional systems

It can be noted that both the models agree quite well throughout the entire time range in the one-dimensional system and for smaller times in the three-dimensional system. The variation in the three-dimensional system at larger times can be attributed to the difference in the robustness of the models owing to the nature of the time integration and grid shift correction.

5.2.2 Semi Analytical Model

The model was compared with the fully numerical model in order to assess its range of validity in terms of temperature, mobility, diffusivity and system size. The simulation conditions are listed in Table 5.4. The simulations were carried out for DP600 under the PE equilibrium condition except when the effect of alloy composition was studied. In the fully numerical model, a grid of 198 austenite and 2 ferrite grid points was used. However, no initial ferrite fraction was considered in the semi analytical simulations. As the initial ferrite fraction in the fully numerical model for a three-dimensional system (8.12×10^{-6}) is quite small, it can be considered to not affect the results to a large extent.

Dimension (-)	System size (μm)	Temper--ature (K)	Mobility pre-factor (molm/Js)	Diffusion pre-factor (m^2/s)	Alloy
1	5	800	0.02	1.5×10^{-4}	A36
3	10	850	0.05	1.5×10^{-5}	DP600
	15	900	0.1	1.5×10^{-6}	
		950	0.2		
		1000	0.5		

Table 5.4: Simulation conditions for the validation of the semi analytical model

Effect of Dimension

In order to compare the two models in one- and three- dimensional systems, the simulations were carried out at an intermediate value of temperature (900 K) and mobility pre-factor (0.1 molm/Js). The resulting ferrite radii was compared as shown in Figure 5.5. The dashed lines in the figure represent the semi analytical model and the solid lines represent the fully numerical model. It was observed that the deviation between the models in both cases increases towards the end of the transformation. However, it should be noted that the semi analytical model predicts a faster transformation in case of the three dimensional system, whereas it predicts a slower transformation in case of the one dimensional system.

It can also be noted that the ferrite radius increases at a faster rate in the three dimensional system. This is because of the availability of a larger amount of space for the carbon to diffuse in to, which causes a faster reduction in the interface carbon concentration and thus, a higher driving force. All the subsequent simulations in this section were carried out for a three-dimensional system.

Effect of System Size

The two models were compared on the basis of the ferrite fraction curves obtained by using various system sizes for a range of mobilities at a constant temperature (900 K).

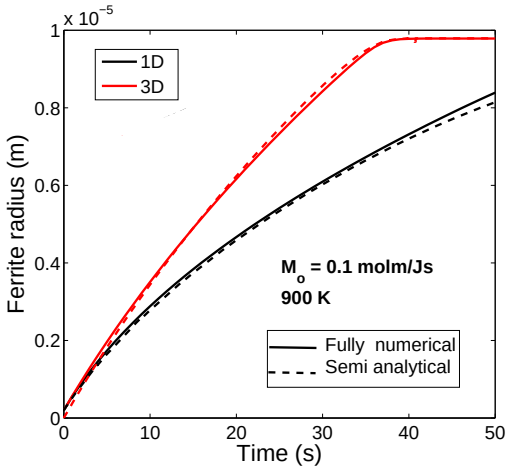

Figure 5.5: Comparison between the fully numerical and semi analytical models in one and three dimensional systems for DP600

The comparison of the models can be seen in Figure 5.6. It can be noted that, for a constant value of mobility, the difference between the semi analytical and fully numerical models for different system sizes is similar in nature. i.e. for all system sizes, the fraction curves obtained using the semi analytical model is similar to the fully numerical model at lower mobilities, and is faster at higher mobilities.

Effect of Temperature

The effect of temperature was studied by comparing the fraction curves obtained using the fully numerical and semi analytical models at constant mobility and system size (10 μm). The comparison is shown in Figure 5.7. It can be noted that a clear trend with regard to the effect of temperature is absent. However, the ferrite transformation using the semi analytical model is found to be slower at lower mobilities at lower temperature, whereas it is faster at all mobilities at higher temperature.

Effect of Mobility

The effect of mobility on the accuracy of the semi analytical model can be seen in Figure 5.8. The simulations were carried out for various temperatures at constant system size (10 μm). It can be seen that with an increase in the value of the mobility pre-exponential factor, the semi analytical model predicts a much faster transformation than the fully numerical model. At lower temperatures and mobility pre-exponential factor values, the semi analytical model predicts a slower transformation than the fully numerical model.

A higher mobility pre-exponential factor represents a faster interface movement, i.e. the interface movement becomes easier compared to the diffusion of carbon in austenite. Thus, the transformation becomes more diffusion controlled, i.e. the diffusion is the rate

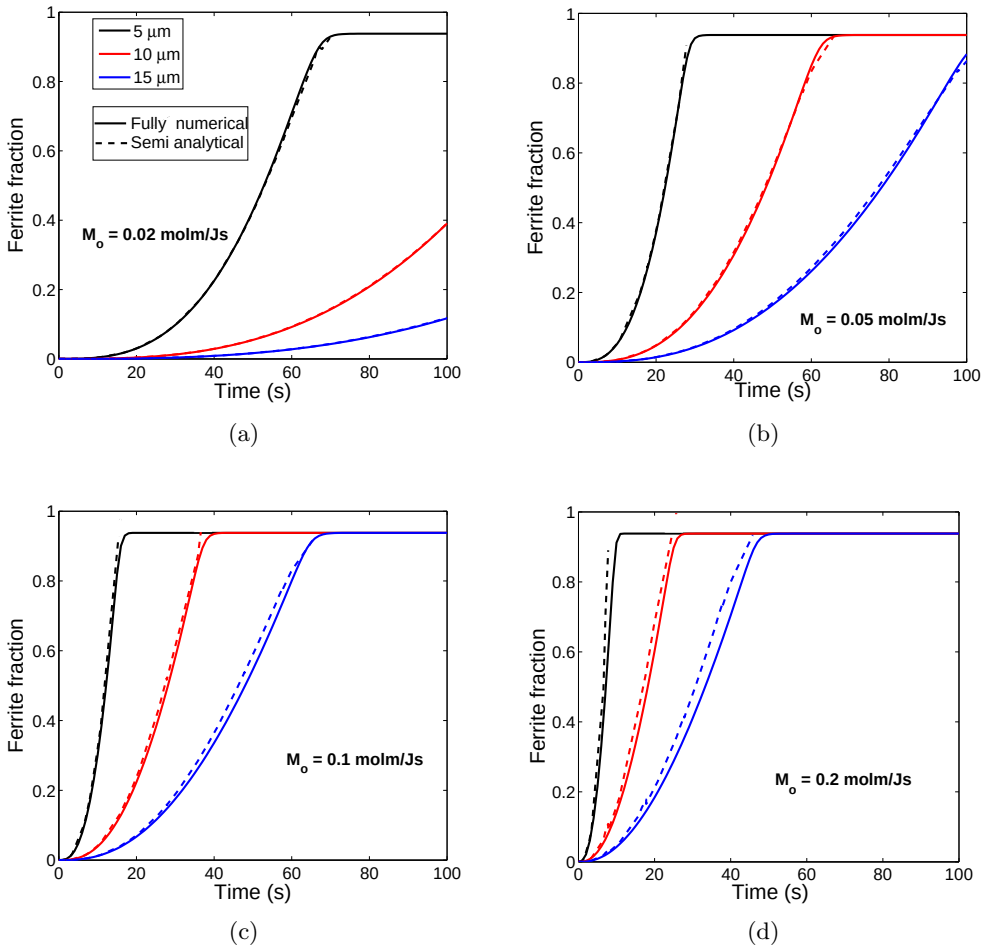

Figure 5.6: Comparison of fraction curves between the fully numerical and semi analytical models at various values of $M_\circ$ (a) 0.02 (b) 0.05 (c) 0.1 (d) 0.2 molm/Js for different system sizes for DP600

limiting event. It can be hypothesised that the semi analytical model starts to deviate to a larger extent from the fully numerical model in more diffusion controlled situations. In order to verify the hypothesis, the effect of the diffusion coefficient was studied.

Effect of Diffusion Coefficient

Generally, a constant value of the diffusion pre-exponential factor as given in Equation 5.13 is used to describe the diffusion of carbon in austenite. However, this study was carried out in order to verify the behaviour of the model at more diffusion controlled situations. It was observed that the change in the diffusion coefficient had more pronounced effect than the change in the mobility of equal order of magnitude. A lower value of the diffusion pre-exponential factor for the diffusion of carbon in the austenite gives rise to a lower value of diffusion coefficient, i.e. the diffusion becomes slow and

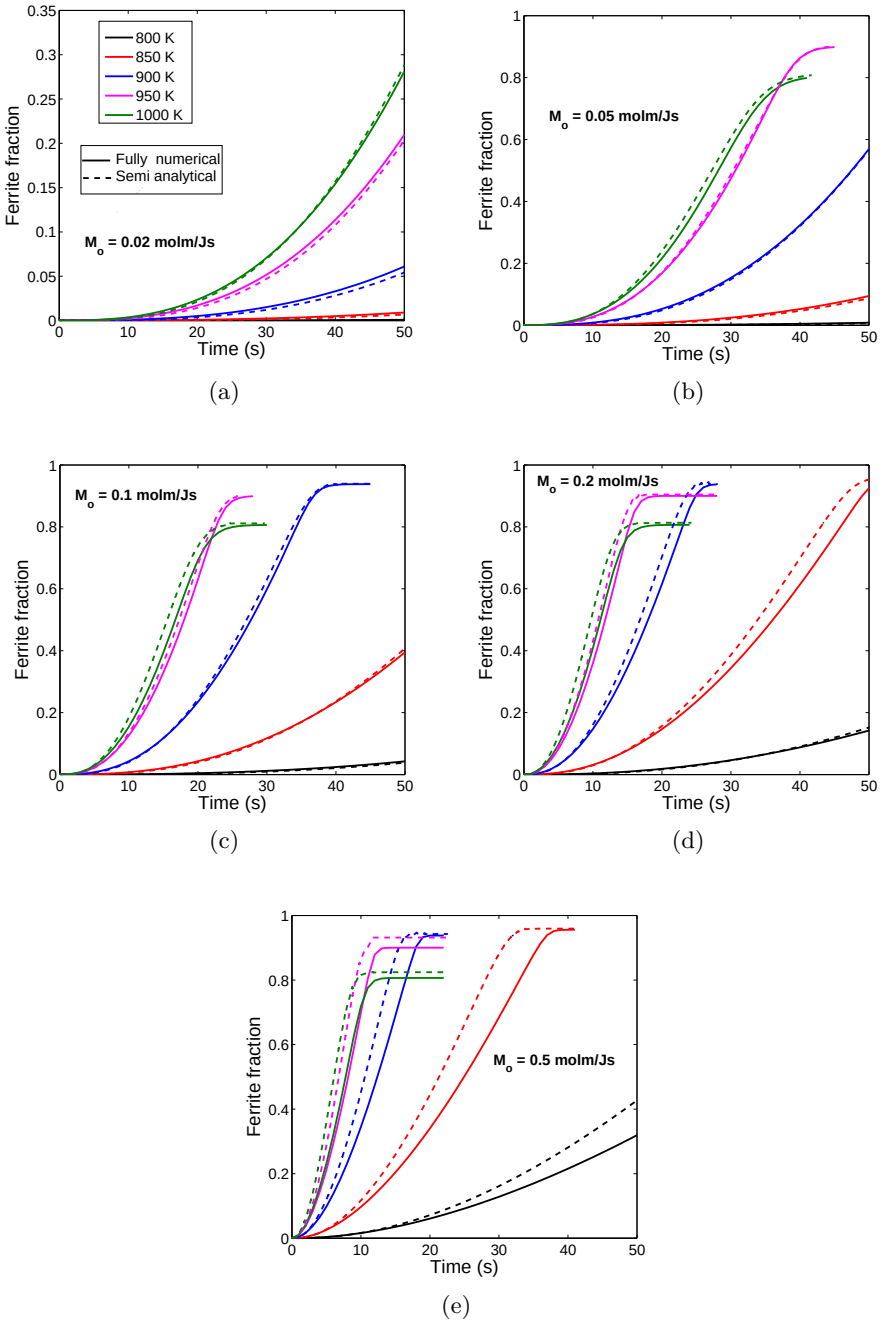

Figure 5.7: Comparison of fraction curves between the fully numerical and semi analytical models at various values of M_o (a) 0.02 (b) 0.05 (c) 0.1 (d) 0.2 (e) 0.5 molm/Js for different temperatures for DP600

thus, limiting. In other words, the transformation becomes more diffusion controlled.

In order to study the effect of diffusion coefficient, simulations were performed at different mobilities at 900 K with a system size of 10 μm. It can be seen from Figure 5.9a that the semi analytical model predicts faster transformation at lower diffusivity.

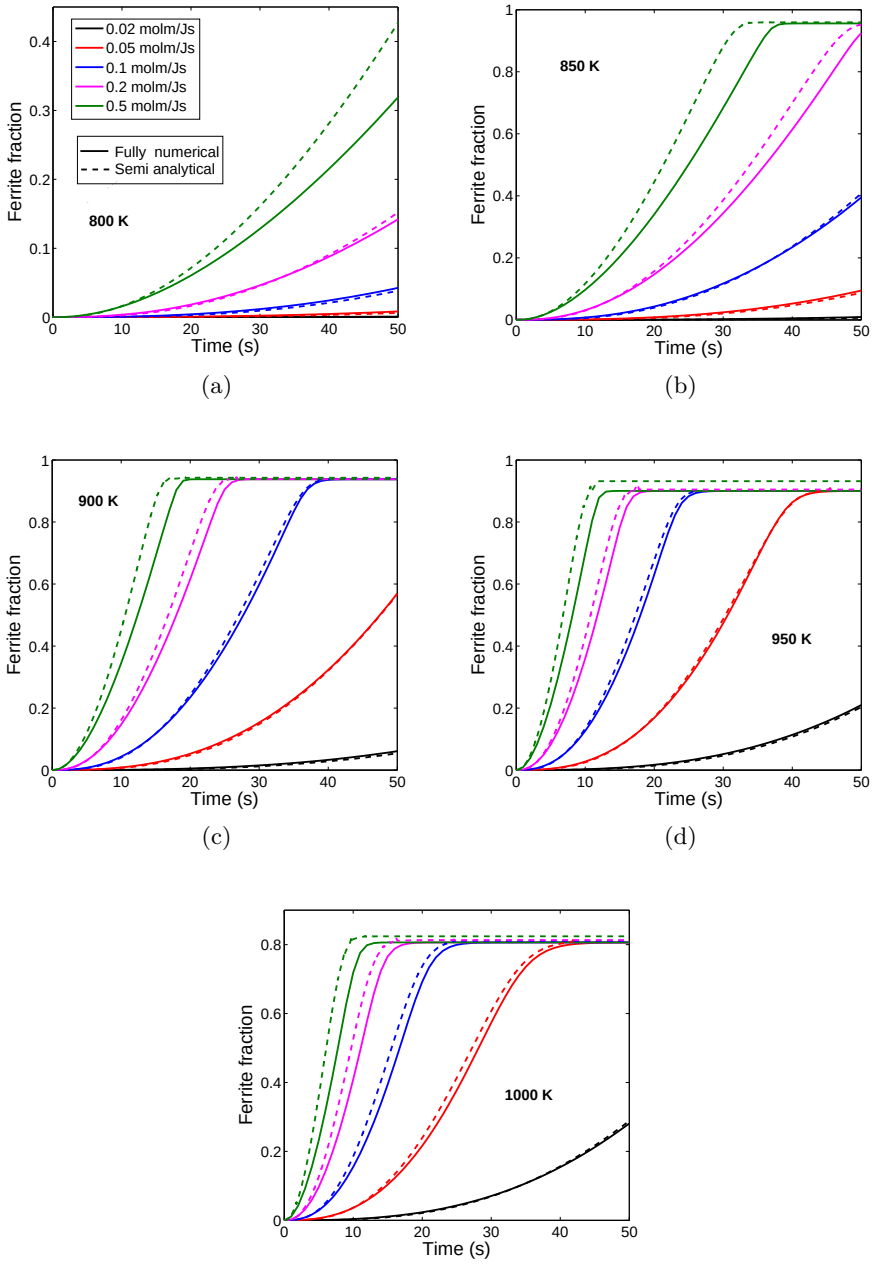

Figure 5.8: Comparison of fraction curves between the fully numerical and semi analytical models at various temperatures (a) 800 (b) 850 (c) 900 (d) 950 (e) 1000 K for different values of mobility pre-exponential factor for DP600

From Figure 5.9b, it can be seen that for a given diffusion coefficient, the deviation of the semi analytical model from the fully numerical model increases with increase in mobility. Thus, it can be concluded that the semi analytical model predicts much faster transformation at higher mobilities and lower diffusivities, i.e. when the transformation

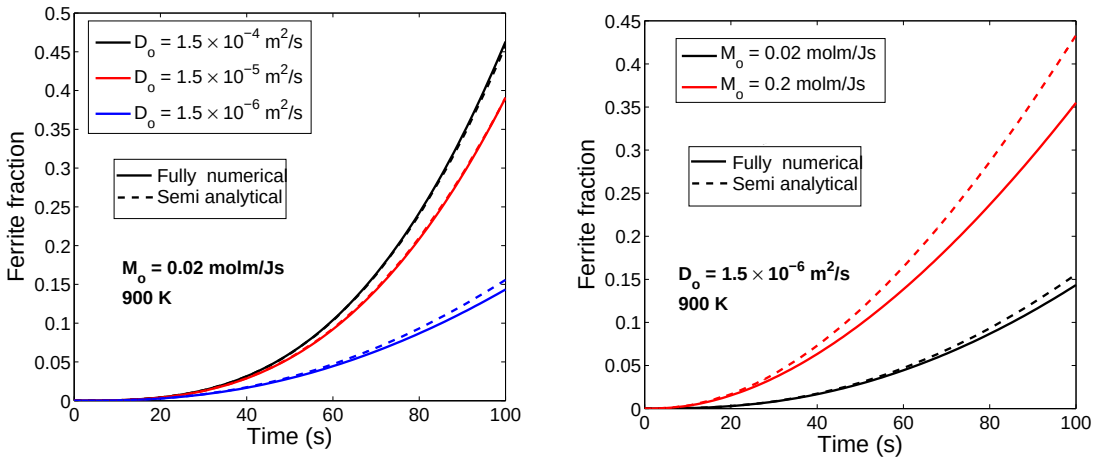

(a) (b)

Figure 5.9: Comparison of fraction curves between the fully numerical and semi analytical models at 900 K for different (a) diffusivities and (b) mobilities for DP600

becomes more diffusion controlled in nature.

The difference between the models could be either due to the difference in the interface carbon concentration or the difference in the carbon profile described in the semi analytical model.

Effect of Alloy Composition

In order to study the versatility of the semi analytical model in terms of the composition of the alloy, simulations were carried out for a plain carbon steel, A36 (Table 4.2). The comparison between the fully numerical and semi analytical model at a temperature of 900 K for different mobilities is given in Figure 5.10. It is seen that the A36 alloy behaves in a similar way as DP600, i.e. the deviation of the semi analytical model from the fully numerical model increases with increase in mobility.

A36 has a higher carbon content and lower substitutional element content (Mn, Si and Cr) than DP600. The comparison of both alloys in terms of their Ae3 temperature is given in Figure 5.11. The thickness of the lines represent the variation in Mn content. A higher Mn content results in a lower Ae3 temperature. It can be seen that A36 has a higher Ae3 temperature than DP600.

With a higher Ae3 temperature, it can be expected that A36 transforms faster than DP600 at a given temperature. Figure 5.12 shows the comparison between the ferrite fraction curves obtained in DP600 and A36 for different mobilities at 900 K. It can be seen that the behaviour of the alloy depends strongly on the interface mobility. At lower mobilities, the A36 is faster than DP600. However, at higher mobilities, DP600 is much faster. This is due to the higher carbon content in A36, which becomes more

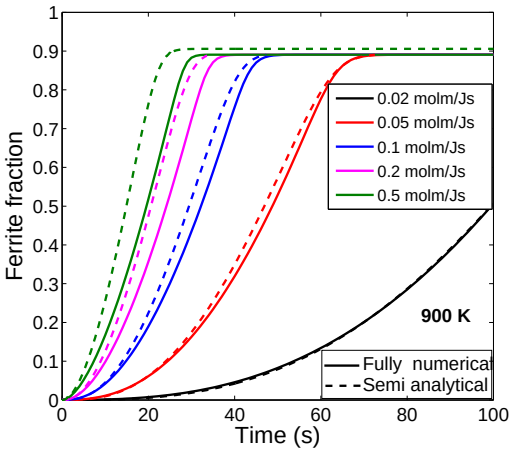

Figure 5.10: Comparison of fraction curves between the fully numerical and semi analytical models for A36 at 900 K for different mobilities

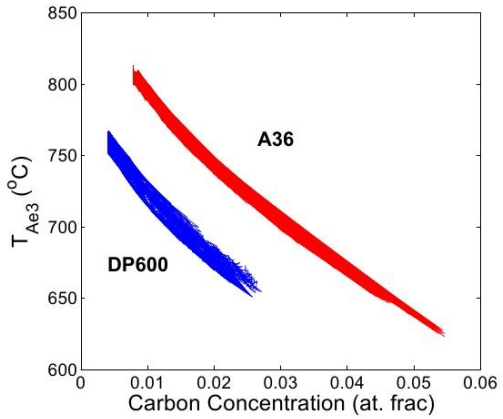

Figure 5.11: Comparison of variation of Ae3 temperature with carbon concentration for A36 and DP600 (Pattabhiraman [2012])

important at more diffusion controlled situations. The higher amount of carbon in the system makes its diffusion much slower. Thus, while trying to select a set of parameters to explain the ferrite transformation curves, the choice of mobility becomes critical.

Effect of Mode Factor

From the above comparison studies, it can be concluded that mobility and diffusivity are the major factors affecting the applicability of the semi analytical model. It can be noted that the semi analytical model deviates to a larger extent at higher mobilities and lower diffusivities, i.e. when the transformation becomes more diffusion controlled.

In order to quantitatively assess their effects, a quantity based on the difference in ferrite fraction between the fully numerical and semi analytical models was proposed. The Root Square Fraction Difference (θ) is the average of square root of the sum of

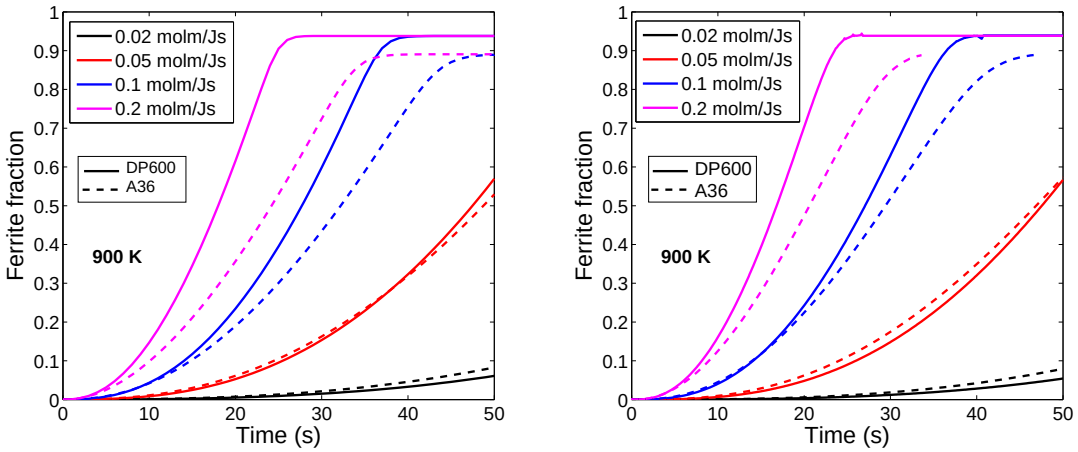

(a) (b)

Figure 5.12: Comparison of fraction curves obtained for A36 and DP600 at 900 K for different mobilities using the (a) the fully numerical and (b) semi analytical model

squares of normalised fraction difference between the two models at various times. This gives the error in percentage of ferrite fraction. It is calculated at a certain temperature and mobility. Mathematically, it can be represented as

$$\theta = \frac{\sqrt{\sum_{i=1}^{n} \left(\frac{f_{fn,i} - f_{sa,i}}{f_{fn,i}}\right)^2}}{n} \cdot 100\%, \tag{5.15}$$

where $f_{sa,i}$ and $f_{fn,i}$ are the ferrite fraction obtained using the semi analytical and finite difference models respectively at given time i, and n is the number of data points (time steps).

In order to quantify the nature of the transformation, an average mode factor was calculated as

$$S_{avg} = \frac{\sum_{i=1}^{n} S_i}{n}. \tag{5.16}$$

The value of the average mode factor for various diffusivities and mobilities is shown in Figure 5.13. Similar to the mode factor defined in Equation 2.8, a value of zero represents fully diffusional controlled transformation and a value of unity represents interface controlled. It can be seen that the average mode factor decreases with increase in mobility and increase in diffusivity, i.e. the transformation becomes more diffusion controlled.

The calculated error (θ) as a function of the mode factor is given in Figure 5.14. The black points represent the data obtained from DP600 and the red points from A36. It can be noted that a lower average mode factor is associated with a higher error. The scatter in the results could be attributed to the variation in mobility, diffusivity and

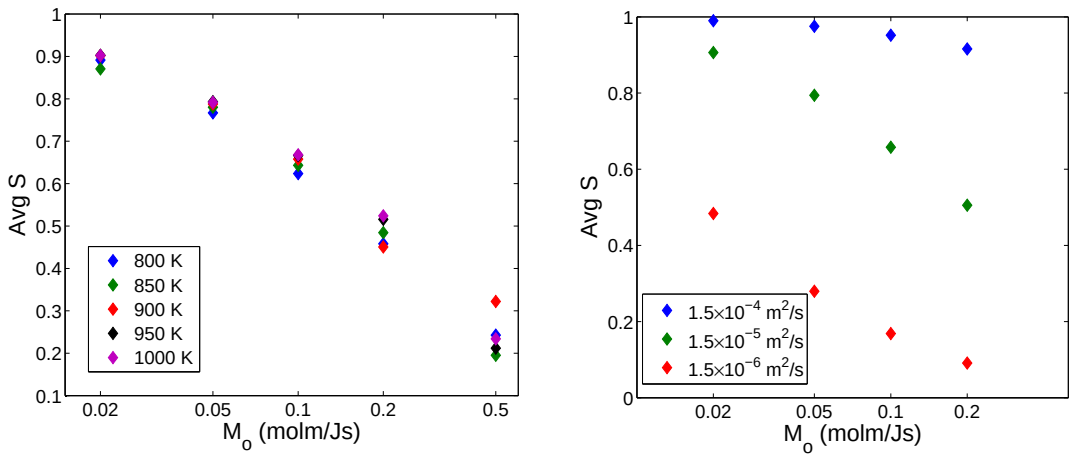

(a) (b)

Figure 5.13: Average mode factor calculated for DP600 for various (a) temperature and (b) diffusivities plotted as a function of mobility

temperature. The difference in ferrite fraction between the two models could be due to an error in the definition of the carbon concentration profile in the austenite or the interface carbon concentration. A detailed study of the carbon concentration profiles was, thus, carried out.

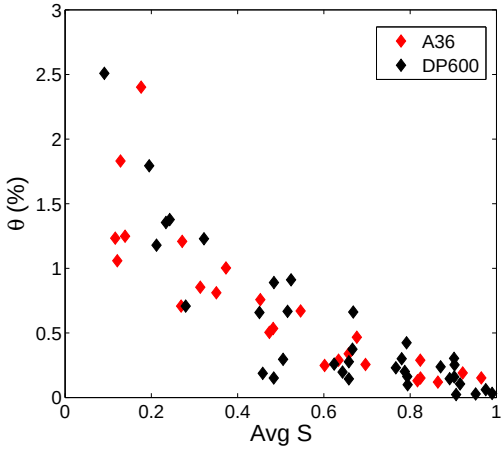

Figure 5.14: Calculated error (θ) as a function of average mode factor for A36 and DP600

Comparison of Carbon Profile

In order to compare the nature of the carbon profiles between the fully numerical and semi analytical model, two conditions of mobility and diffusivity were chosen. In one condition, the ferrite transformation kinetics was almost accurately defined by the semi

analytical model. While in the other case, the semi analytical model predicted faster transformation kinetics. The fraction curves obtained in both these cases are given in Figure 5.15.

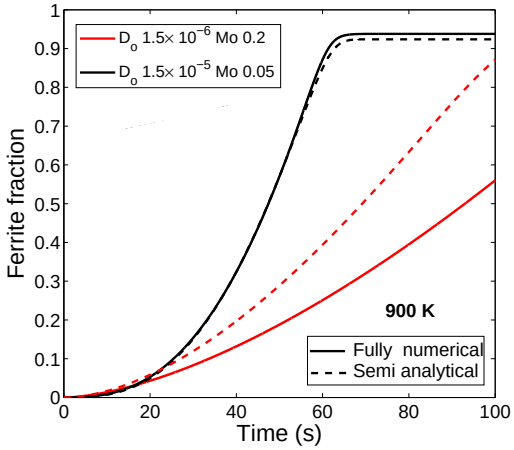

Figure 5.15: Comparison of ferrite fraction curves between a more diffusion controlled and interface controlled transformations for DP600

The carbon profile obtained from a more interface controlled transformation is shown in Figure 5.16. The simulation was carried out with a mobility pre-exponential factor of 0.05 molm/Js and diffusivity pre-exponential factor of 1.5×10^{-5} m^2/s at a temperature of 900 K. It can be observed from Figure 5.16a that the interface carbon concentration predicted by the semi analytical model is a little different from that of the fully numerical model, and is much lower than the equilibrium carbon concentration for most part of the transformation. It can be noted from 5.16b, that the carbon profile in the semi analytical model is described decently well at larger times. However, some difference in the nature of the profile can be noted at smaller times.

The interface carbon concentration and the carbon profiles in a case where the semi analytical model over predicts the transformation is shown in Figure 5.17. The simulation was carried out with a mobility pre-exponential factor of 0.2 molm/Js and diffusivity pre-exponential factor of 1.5×10^{-6} m^2/s at a temperature of 900 K. From Figure 5.17a, it can be seen that the interface carbon concentration between both models is similar and is close to the equilibrium carbon concentration for most part of the transformation. However, the carbon profile as described by the semi analytical model is much different from the fully numerical model as seen in Figure 5.16b. The interface in the semi analytical model moves much faster than that in the fully numerical model, as observed in the fraction curves.

However, it can be noted that, at a given interface position, the carbon profile predicted by the semi analytical model is same as the one in the fully numerical model. The interface position is reached by the semi analytical model at 60.11 s and in the fully

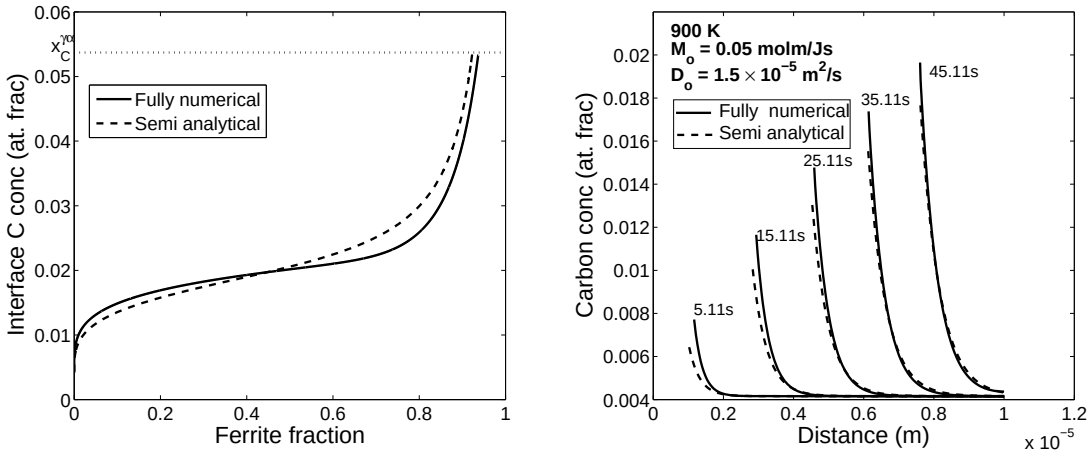

(a) (b)

Figure 5.16: Comparison of (a) interface carbon concentration and (b) carbon profile obtained using the fully numerical and semi analytical models at 900 K for $M_\circ$ of 0.05 molm/Js and $D_\circ$ of 1.5×10^{-5} m^2/s

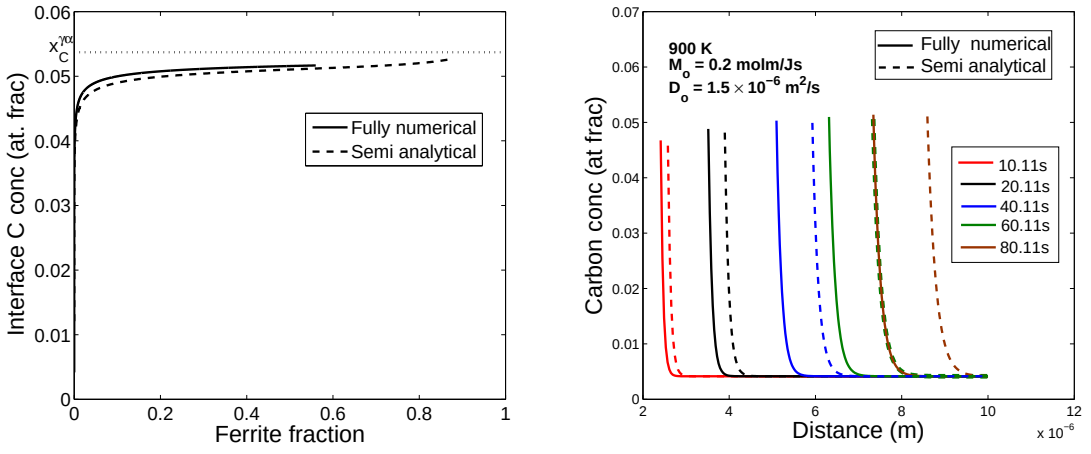

(a) (b)

Figure 5.17: Comparison of (a) interface carbon concentration and (b) carbon profile obtained using the fully numerical and semi analytical models at 900 K for $M_\circ$ of 0.2 molm/Js and $D_\circ$ of 1.5×10^{-6} m^2/s

numerical model at 80.11 s. This shows that the mass balance calculations in the semi analytical model based on the position of the interface, yields accurate value of $z_\circ$.

In the definition of the semi analytical model, prior transformation history of the material, in terms of the ferrite fraction, is not accounted for. This, however, is inherently present in the definition of the fully numerical model. Thus, it can be postulated that the effect of time in terms of the prior history becomes critical for diffusion controlled

transformations. This can be further ascertained by the nature of the carbon profiles in fully diffusion controlled and interface controlled transformations. The carbon profiles are shown in Figure 5.18. The carbon profile in case of interface controlled transformation is flat in nature as indicated by the dashed lines in the figure. While the carbon concentration in diffusion controlled transformation has a certain curvature, indicated by solid lines in the figure. Thus, in case of a interface controlled transformation, it does not matter how a certain ferrite fraction was reached, as the carbon profile will look similar in all cases. In contrast, in case of the diffusion controlled transformation, the curvature of the carbon profile will be affected by prior transformation.

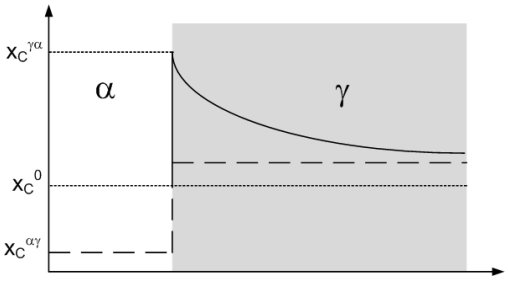

Figure 5.18: Schematic of carbon concentration profiles observed in interface controlled and diffusion controlled transformations

Effect of Soft-Impingement Correction

As explained in Section 2.3, two methods have been proposed for correction in the interface carbon concentration due to soft-impingement between the growing ferrite grains. The two soft-impingement correction methods namely, 'mode factor soft-impingement' (Equation 2.10) and 'fraction soft-impingement' (Equation 2.11), were compared in order to study the accuracy of the methods.

The comparison between the ferrite fractions obtained with the semi analytical model with either of the soft-impingement correction and the fully numerical model is given in Figure 5.19. The simulations were carried out at 900 K. It can be seen that both the correction methods give similar results at low ferrite fractions and low mobilities. However, at higher ferrite fractions, the kinetics described by the 'fraction soft-impingement' correction is much slower than that by the 'mode factor soft-impingement' correction as well as the fully numerical model. Thus, at higher mobilities, the 'mode factor soft-impingement' method over predicts the ferrite fraction, while the 'fraction soft-impingement' method under predicts.

The correction by the 'fraction soft-impingement' method is based on the fraction of ferrite formed. Accordingly, the carbon concentration at the interface reaches the equilibrium carbon concentration when the equilibrium ferrite fraction is reached. The increase in the carbon concentration at the interface is proportional to the ferrite fraction.

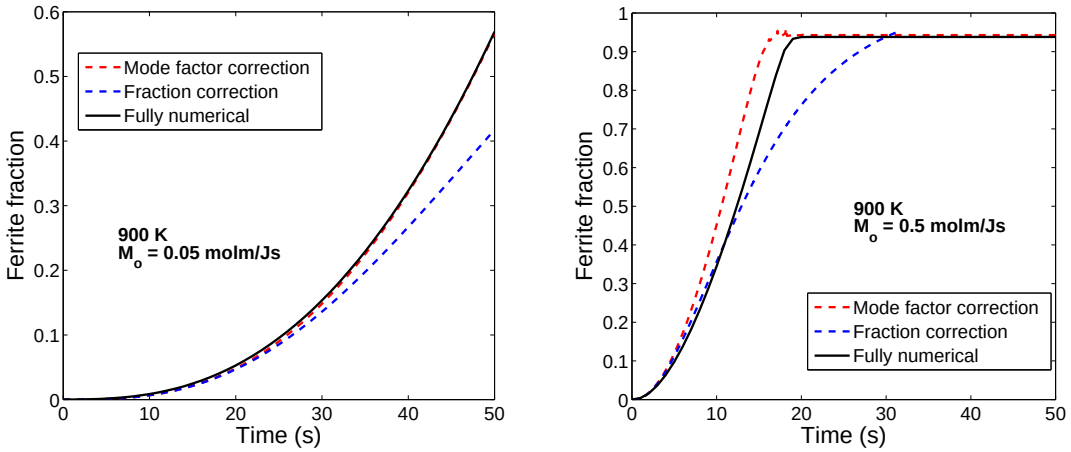

(a) (b)

Figure 5.19: Comparison of fraction curves obtained in the semi analytical model using the 'fraction' and 'mode factor' soft-impingement corrections with the fully numerical model for DP600 at 900 K for mobilities of (a) 0.05 and (b) 0.5 molm/Js

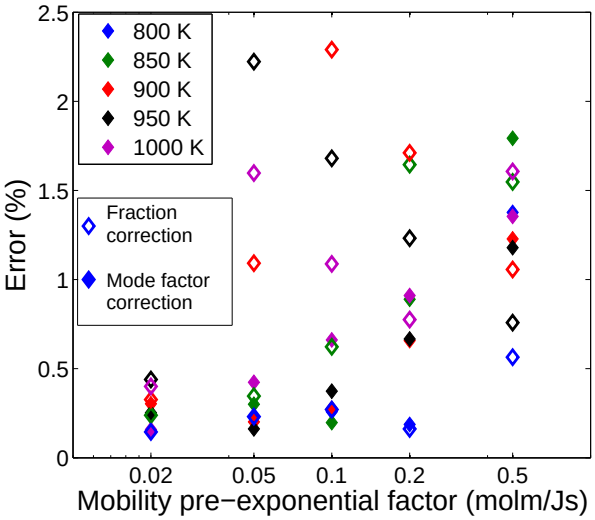

Figure 5.20: Error obtained in the semi analytical model calculated using the fraction and local soft-impingement methods plotted as a function of mobility in DP600

This means that the soft-impingement effect is higher at higher ferrite fractions, which can be seen from the slower ferrite formation kinetics. However, the carbon concentration is equal to the bulk carbon concentration only at the start of the transformation, when no ferrite is formed. This means that this method can describe interface controlled transformations only at the start of the transformation.

In contrast, the upper and lower limits of the carbon concentration in the 'mode factor soft-impingement' correction are influenced by the mode factor. The mode factor

varies between zero for diffusion controlled transformations to unity for interface controlled transformations. Thus, the situations wherein the interface carbon concentration is closer either to the bulk or the equilibrium concentration for most part of the transformation can be explained better.

The error obtained in the calculation of the ferrite fraction (θ) using the two soft-impingement correction methods is given in Figure 5.20. It can be noted that the semi analytical model with 'mode factor soft-impingement' correction results in a lower error when compared to the 'fraction soft-impingement correction'. The large spread of the error obtained using the 'fraction soft-impingement' at each mobility shows the dependence of the method on the temperature, which affects the equilibrium ferrite fraction. The temperature dependence, however, is not very evident in the 'local soft-impingement' method.

It can be concluded that the 'mode factor soft-impingement' correction is more accurate than 'fraction soft-impingement' correction for the given range of conditions. Thus, the 'mode factor soft-impingement' correction will be used in the subsequent simulations.

In this chapter, the implementation of the fully numerical and semi analytical models were explained. The semi analytical model was compared with the fully numerical model for its validity under various conditions of temperature, mobility pre-exponential factor and diffusion pre-exponential factor. It was found that the error obtained using the semi analytical model increases with increase in mobility and decrease in diffusivity. i.e. the semi analytical model deviates from the fully numerical model when the transformation becomes more diffusion controlled in nature. Two soft-impingement corrections used in the semi analytical model were compared. The 'mode factor soft-impingement' correction was found to be more accurate than 'fraction soft-impingement' correction for a given range of conditions.

Chapter 6

Gradual Transition Approach

In order to explain the kinetic transition from PE to LENP, a gradual transition approach was developed. The approach is based on the concept of P-factor as described by Capdevila et al. [2011] and the mixed equilibrium approach by Thibaux [2006]. This chapter explains the formulation of the approach and its implementation in the fully numerical and semi analytical models.

6.1 Approach Formulation

In the proposed gradual transition approach, it is assumed that the nucleation and the initial growth takes place in PE condition. For nucleation, the assumption is in accordance with the work by Zurob et al. [2008] and Hutchinson et al. [2004]. It is reasonable to consider the PE condition, given the fact that the composition of the matrix around a nucleus does not change considerably owing to the small size of the nucleus. Thus, there will be no building up of a concentration spike, characteristic to the LENP condition as explained in Section 3.1. The absence of a substitutional element peak at shorter times was experimentally shown by Capdevila et al. [2011], which shows that ferrite grows under PE conditions during early stages.

The gradual PE to LENP transition is based on the physical explanation offered by Capdevila et al. [2011]. In the austenite-to-ferrite transformation, an unbalanced flux of the substitutional element (X) is assumed to flow across the interface from the ferrite to austenite. This can be attributed to the difference in chemical potentials between Fe and X. With the passage of time, the interface velocity decreases and thus, the X atoms begin to diffuse in the austenite at a greater rate compared to the interface movement. Theoretically, in the mixed mode model, a higher interface velocity results in an increase in the substitutional element concentration of the spike while a lower velocity results in an increase in the width of the spike. In order to calculate the building up of the Mn concentration in the spike, the mixed mode equations has to be solved for Mn in

addition to that for carbon. In order to save computational time, the height of the spike is assumed to be proportional to the width of the spike. Thus, the building up of the spike is described in terms of the increase in width of the spike. It is assumed that the spike starts to form at a certain velocity and is fully developed at a much lower velocity. The transformation proceeds in a mixed-condition between these two critical velocities. Complete LENP equilibrium is reached when the spike is fully formed, i.e. reaches a certain width.

The PE to LENP transition is modelled on the basis of the P-factor defined by Capdevila et al. [2011]. The steps followed to model the transition in the fully numerical model is explained here. At each time step j, the P-factor is calculated based on the velocity of the previous time step as

$$P_j = \frac{D^{\gamma}_{\mathrm{X,j}}}{v_{j-1}}. \tag{6.1}$$

The P-factor denotes the characteristic width of the substitutional element concentration profile in the austenite as shown in Figure 6.1. (Porter and Easterling [1992]) A lower value of the P-factor denotes a thinner spike. The P-factor at each time step is then used to calculate the transition parameter (K_T) defined as

$$K_{T,j} = \frac{P_j - P_{\mathrm{PE}}}{P_{\mathrm{LENP}} - P_{\mathrm{PE}}}, \tag{6.2}$$

where P_{PE} is the value of P-factor when the spike starts to form and P_{LENP} is the value when the spike is fully formed, i.e. the spike is said to become stable at a width of P_{PE} and is treated to be completely formed at a width of P_{LENP}. For values of P_j lower than P_{PE}, it is assumed that the 'spike' is unstable because of the high interface velocity, and thus, does not physically exist.

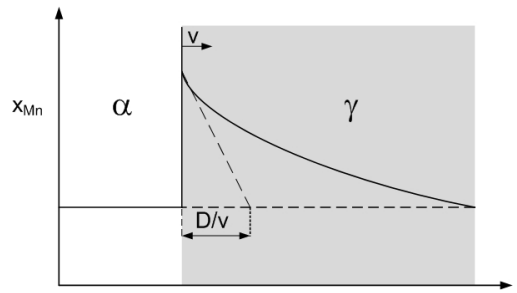

Figure 6.1: Physical representation of P-factor (Porter and Easterling [1992])

In other words, the system will be in complete PE condition for P-factor values lower than P_{PE} and in complete LENP condition for values greater than P_{LENP}. The values of P_{PE} and P_{LENP} will be chosen so as to obtain a good agreement with the experimental data. The critical value of P-factor obtained by Capdevila et al. [2011] refers to the

value at which the equilibrium becomes completely LENP in nature and is found to be in the order of 10^{-10} m. While, the critical value defined by Zurob et al. [2008] refers to the start of the deviation from PE equilibrium and was found be in the order of 10^{-11} m. However, in both cases the value of the diffusion coefficient for Mn used for calculating the critical P-factor is not given. Thus, an estimate of the interface velocity which results in the given value of the spike width cannot be calculated. However, based on these results, the values of P_{PE} and P_{LENP} is expected to be in a similar order of magnitude, i.e. between 10^{-11} and 10^{-10} m. This would mean that LENP equilibrium condition is maintained for spike width greater than 10^{-10} m.

The dependence of the P-factor on the diffusion coefficient of the substitutional element in austenite suggests that the critical velocity at which the transition takes place is different at different temperatures. The value of the transition parameter varies between zero for fully PE condition ($P_j = P_{\mathrm{PE}}$) to unity for fully LENP condition ($P_j = P_{\mathrm{LENP}}$).

The transition parameter is then used to calculate the driving force at each time step as by averaging the driving forces computed using the PE and LENP conditions, over the transition parameter as

$$\Delta G_j = \Delta G_j^{\mathrm{PE}} + K_T \times \left(\Delta G_j^{\mathrm{LENP}} - \Delta G_j^{\mathrm{PE}}\right), \tag{6.3}$$

where ΔG_j is the averaged driving force and ΔG_j^{PE} and $\Delta G_j^{\mathrm{LENP}}$ are the driving forces calculated using PE and LENP conditions respectively. This averaged driving force is then used to calculate the interface velocity according to Equation 2.14.

The carbon concentration of ferrite in equilibrium with austenite is calculated in a similar manner by averaging over K_T as

$$x_{\mathrm{C},j}^{\alpha\gamma} = x_{\mathrm{C},j}^{\alpha\gamma,\mathrm{PE}} + K_T \times \left(x_{\mathrm{C},j}^{\alpha\gamma,\mathrm{LENP}} - x_{\mathrm{C},j}^{\alpha\gamma,\mathrm{PE}}\right), \tag{6.4}$$

where $x_{\mathrm{C},j}^{\alpha\gamma}$ is the averaged equilibrium carbon concentration in ferrite and $x_{\mathrm{C},j}^{\alpha\gamma,\mathrm{PE}}$ and $x_{\mathrm{C},j}^{\alpha\gamma,\mathrm{LENP}}$ are the equilibrium carbon concentrations in ferrite calculated using PE and LENP conditions respectively.

The carbon concentration of austenite in equilibrium with ferrite is calculated as

$$x_{\mathrm{C},j}^{\gamma\alpha} = x_{\mathrm{C},j}^{\gamma\alpha,\mathrm{PE}} + K_T \times \left(x_{\mathrm{C},j}^{\gamma\alpha,\mathrm{LENP}} - x_{\mathrm{C},j}^{\gamma\alpha,\mathrm{PE}}\right), \tag{6.5}$$

where $x_{\mathrm{C},j}^{\gamma\alpha}$ is the averaged equilibrium carbon concentration in austenite and $x_{\mathrm{C},j}^{\gamma\alpha,\mathrm{PE}}$ and $x_{\mathrm{C},j}^{\gamma\alpha,\mathrm{LENP}}$ are the equilibrium carbon concentrations in austenite calculated using PE and LENP conditions respectively.

The equations 6.1 to 6.5 are repeated at each time step. This approach is termed as the 'average driving force' method.

In a variation of the above method, the interface velocity can initially be calculated separately for the PE and LENP conditions and then averaged over K_T at the end of each time step as

$$v_j = v_j^{\mathrm{PE}} + K_T \times \left(v_j^{\mathrm{LENP}} - v_j^{\mathrm{PE}} \right), \tag{6.6}$$

where v_j is the averaged interface velocity and v_j^{PE} and v_j^{LENP} are the interface velocities calculated using PE and LENP conditions respectively.

However, in the CA model, the velocity of the grain boundary is calculated based on the average carbon concentration of the grain. The average carbon concentration of the grain is calculated based on an infinitely large system, with no soft impingement effects. Also, in the CA model, the values of the velocity and the driving force in the previous time step are not stored. Thus, the transition parameter at each time step is calculated using the velocity at the same time step. This is complicated by the velocity dependence of the transition parameter. This is solved by solving the equations 6.2 and 6.6 simultaneously. Thus, the mixed velocity at each time step can be obtained as

$$v_j = \frac{1}{2} \left(\pm \sqrt{4.Y.D^{\gamma}_{\mathrm{X,j}} + (v_j^{PE} - Y.P_{PE})^2} - Y.P_{PE} + v_j^{PE} \right), \tag{6.7}$$

where $Y = \frac{v_j^{LENP} - v_j^{PE}}{P_{LENP} - P_{PE}}$.

This is termed as the 'average velocity' method. The 'averaging' of the velocity starts when P-factor reaches a value equal to P_{PE}. The equilibrium condition becomes completely LENP once the value of the square root term in Equation 6.7 becomes complex. This quadratic equation yields two positive roots, both of which lie between v_j^{PE} and v_j^{LENP}. The value close to v_j^{PE}, as given by the positive value of the determinant, is chosen. This is done to indicate that the equilibrium will be more closer to the PE condition at the start of the kinetic transition. Also, the end point of the transition is not clearly observed as is taken as the point at which the determinant becomes negative.

The P-factor is calculated on the basis of grain boundary diffusion of the substitution element. The grain boundary diffusion coefficient is calculated as 'n' times the bulk diffusion coefficient. For a Fe-C-Mn alloy, the diffusion coefficient is given as

$$D^{\gamma,\mathrm{GB}}_{\mathrm{Mn}} = n \times D^{\gamma,\mathrm{bulk}}_{\mathrm{Mn}}, \tag{6.8}$$

where 'n' has a value between 400 and 700 (Gamsjäger et al. [2006]). This is much larger than a value of 30 used by Capdevila et al. [2011]. However, the activation energy and diffusion pre-exponential coefficient used for the calculation of the diffusion of Mn by Capdevila et al. [2011] is unknown.

The diffusion coefficient for bulk diffusion of Mn in austenite is given by (Landolt-

Bornstein)

$$D_{\mathrm{Mn}}^{\gamma,\mathrm{bulk}} = \left(1.6 \times 10^{-5}\, m^2/s\right) \times \exp\left(\frac{-2.62 \times 10^5\, KJ/mol}{\mathrm{RT}}\right).$$

6.2 Analysis of the Transition Behaviour

Spike build up is defined as the increase in the width of the spike and is described in terms of the transition parameter. A value of the transition parameter between zero and unity refers to a partial build up of the spike and thus, an equilibrium condition intermediate to that of PE and LENP. This refers to the gradual nature of the PE to LENP transition. The equilibrium condition is closer to either PE or LENP depending up on the value of the transition parameter. The transition parameter increases till it reaches unity and is maintained thereafter.

6.2.1 Transition during Isothermal Transformation

In order to study the behaviour of the gradual transition, a simulation was carried out for DP600 at a constant temperature of 898.15 K (625 °C) for 30 s with a mobility pre-factor of 0.05 molm/Js in a one-dimensional system. A P_{PE} of $6{\times}10^{-11}$ m and P_{LENP} of $1.5{\times}10^{-10}$ m were used in the simulation. These values are similar in magnitude as obtained by Capdevila et al. [2011] and Zurob et al. [2008]. Further, the specific values were chosen so as to ensure that the transition occurs within the course of the simulation.

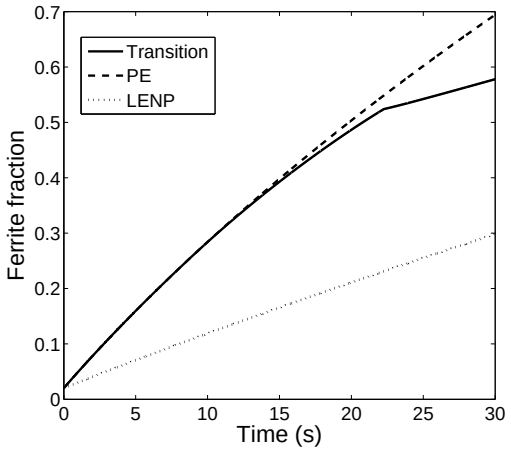

Figure 6.2: Ferrite fraction curves obtained using gradual transition approach and complete LENP and PE controlled transformations

The ferrite fraction curves obtained are shown in Figure 6.2. The solid lines represent the fraction curve obtained with gradual transition from PE to LENP. The dashed and dotted lines represent the fraction curves obtained under complete PE and LENP

conditions respectively. It can be seen that the final ferrite fraction obtained with the transition is in between the fractions obtained using completely PE and LENP conditions. This is similar to the behaviour reported by Capdevila et al. [2011] and Thibaux [2006].

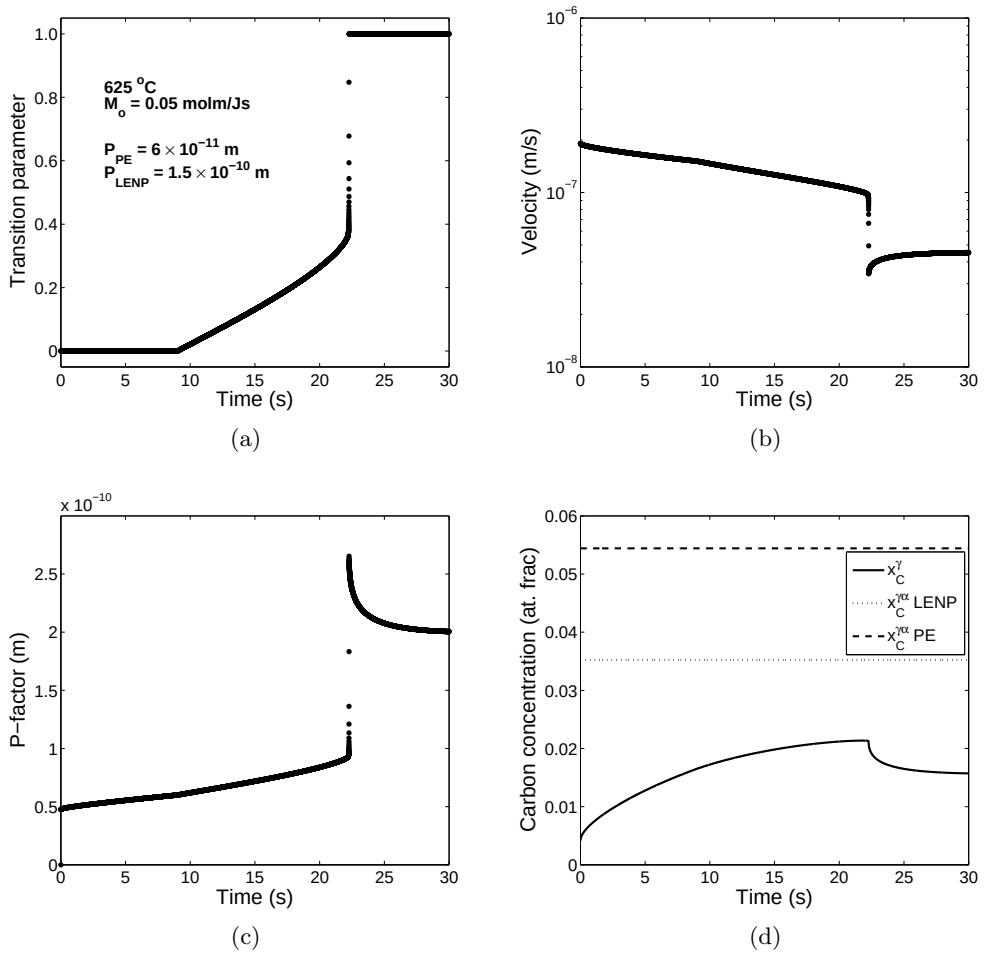

Figure 6.3: Behaviour of (a) transition parameter (b) velocity (c) P-factor and (d) interface carbon concentration during the gradual transition

The variation of the transition parameter during the transformation is shown in Figure 6.3. The accompanying changes in velocity, P-factor and the interface carbon concentration in austenite (x_{C}^{γ}) are also shown. The transition parameter increases at slower rate in the start of the transition as seen in Figure 6.3a. However, the end of the transition is quite rapid in nature. This can be explained in terms of the dependence of the transition parameter on the interface velocity. The transition behaves in an auto-catalytic manner, i.e. when the interface velocity decreases, the transition parameter is increased. This causes the transformation to become more LENP in nature, which further reduces the interface velocity.

It can be seen from Figure 6.3d that the interface carbon concentration increases continuously till the transition parameter reaches a value of unity. At this point, the carbon concentration starts to decrease. It can be hypothesised that the interface velocity, at this point, becomes so low that the diffusion of the carbon in austenite occurs at a higher rate in comparison to the movement of the interface. After a certain period of time, when the interface concentration decreases to a certain extent, the driving force becomes high enough to facilitate a faster interface movement. This, again, causes the interface concentration to increase till the equilibrium carbon concentration is reached ($x_{\mathrm{C}}^{\gamma\alpha}$). Also, in this case, it can be noted that the interface carbon concentration remains well below the LENP and PE equilibrium concentration through out the transformation. This, however, depends on the values of P_{PE} and P_{LENP}.

6.2.2 Effect of Critical Interval

The difference between the P_{PE} and $\mathrm{P_{LENP}}$ values is termed as the 'critical interval'. In order to study the effect of the critical interval, two simulations were carried out with a value of P_{LENP} of $1.5{\times}10^{-10}$ m and $2{\times}10^{-10}$ m at a temperature of 898.15 K (625 °C) with a mobility pre-factor of 0.05 molm/Js in a one-dimensional system in DP600. The value of P_{PE} was kept constant at $6{\times}10^{-11}$ m. It can be seen from Figure 6.4 that a smaller interval leads to faster increase in the value of the transition parameter, which, in turn, refers to a faster spike build up. It is, further, noted that the difference in the critical interval in the order of about $0.5{\times}10^{-10}$ m results in the increase in the transition time by about 26 seconds.

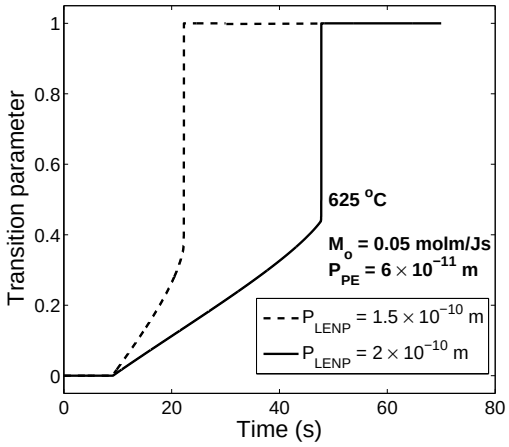

Figure 6.4: Effect of critical interval on the transition parameter

6.2.3 Effect of Mobility

The effect of the mobility on the transition factor can be seen in Figure 6.5. Mobility pre-exponential factor values of 0.04 and 0.05 molm/Js was used. The other conditions were same as above with a P_{LENP} of 1.5×10^{-10} m. It can be seen that a lower mobility gives rise to a lower velocity, which in turn leads to a higher P-factor value and thus, larger value of the transition parameter. Thus, a lower mobility gives rise to an faster transition from PE to LENP for constant values of P_{PE} and P_{LENP}.

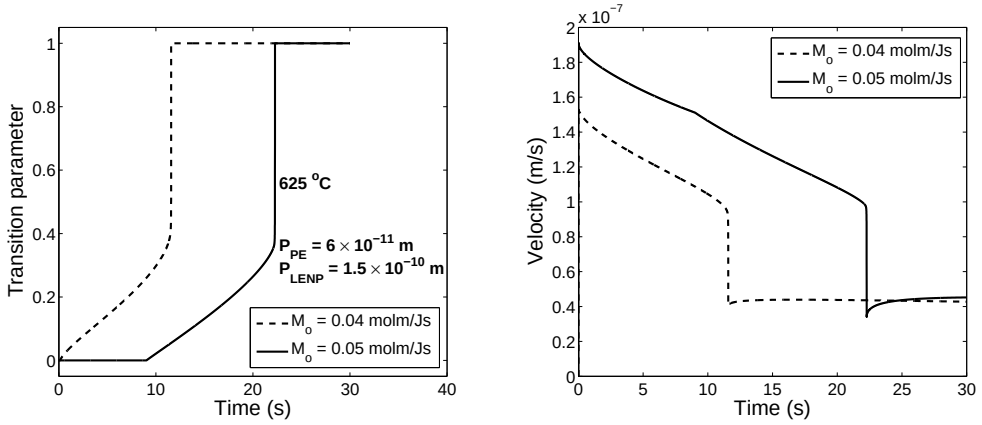

(a) (b)

Figure 6.5: Effect of mobility on (a) transition parameter and (b) velocity of transformation

Thus, it can be concluded that transition behaviour depends on both the mobility pre-exponential factor and the critical interval. In the CA model, the mobility pre-exponential factor is used as a fitting parameter in order to explain the nature of the ferrite transformation curves. The difficulty lies in obtaining universal values of the critical interval and mobility pre-exponential factor in order to explain the transition over a range of conditions viz. alloy composition and temperature.

6.2.4 Final Ferrite Fraction

The final ferrite fraction obtained using the gradual transition approach at a given temperature depends on mobility and critical interval. It is observed that at certain conditions of mobility and critical interval, the final ferrite fraction obtained lies in-between the ferrite fractions calculated for PE and LENP equilibrium. The equilibrium ferrite fractions are calculated using Thermo-calc®. This observation is of considerable importance because, at the later stages of the transformation, when the system is thermodynamically in LENP condition, the amount of ferrite formed is higher than that determined by the LENP equilibrium.

An example of such a situation is shown in Figure 6.6, which shows the ferrite fraction as a function of time. The simulation was carried out at a temperature of 898.15 K (625 °C) with a mobility pre-factor of 0.2 molm/Js in a one-dimensional system in DP600. A P_{PE} of 6×10^{-11} m and P_{LENP} of 2×10^{-10} m was used. The arrow in the figure represents the point at which the system reaches complete LENP equilibrium. It can be noted that the ferrite fraction increases above the LENP equilibrium ferrite fraction represented by the red dashed line.

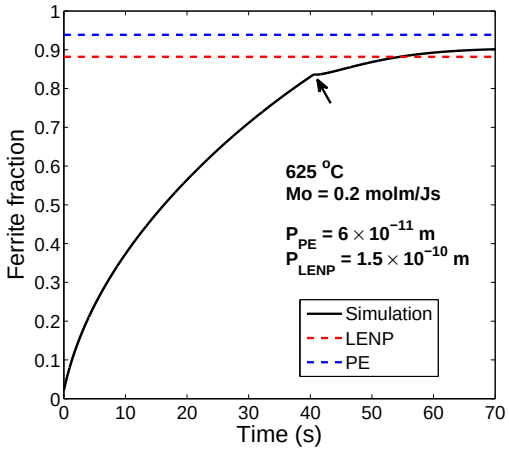

Figure 6.6: Nature of ferrite fraction curve obtained using the gradual transition approach

As calculated using the lever-rule, at a given temperature, austenite and ferrite are associated with a certain carbon concentration. This has been termed as the 'equilibrium carbon concentration' in Section 2.3. These equilibrium carbon concentrations are different for the PE and LENP conditions. In the mixed mode model, it has been assumed that the ferrite is formed with equilibrium carbon concentration at the interface. And during the transition period, the equilibrium carbon concentration is calculated as an average over transition parameter as given in Equation 6.4. The equilibrium carbon concentration in ferrite, at a given temperature, is lower in the LENP condition than in PE. Thus, at initial stages of the transformation, when the system is in PE condition, the ferrite is formed with higher amount of carbon than it would have if it was in LENP condition. Under these conditions, the austenite gets saturated with carbon in accordance to the PE condition. Therefore, when the system reaches complete LENP condition, the austenite is not saturated with respect to carbon. This allows for the driving force for the ferrite to grow above the equilibrium LENP ferrite fraction.

For DP600 at a temperature of 625 °C, the difference between the carbon concentration in austenite obtained using PE and LENP equilibrium conditions is given in Figure

6.7. The carbon concentration in austenite is calculated using the lever-rule as

$$x_{\mathrm{C}}^{\gamma\alpha,eqm} = \frac{(\alpha_f \times x_{\mathrm{C}}^{\alpha\gamma,eqm}) - x_{\mathrm{C}}^{\circ}}{\alpha_f - 1}, \tag{6.9}$$

where eqm refers to either PE or LENP condition and α_f is the fraction of ferrite formed at a given time. $x_{\mathrm{C}}^{\alpha\gamma,\mathrm{PE}}$ and $x_{\mathrm{C}}^{\alpha\gamma,\mathrm{LENP}}$ have a value of $8.68{\times}10^{-4}$ and $2.68{\times}10^{-4}$ at. frac. respectively at the given temperature.

Then, the difference between the carbon concentrations is calculated as

$$\text{Difference} = \frac{\left| x_{\mathrm{C}}^{\gamma\alpha,\mathrm{PE}} - x_{\mathrm{C}}^{\gamma\alpha,\mathrm{LENP}} \right|}{x_{\mathrm{C}}^{\gamma\alpha,\mathrm{PE}}} \,\%. \tag{6.10}$$

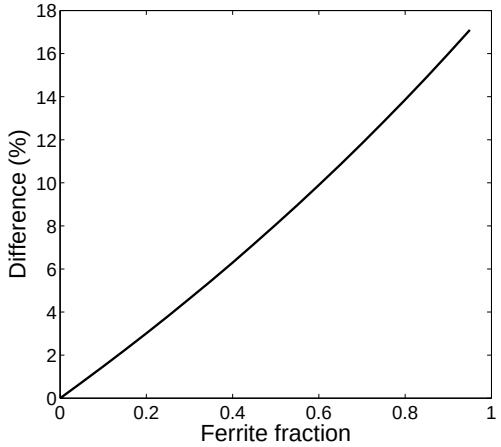

Figure 6.7: Difference in carbon concentration in austenite in PE and LENP conditions as a function of ferrite fraction

For a given ferrite fraction, the carbon concentration in austenite is lower in PE than in LENP condition. It can be seen from Figure 6.7 that the difference increases with increase in ferrite fraction. Thus, it can be postulated that a transition to PE at lower ferrite fractions will not affect the final ferrite fraction to a larger extent. However, for transitions occurring at higher fractions, the difference between the carbon concentration in austenite in PE and LENP conditions is large enough to provide for a final ferrite fraction above the LENP equilibrium fraction. But, the critical ferrite fraction after which the transition will result in higher final ferrite fraction is unknown.

6.3 Validation

The comparison between the 'average driving force' and 'average velocity' methods implemented in the fully numerical model in shown in Figure 6.8. The figure shows the

variation of the transition parameter with time. The simulation was carried out at a temperature of 898.15 K (625 °C) with a mobility pre-factor of 0.05 molm/Js in a one-dimensional system in DP600. A P_{PE} of $6{\times}10^{-11}$ m and P_{LENP} of $2{\times}10^{-10}$ m was used. It can be seen that the transition is completed a little faster in the 'average velocity' method than in the 'average driving force' method.

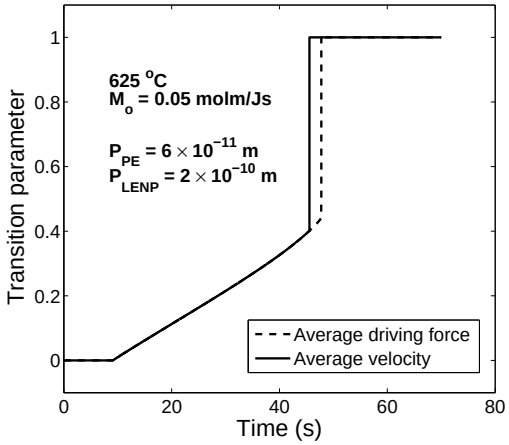

Figure 6.8: Comparison between the transition in 'average driving force' and 'average velocity' methods in the fully numerical model

Further, it can be noted that the increase of the transition parameter is quite rapid towards the end of the transition. The transition parameter increases from 0.4 to 1 in a second. Thus, the assumption of the end point of the transition as the point of negative determinant of the root in Equation 6.7 is considered to be valid. And it gives a value with an error in the order of less than a second.

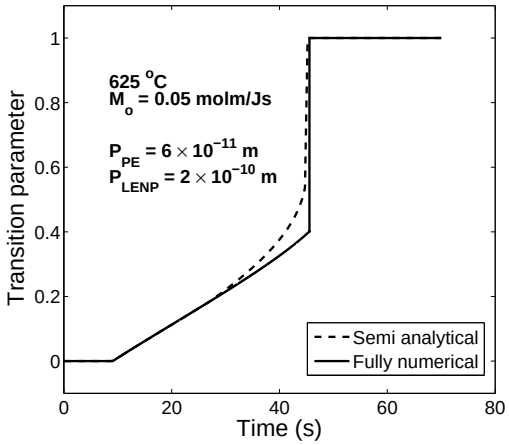

Figure 6.9: Comparison between the transition in fully numerical and semi analytical models using the 'average velocity' method

The comparison between the 'average velocity' method implemented in the fully numerical and semi analytical models is shown in Figure 6.9. The figure shows the variation of the transition parameter. It can be seen that the transition occurs more smoothly in the semi analytical model that the fully numerical model. This could be due to the difference in the implementation of the method in the two models. In the fully numerical model, a single interface concentration is used to calculate the mixed interface velocity. However, in the semi analytical model, the interface velocities according to the PE and LENP conditions are obtained from two different interface carbon concentrations. In other words, in the fully numerical model, the calculation is performed only once, using the interface carbon concentration of the previous time step to calculated two interface velocities according to the PE and LENP conditions. This is then averaged over the transition parameter. But, in the semi analytical model, the calculation is performed twice, separately for the PE and LENP conditions, which results in two different interface carbon concentrations. These give rise to two interface velocities, which are then averaged to obtain a single value of interface velocity according to Equation 6.7.

In this chapter, a gradual transition approach to describe the kinetic transition from PE to LENP condition was formulated. The approach is based on the P-factor, which is inversely proportional to the interface velocity. It denotes the width of the concentration spike of the substitutional element. It is assumed that PE conditions are maintained at the interface till a certain value of P-factor is reached. At this point, the equilibrium starts to deviate from PE towards LENP. LENP conditions is completely attained at a certain value of P-factor. A mixed equilibrium exists between the two criticial P-factor values. The transition approach was implemented in the fully numerical and semi analytical models and its behaviour was studied.

Chapter 7

Isothermal Transformation Studies

The ultimate goal of this work is to obtain a universal set of nucleation and growth parameters which can describe the transformation behaviour of austenite to ferrite in different grades of steels during different heat treatment cycles. In this chapter, the CA model has been used to reproduce the ferrite transformation behaviour in terms of the fraction curve and microstructure during isothermal holding. An attempt has been made to identify a unique set of parameters which is capable of explaining the isothermal austenite-to-ferrite transformation behaviour in DP600 at temperatures given in Chapter 4.

7.1 Cellular Automata Model Settings

The simulation volume in the CA model consisted of a grid of $300 \times 300 \times 300$ grid points with a grid spacing of 0.25 μm. This represents a cubic section of length 75 μm. An initial Voronoi austenite microstructure with a number averaged grain size of about 11.9 μm was used. The initial microstructure is shown in Figure 7.1.

The annealing cycle used in the simulations consisted of an initial quench from a temperature of 1100 K (826.85 °C) followed by isothermal holding at the required temperature. The initial heating and austenizing steps explained in Section 4.2 were not simulated in order to minimise the calculation time without significantly affecting the results.

In order to distinguish between the various potential nucleation sites, a variation in Mn content in the form of a sine wave was introduced. The Mn concentration affects the Ae3 temperature as shown in Figure 7.2. This, in turn, affects the nucleation behaviour as given in Equation 2.16. An example of the sine profile used in the simulations is given in Figure 7.3. This profile has an amplitude of 0.001 at. frac. of Mn with the mean

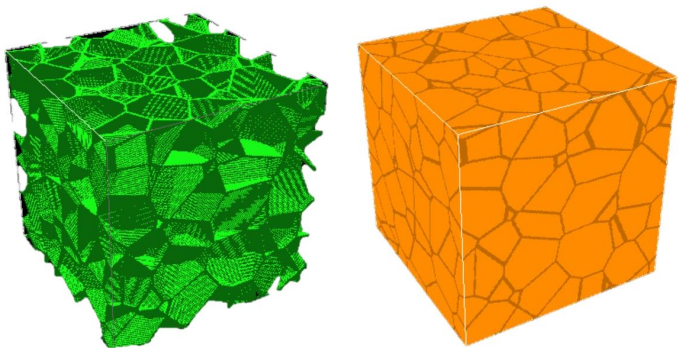

(a) (b)

Figure 7.1: Initial austenite grain structure (a) three dimensional view of the grains (b) side planes of the simulation volume (cube)

equal to the average Mn concentration in the alloy (0.01646 at. frac.). Mn concentration profiles of a similar order of magnitude have been experimentally observed in DP600 in the rolling direction (Rudnizki et al. [2011]). However, such observations in the transverse direction for this alloy is presently unavailable. The wavelength was chosen such that five Mn bands are accommodated in the length of the simulation cube. This distance was decided on the basis of the banding found in the experimental micrographs shown in Figure 4.7. The amplitude and the number of Mn bands used have an effect on the final ferrite microstructure.

The use of a Mn concentration profile to differentiate the nucleation sites necessitates the presence of experimental data of such profiles. It is , thus, difficult to accurately simulate the transformation in alloys where such data is not available. Theoretically, it is also possible to differentiate the nucleation sites on the basis of the 'effective activation energy for nucleation' (L) given in Equation 2.17 instead of the Mn concentration. This does not require the experimental data regarding the Mn profile in the alloy. This option, however, is not currently supported by the CA model.

7.2 Manganese Banding

In order to identify a correct description of the initial Mn profile in terms of its amplitude, a study of its effect on the final ferrite microstructure at various temperatures was carried out. The chosen Mn amplitude should be able to reproduce the trend of banding as seen in Figure 4.7, i.e. the presence of Mn banding at a temperature of 700 °C and its absence at 625 °C. Amplitudes of 1×10^{-5}, 1×10^{-4} and 1×10^{-3} at. frac. Mn with 10 bands was used for the comparison studies. The simulations was carried out for a single ferrite grain growing inside a single austenite grain with a diameter of 0.25 μm. Mobility pre-exponential factor of 0.1 molm/Js was used. The microstructures obtained after 50 s of

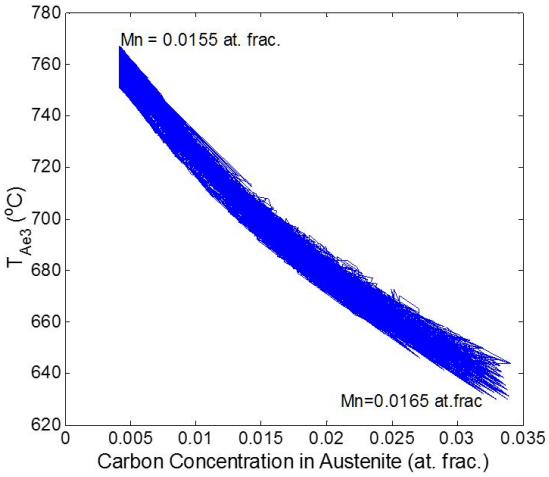

Figure 7.2: Variation of Ae3 temperature with carbon and manganese concentrations in DP600

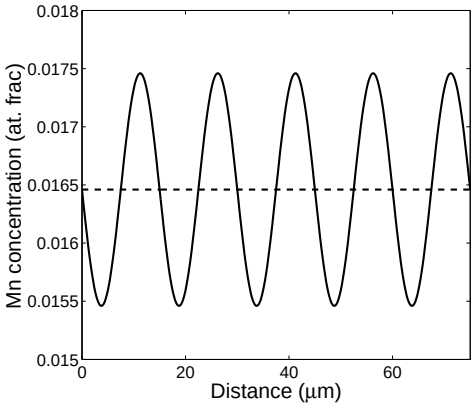

Figure 7.3: Schematic of Mn concentration profile in the x-direction used in the CA simulations

simulation under PE conditions are given in Table 7.1. The microstructures represent the xy-plane of the cube.

It can be seen that at the lowest Mn amplitude (1×10^{-5} at. frac.), a banded microstructure is not observed at any of the temperatures. It could be that the difference in the Mn concentration of this order of magnitude is not sufficient to cause an appreciable difference in the Ae3 temperature and thus, the driving force. However, at the highest Mn amplitude (1×10^{-3} at. frac.), the influence of temperature on banding can be noted. The effect of Mn concentration profile becomes stronger as the temperature becomes closer to the Ae3 temperature. Thus, a small difference in the Mn concentration is reflected as a large difference in the driving force. This causes the ferrite grain to grow only in the most preferred direction, thereby resulting in a rod like grain as seen in the simulation carried out at 750 °C.

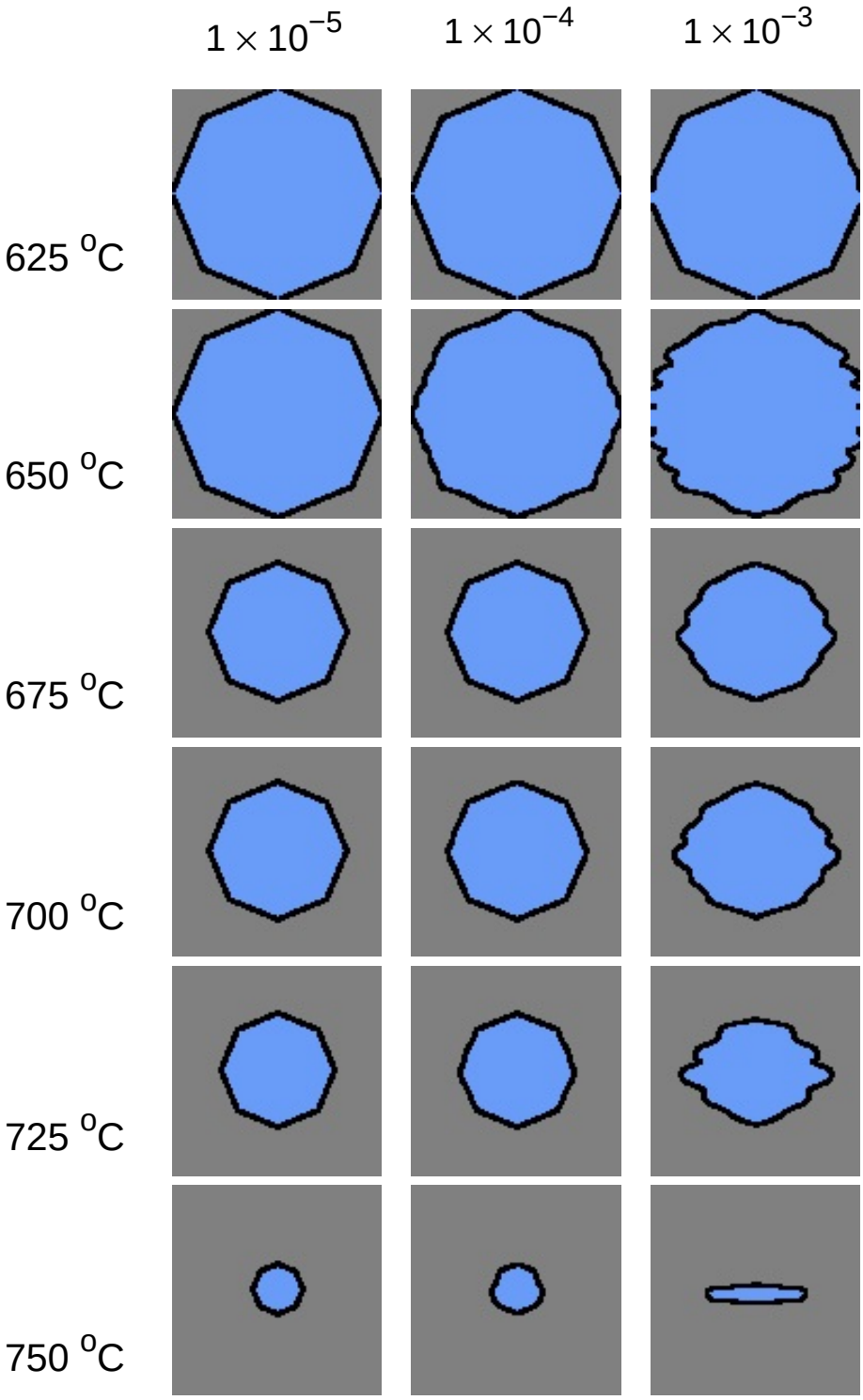

Table 7.1: Effect of initial Mn amplitude on ferrite microstructure at different temperatures for DP600. The rows and the columns represent various temperatures and Mn amplitudes (at. frac.) respectively.

For further simulations in the CA model, a Mn sine profile with an amplitude of 1×10^{-3} at. frac. was used.

7.3 Isothermal Transformation

Complete description of the austenite-to-ferrite transformation requires the correct prediction of the ferrite formation kinetics in terms of the fraction curve, final ferrite fraction, and the microstructure in terms of the Mn banding and ferrite grain size. The comparison between the experimental and the simulated results in terms of the above four features are given here.

7.3.1 Simulation Parameters

The values of various input parameters used in the CA model for simulating the ferrite formation at various temperatures is given in Table 7.2. The given set of parameters was capable of explaining the transformation behaviour, in terms of the ferrite fraction curve, at all temperatures. However, in order to reproduce the trend in the ferrite grain sizes, edge nucleation had to be incorporated at lower temperatures. The fraction of edge cells used for the nucleation process at various temperature is given in Table 7.3. The value of 'effective activation energy for nucleation' (L) for edge nucleation was used as 10^{-11} JK^2. A higher value of L represents a lower nucleation rate as given by Equation 2.16. This is representative of the fact that the austenite grain corners are the most preferred sites for ferrite nucleation, followed by the austenite grain edges. The value of the nucleation pre-exponential factor (K) for the edge nucleation is same as that of the corner nucleation. The use of a different pre-exponential factor for edge and corner nucleation is currently not supported by the CA model. Also, in this case, it is assumed that the number of potential nucleation sites in the grain edges is dictated by the fraction of edge cells used.

K_{corner} (-)	L_{corner} (JK^2)	$M_\circ$ (molm/Js)	P_{PE} (m)	P_{LENP} (m)	Q_d (KJ/mol)	n (-)
10	10^{-14}	0.65	5×10^{-12}	9×10^{-12}	240	600

Table 7.2: Values of various parameters used in the CA model for simulating austenite-to-ferrite transformation in DP600

The high value of the mobility pre-exponential factor represents a more diffusion controlled nature of the transformation. The accuracy of the semi analytical model at these conditions was studied in Section 5.2. As shown previously, the error obtained in the calculation of the ferrite fraction using the semi analytical model is acceptable.

The 'effective activation energy for nucleation' (L) is a collective factor representing the driving force for nucleation, the undercooling, the shape of the nucleus and the in-

Temperature (°C)	Edge Factor (-)
700	0
650	0.1
625	0.3

Table 7.3: Details of edge nucleation used in the CA model for simulating austenite-to-ferrite transformation in DP600

terfacial energies as given in Equation 2.17. The value of L can be used to calculate the value of Ψ which represents the effects of the shape of the nucleus and the interfacial energies. The uncertainties in determining Ψ leads to difficulties in the prediction of the nucleation rate and hence, its calculation is important. Several models have been proposed earlier for calculating Ψ. A model proposed by Clemm and Fisher [1955] considered grain corner nucleation with incoherent grain boundaries and a value of 3.3×10^{-3} J^3/m^2 was calculated. Experimentally, the value of Ψ was calculated by Offerman et al. [2002] using nucleation rates obtained from synchrotron studies. A value of 5×10^{-8} J^3/m^2 was obtained. It is five orders of magnitude lower than the value predicted by Clemm and Fisher [1955]. The low value obtained by Offerman et al. [2002] was attributed to the possibility of formation of initial nuclei with metastable crystallographic structures and the accuracy of conventional thermodynamics to predict the driving force for such small systems. Here, the value of Ψ is calculated from the parameter obtained from the CA model.

The driving force for nucleation (Δg_v) obtained from Thermo-calc® is plotted as a function of the undercooling for DP600. The value of χ used in Equation 2.17 is obtained as the slope of this curve. A linear approximation of this curve was used in determining the slope. The various values of Ψ calculated previously by Offerman et al. [2002] and Clemm and Fisher [1955] differ by a few orders of magnitude. The focus here is to obtain a measure of the order of magnitude of Ψ. Thus, the linearisation can be assumed to be a reasonable approximation. The plot of driving force for nucleation with the undercooling and the linear fit are given in Figure 7.4. The value of χ is calculated to be 3.1 J/molK. The calculated Ψ values are given in Table 7.4.

Nucleation site (-)	L (JK^2)	Ψ (J^3/m^2)
Corner	10^{-14}	1.3×10^{-3}
Edge	10^{-11}	1.3×10^{-1}

Table 7.4: Value of Ψ calculated for various nucleation sites

The value of Ψ calculated from the CA model for corner nucleation has a value closer to that of Clemm and Fisher [1955], which is five orders of magnitude larger than that of

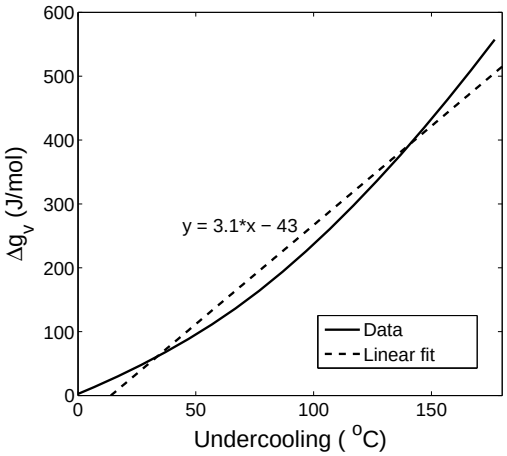

Figure 7.4: Variation of driving force for nucleation with undercooling

Offerman et al. [2002]. In order to understand the physical significance of the obtained value, a more detailed study needs to be carried out.

It can be noted from Table 7.2 that the values of P_{PE} and P_{LENP} obtained are about 2 orders of magnitude lower than those obtained by Capdevila et al. [2011] and Zurob et al. [2008]. However, a direct comparison cannot to be made between the values as the value of diffusion coefficient of Mn by Capdevila et al. [2011] and Zurob et al. [2008] is not known. The difference in the P-factor between the three simulations could be due to the difference in the nature of ferrite growth, in terms of the geometry of the interface. Capdevila et al. [2011] used a large austenite grain size of 76 μm and the growth is mostly confined to the grain boundary. Zurob et al. [2008] studied the growth of ferrite using decarburisation experiments. The growth of ferrite in both cases is planar in nature. However, in the CA simulations, a small austenite grain size (12 μm) is used. The growth of ferrite is spherical in nature. It is expected that the difference in the interface geometry behaves in a similar way as the system geometry used in the fully numerical model (Figure 5.4), where faster growth in a three-dimensional system was observed. A faster interface velocity represents a lower value of P-factor.

7.3.2 Ferrite Fraction Curve

The comparison between the simulated and the experimental ferrite fraction curves are given in Figure 7.5. It can be noted that the model accurately describes the transformation behaviour at lower ferrite fractions. At higher fractions, the simulated transformation is faster than the experimental at lower temperatures and slower at 700 °C. Considering the experimental error in the determination of the ferrite fraction curve, this difference is considered to be valid.

In the previous version of the CA model, without the implementation of the gradual

transition approach, different values of mobility pre-exponential factor, fraction of edge nucleation and equilibrium conditions had to be used at different cooling rates in order to obtain an accurate representation of the transformation kinetics. (Pattabhiraman [2012]) In this work, however, the mobility pre-exponential factor is constant for all temperatures, though the fraction of edge nucleation is different. The difference in the equilibrium condition between the temperatures is accounted for by the variation in the P-factor. In other words, the number of parameters that was manually adjusted in order to describe the transformation at various conditions has decreased with the implementation of the gradual transition approach.

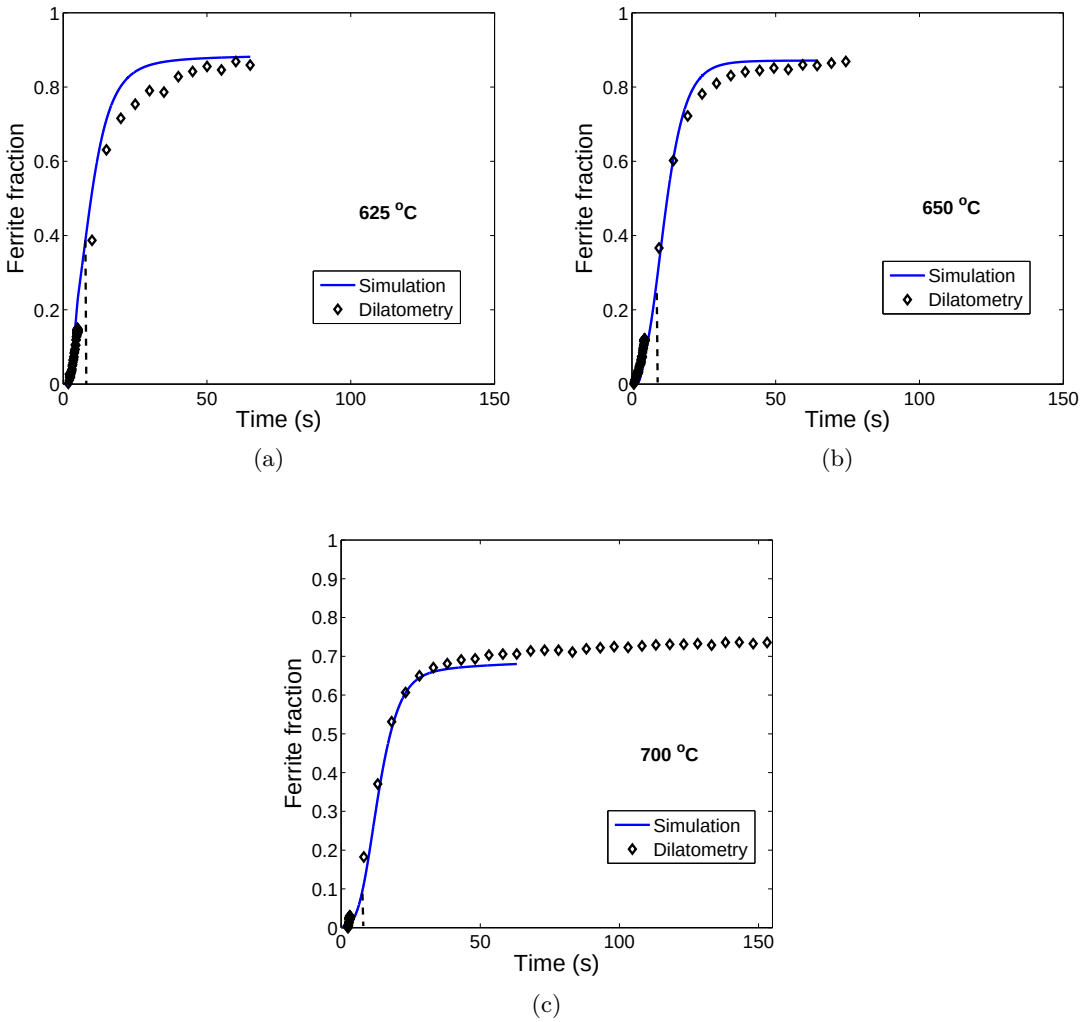

Figure 7.5: Comparison of simulated and dilatometric ferrite fraction curves obtained at (a) 625 °C (b) 650 °C and 700 °C.

At each temperature, full LENP condition is established at different times as described by the value of P_{LENP}. These times are indicated by the dashed lines in Figure

7.5. It can be noted that the LENP equilibrium is reached much faster at 700 °C than at 625 °C. This means that the transformation occurs under PE conditions for longer times at lower temperatures. PE, being a constrained equilibrium defined by the virtue of the reduced mobility of substitutional atoms with decreasing temperature, is preferred at lower temperatures. However, this is different from the observation by Zurob et al. [2008] wherein PE conditions were found at higher temperatures and LENP at lower temperatures for a Fe-C-Mn alloy.

7.3.3 Final Ferrite Fraction

The comparison between the final ferrite fractions obtained from the simulations and microscopic studies are given in Figure 7.6. The error bars in the figure represents the standard error of the mean (sem) given as

$$sem = \frac{SD}{\sqrt{n}} \tag{7.1}$$

where SD is the standard deviation of the sample mean and n is the sample size.

A decrease in ferrite fraction with increase in temperature is noted. From the figure, it can be seen that the model predicts the final ferrite fraction accurately at lower temperatures. However, the fraction obtained at 700 °C is lower than the experimental fraction. The absolute difference between the two fractions is 0.063 and is considered to be within experimental limits of error.

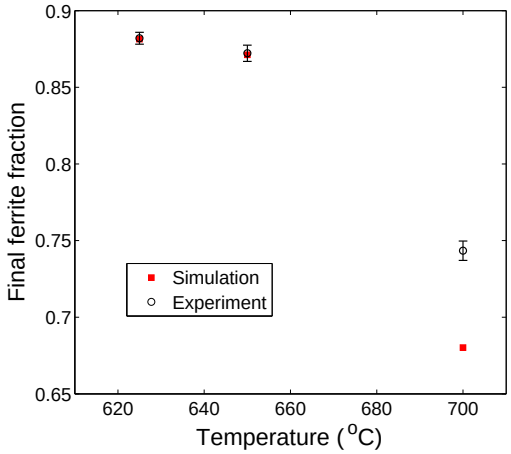

Figure 7.6: Final ferrite fractions obtained at different isothermal holding temperatures

7.3.4 Ferrite Microstructure

The microstructure obtained after isothermal holding at different temperatures are given in Figure 7.7. The inset shows the simulated microstructure. The scales of the simulated

and experimental micrographs are equal. The grey coloured phase in both microstructures represent pearlite. Ferrite is represented in blue and brown colour in the simulated and experimental microstructures respectively.

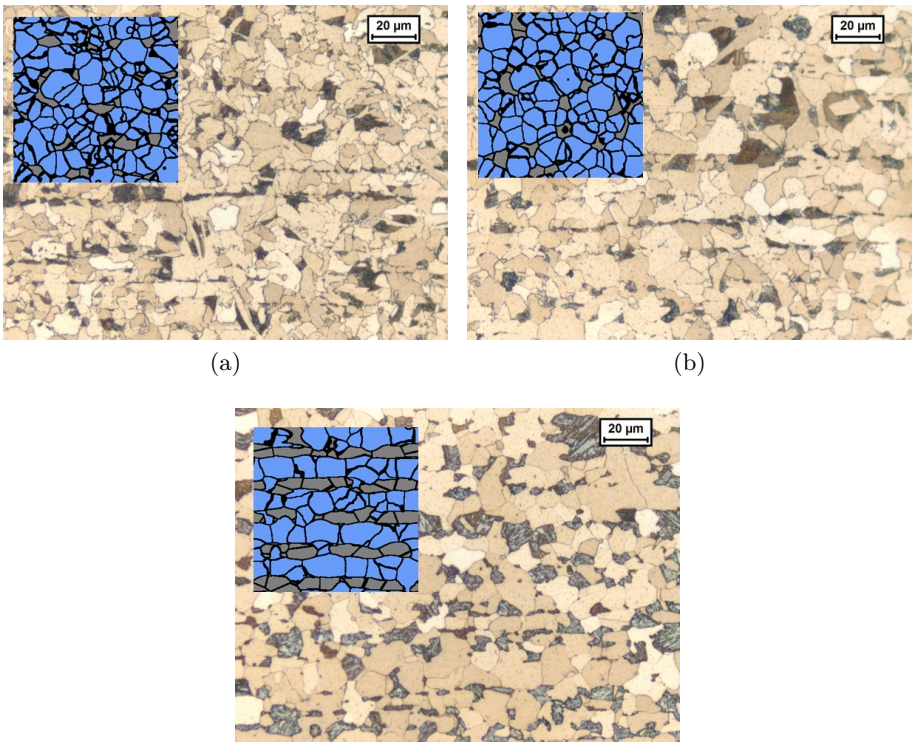

(a) (b)

(c)

Figure 7.7: Comparison of simulated and experimental microstructures obtained after isothermal transformation at (a) 625 °C (b) 650 °C (c) 700 °C

It can be seen from the figure that the simulated microstructure is a good representation of the experimental microstructure. It can also be noted that the model is capable of reproducing the trend of Mn banding in the microstructure, i.e. stronger banding with increasing temperature.

7.3.5 Ferrite Grain Size

The number averaged ferrite grain sizes obtained for the different conditions were compared. The comparison is given in Figure 7.8. The error bars represent the standard error of the mean (sem) given in Equation 7.1. An increase in ferrite grain size with an increase in temperature was noted. The behaviour of the simulated ferrite grain size is similar to that of the final ferrite fraction. The ferrite grain size calculated at 700 °C is lower than the experiment grain size. However, the grain sizes at lower temperatures are accurately predicted.

The variation of number of ferrite grains and average ferrite grain size as a function

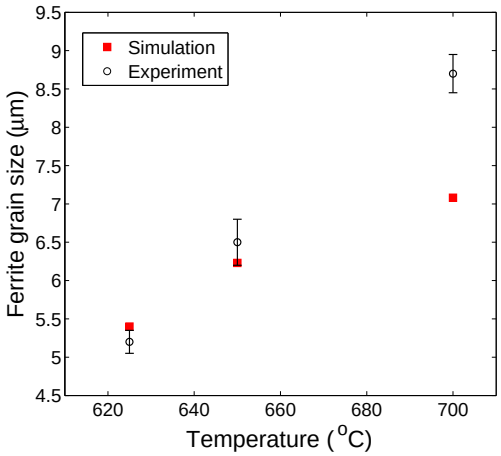

Figure 7.8: Ferrite grain sizes obtained at different isothermal holding temperatures

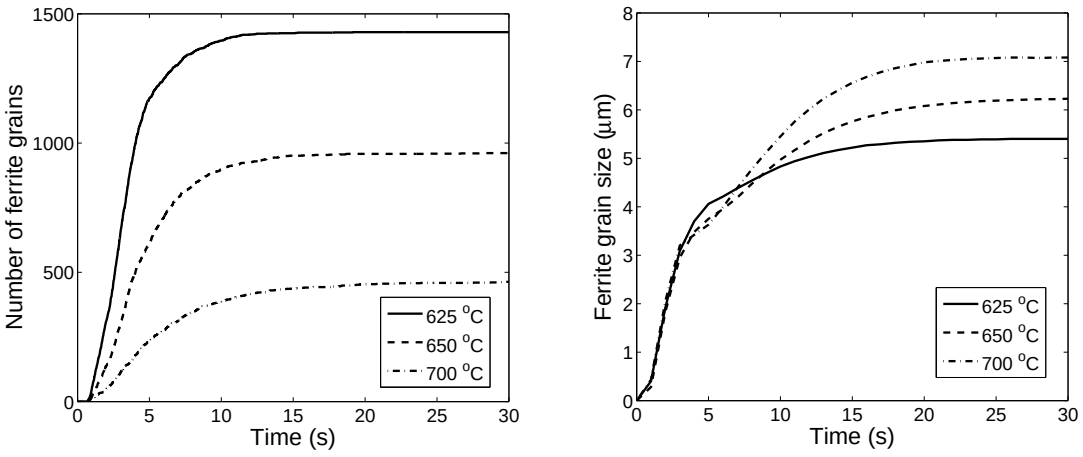

(a) (b)

Figure 7.9: Change in (a) number of ferrite grains and (b) ferrite grain size with time at various temperatures

of time at the different temperatures is given in Figure 7.9. All ferrite grains are formed within the first 10 seconds of transformation and are fully grown by 15 seconds. This is also reflected in the flat nature of the ferrite fraction curve shown in Figure 7.5. The change in the rate of ferrite grain growth with the transition from PE to LENP can be noted in Figure 7.9b. The growth is slower under LENP conditions.

From the above discussion, it can be seen that the improved version of the CA model was able to predict the isothermal austenite to ferrite transformation at different temperatures in terms of the ferrite transformation kinetics and the microstructure. However, the fraction of austenite grain edge cells used for nucleation had to be manually adjusted in order to reproduce the trend in ferrite grain size.

Chapter 8

Conclusions and Recommendations

The austenite-to-ferrite transformation in steel using a three-dimensional cellular automata (CA) model was studied in this work. The improvement and its subsequent validation formed an important part of the study. This chapter contains the major conclusions and recommendations for future study.

8.1 Conclusions

The main objective of the work is to obtain a single set of nucleation and growth parameters in the cellular automata (CA) model for describing the austenite-to-ferrite transformation in steels. A simplified 'semi analytical model' is used to describe the growth characteristics. In order to ascertain that the error in the CA model does not stem from this simplification, a critical assessment of its validity was carried out. The conditions of discrepancy were identified. In the second part of the thesis, the areas of improvement in the CA model was identified. A transition from para equilibrium (PE) to local equilibrium with negligible partitioning (LENP) was formulated and implemented in the CA model. The model was then validated by comparing the ferrite transformation rate and microstructure obtained at various isothermal holding temperatures with the experimental data. The major conclusions are given here.

8.1.1 Validity of Semi Analytical Model

The semi analytical model assumes an exponential carbon profile ahead of the interface in the austenite. It was compared with the fully numerical model wherein the carbon profile is calculated by solving the diffusion equations at each grid point. The comparisons were carried out over a range of temperature, mobility, diffusivity and alloy compositions.

Nature of Transformation

It was found that the accuracy of the semi analytical model depends on the nature of the transformation. A more diffusion controlled transformation, in terms of higher interface mobility and/or lower diffusion coefficient, results in a larger difference between the two models. It is postulated that the dependence of the model accuracy on the nature of transformation is due to the difference in the nature of the carbon concentration profile in austenite. Completely interface controlled transformation proceeds with a flat profile, while completely diffusion controlled transformation is associated with a curved profile. Thus, the definition of the shape of the carbon concentration profile has a significant effect in describing more diffusion controlled transformations than interface controlled transformations.

Importance of Mobility

Comparison of alloys with different carbon contents showed that the mobility pre-exponential factor has a great influence on the rate of transformation. Thermodynamically, an alloy with a higher Ae3 temperature is expected to transform faster than an alloy with lower Ae3 temperature. This was found to be true only at low mobilities. At higher mobilites this, however, was reversed. In other words, the composition of the alloy has a greater effect on the rate of transformation as the transformation becomes more diffusion controlled in nature. Thus, the selection of a single value of the mobility pre-exponential factor for describing the transformation behaviour of different alloys is quite critical.

Soft Impingement Correction

The semi analytical model is defined for grains growing in infinitely large systems. In order to account for the overlapping of carbon profiles of neighbouring grains due to the constriction in physical space, soft impingement corrections are defined. Two such methods of correction, namely 'mode factor soft-impingement' and 'fraction soft-impingement' were compared. It was found that the 'mode factor impingement' describes the transformation more accurately for a wider range of parameters than the 'fraction impingement'.

8.1.2 Gradual Transition Approach

A gradual transition approach for describing the transition from para equilibrium (PE) to local equilibrium with negligible partitioning (LENP) was formulated. The approach is based on the definition of a 'P-factor' which denotes the width of the spike of the substitutional alloying element in austenite. This approach makes use of the fact that a substitutional alloying element spike is present under LENP condition, while is absent

in PE condition. An increase in the value of the P-factor represents the building up of the spike. Two critical values of the P-factor denoting the start and completion of the spike build-up are defined. A value of calculated P-factor in between the critical values denote an equilibrium condition intermediate to the PE and LENP conditions. The studies showed that the transition behaviour is dependent on the selection of the mobility pre-exponential factor and the critical values.

8.1.3 Isothermal Transformation Studies

The CA model, after the implementation of the gradual transition, was used to study the isothermal austenite-to-ferrite transformation behaviour in DP600. The studies were carried out at temperatures of 625, 650 and 700 °C. A set of nucleation and growth parameters in terms of effective activation energy for nucleation (L), nucleation pre-exponential factor (K), mobility pre-exponential factor ($M_\circ$), critical interval (P_{PE} and P_{LENP}) were identified. The obtained set of parameters was capable of describing the ferrite transformation kinetics in terms of the ferrite fraction curve. The trend with respect to the final ferrite fraction obtained and microstructural banding was also reproduced. However, the decrease in grain size with temperature could not be predicted. In order to do so, the nucleation parameter denoting the amount of grain edge available for nucleation was manually adjusted.

8.2 Recommendations

In order to work towards a predictive nature for the CA model, several recommendations are given.

The model uses a variation in Mn concentration in order to create a difference between a class of nucleation sites. This, however, is not effective when the amount of Mn variation in an alloy is unknown. It would be more prudent to introduce a variation on the basis of the 'effective activation energy' (L).

The transition from PE to LENP has been defined to be gradual in nature. However, the value of the critical interval (difference between P_{PE} and P_{LENP}) obtained from the isothermal transformation studies in DP600 is quite small. Thus, the possibility of a sharp transition needs to be investigated. A sharp transition is computationally advantageous than the gradual transition. Also, the definition of the transition approach needs to be broadened in order to accommodate transformation during cooling. This is complicated by the fact that the P-factor decreases during cooling.

In the isothermal transformation studies carried out, the value of Mn amplitude in the sine profile used was experimentally observed in the rolling direction. Results of such studies in the transverse direction, is at present, unavailable. The inability to predict

the trend in the ferrite grain size could be due to the use of an incorrect value of the Mn amplitude. Thus, experimental studies need to be performed to validate the same.

The inability of the model to predict the trend in grain size even after the use of an accurate Mn amplitude would mean that the model is over-simplified and there exists other processes which affect the transformation and have not been considered. For example, solute drag in the moving interface could be once such process which could result in lower transformation rate and lower grain sizes.

Bibliography

C. Bos and J. Sietsma. A mixed-mode model for partitioning phase transformations. *Scripta Materialia*, 57(12):1085–1088, 2007.

C. Bos, MG Mecozzi, and J. Sietsma. A microstructure model for recrystallisation and phase transformation during the dual-phase steel annealing cycle. *Computational Materials Science*, 48(3):692–699, 2010.

C. Bos, MG Mecozzi, DN Hanlon, MP Aarnts, and J. Sietsma. Application of a three-dimensional microstructure evolution model to identify key process settings for the production of dual-phase steels. *Metallurgical and Materials Transactions A*, 42(12): 3602–3610, 2011.

JR Bradley and HI Aaronson. Growth kinetics of grain boundary ferrite allotriomorphs in fe-cx alloys. *Metallurgical and Materials Transactions A*, 12(10):1729–1741, 1981.

W. D. Callister. *Material science and engineering: an introduction*. John Wiley and sons, Inc., 2007.

C. Capdevila, J. Cornide, K. Tanaka, K. Nakanishi, and E. Urones-Garrote. Kinetic transition during ferrite growth in fe-c-mn medium carbon steel. *Metallurgical and Materials Transactions A*, 42(12):3719–3728, 2011.

H. Chen and S. van der Zwaag. Analysis of ferrite growth retardation induced by local mn enrichment in austenite created by prior interface passages. *Acta Materialia*, Online, 2012.

P.J Clemm and J.C Fisher. The influence of grain boundaries on the nucleation of secondary phases. *Acta Metallurgica*, 3(1):70 – 73, 1955. ISSN 0001-6160. doi: 10.1016/0001-6160(55)90014-6. URL `http://www.sciencedirect.com/science/article/pii/0001616055900146`.

DE Coates. Diffusion-controlled precipitate growth in ternary systems i. *Metallurgical Transactions B*, 3(5):1203–1212, 1972.

M. Enomoto. Local conditions at moving α/γ boundaries of proeutectoid ferrite transformation in iron alloys. *Metallurgical and Materials Transactions A*, 37(6):1703–1710, 2006.

E. Gamsjäger, M. Militzer, F. Fazeli, J. Svoboda, and FD Fischer. Interface mobility in case of the austenite-to-ferrite phase transformation. *Computational materials science*, 37(1):94–100, 2006.

M. Hillert and J. Agren. On the definitions of paraequilibrium and orthoequilibrium. *Scripta Materialia*, 50(5):697–699, 2004.

CR Hutchinson, A. Fuchsmann, and Y. Brechet. The diffusional formation of ferrite from austenite in fe-c-ni alloys. *Metallurgical and Materials Transactions A*, 35(4): 1211–1221, 2004.

G. Inden. Computer modelling of diffusion controlled transformations. *NATO science series*, 108:135–153, 2003.

G. Inden and R. Hutchinson. Interfacial conditions at the moving interfac during growth of ferrite from austenite in fe-c-(x) alloys. *Material Science and Technology: Austenite formation and decomposition*, pages 65–79, 2003.

T. A. Kop. *A dilatometric study of the austenite/ferrite interface mobility.* PhD thesis, Delft University of Technology, 2000.

Landolt-Bornstein. *Landolt-Bornstein database.* Springer Materials.

M. G. Mecozzi. *Phase field modelling of the austenite to ferrite transformations in steels.* PhD thesis, Delft University of Technology, 2007.

M.G. Mecozzi, M. Santofimia, and J. Sietsma. Modelling of microstructure development. Technical report, Delft University of Technology, 2012.

M. Militzer, R. Pandi, and EB Hawbolt. Ferrite nucleation and growth during continuous cooling. *Metallurgical and Materials Transactions A*, 27(6):1547–1556, 1996.

G E Murch. Ferrite and austenite diffusion bulk and interfacial. *Encyclopedia of materials: Science and Technology*, 2001.

W.D. Murray and F. Landis. Numerical and machine solutions of transient heat-conduction problems involving melting or freezing. *J. Heat Transfer. C*, 81:106–112, 1959.

S. E. Offerman, N. H. Van Dijk, J. Sietsma, S. Grigull, E. M. Lauridsen, L. Margulies, H. F. Poulsen, M. T. Rekveldt, and S. Van der Zwaag. Grain nucleation and growth during phase transformations. *Science*, 298(5595):1003–1005, 2002.

H. Pattabhiraman. Study of transformation behaviour of dual phase steel with continuous nucleation using cellular automata model. Technical report, Delft University of Technology, TATA Steel, 2012.

D. A. Porter and K. E. Easterling. *Phase transformations in metals and alloys*. Chapman and Hall, 1992.

G. Purdy, J. Ågren, A. Borgenstam, Y. Bréchet, M. Enomoto, T. Furuhara, E. Gamsjager, M. Gouné, M. Hillert, C. Hutchinson, et al. Alemi: A ten-year history of discussions of alloying-element interactions with migrating interfaces. *Metallurgical and Materials Transactions A*, 42(12):3703–3718, 2011.

J. Rudnizki, M. G. Mecozzi, and C. Bos. Experimental data for the validation of the through-process model in the production of dual phase steels. Technical report, Materials Innovation Institute, M2i, 2011.

SalzgitterFlachstahl, April 2013. URL `http://www.salzgitter-flachstahl.de/en/News/Archiv/2005/Automotive_Anwendungen//`.

V. I. Savran. *Austenite formation in C-Mn steel*. PhD thesis, Delft University of Technology, 2009.

J. Sietsma and S. van der Zwaag. A concise model for mixed-mode phase transformations in the solid state. *Acta Materialia*, 52:4143–4152, 2004.

SteelUniversity, April 2013. URL `http://steeluniversity.org/`.

TATASteel, April 2013. URL `http://www.tatasteeleurope.com/showsteelsection`.

P. Thibaux. Simplified modelling of the pe/lenp transition. Technical report, ALEMI, ArcelorMittal, 2006.

P. Tsipouridis. *Mechanical properties of dual phase steels*. PhD thesis, TU Munich, 2006.

S.M.C. Van Bohemen, Personal consulatation .

S.M.C. Van Bohemen, C. Bos, and J. Sietsma. Simulation of ferrite formation in fe-c alloys based on a three-dimensional mixed-mode transformation model. *Metallurgical and Materials Transactions A*, 42(9):2609–2618, 2011.

A. van der Ven and L. Delaey. Models for precipitate growth during the gamma-> alpha+ gamma transformation in fe-c and fe-cm alloys. *Progress in materials science*, 40(3):181–264, 1996.

Y. van Leeuwen. *Moving interfaces in low-carbon steel: A phase transformation model*. PhD thesis, Delft University of Technology, 2000.

WorldAutoSteel, April 2013. URL http://www.worldautosteel.org/steel-basics/steel-types/dual-phase-dp-steels/.

HS Zurob, CR Hutchinson, A. Béché, GR Purdy, and YJM Bréchet. A transition from local equilibrium to paraequilibrium kinetics for ferrite growth in fe-c-mn: A possible role of interfacial segregation. *Acta Materialia*, 56(10):2203–2211, 2008.

HS Zurob, CR Hutchinson, Y. Bréchet, H. Seyedrezai, and GR Purdy. Kinetic transitions during non-partitioned ferrite growth in fe-c-x alloys. *Acta Materialia*, 57(9):2781–2792, 2009.

HS Zurob, D. Panahi, CR Hutchinson, Y. Brechet, and GR Purdy. Self-consistent model for planar ferrite growth in fe-c-x alloys. *Metallurgical and Materials Transactions A*, pages 1–16, 2012.

List of Figures

List of Tables